THE GEOLOGY OF THE ADELAIDEAN-KANMANTOO GROUP SEQUENCES IN THE EASTERN MOUNT LOFTY RANGES

by

Stephen Toteff

B.Sc. (Hons.), University of Adelaide

Volume 2

Department of Geology and Mineralogy,

University of Adelaide.

November, 1977.

Awarded Dec. 1978

Figure 2

(in pocket, inside back cover).

Figure 3

Correlation of Marino Group sections in the Nairne-Mt. Barker Creek area with the Marino Group in the western Mt. Lofty Ranges.

Description of lithologies shown in the stratigraphic columns (in map pocket inside back cover):

Nairne

1. Kaolinized pale grey metasiltstones with minor scapolite.
2. Scapolite-rich metasiltstones.
3. Grey weakly laminated metasiltstones. Thin beds scapolite-bearing.
4. Fine to medium-grained feldspathic metasandstones which are weakly laminated. Some ripple marks present.
5. Grey metasiltstones and very fine metasandstones with scapolite-rich more micaceous horizons.
6. Kaolinized poorly sorted fine to coarse feldspathic meta-sandstones and quartzite.
7. Grey laminated metasiltstones and very fine metasandstones. Thin more micaceous beds with minor scapolite.
8. Poorly sorted fine to medium-grained metasandstone and quartzite. Weakly laminated with occasional ripples.
9. Kaolinized well laminated metasiltstones, scapolite-bearing in parts.
10. Poorly sorted medium to coarse-grained feldspathic meta-sandstone and meta-arkose. Thin metasiltstone interbeds.
11. Fine to medium-grained grey metasandstone.
12. Well laminated grey metasiltstones with occasional scapolite-bearing horizons.
13. Grey, weakly laminated fine metasandstone.
14. Coarse poorly sorted meta-arkose.
15. Grey scapolite-rich metasiltstones.
16. Moderately laminated metasiltstones. Thin (to 2.5 cm) fine feldspathic metasandstone interbeds and occasional scapolite-bearing horizons. Some small-scale cross-bedding and ripple marks.
17. Based on field work due south of Nairne: poorly outcropping thin meta-arkoses and scapolite-bearing metasiltstones.

17a. No exposures.

Figure 3 (Description of lithologies continued).

18. Andalusite schists, quartz-micaschists.
19. Metasiltstones, minor micaschists and andalusite schists.

Mt. Barker Creek

1. Well laminated feldspathic metasiltstones and quartz-micaschists.
2. Metasiltstones, minor quartz-micaschists.
3. Laminated metasiltstones with interbeds of weakly laminated less micaceous feldspathic metasiltstones, increasing in abundance up the sequence.
4. Partly calcareous metasiltstones with common interbeds of resistant feldspathic metasiltstones grading to very fine metasandstones. Minor quartz-micaschists.
5. Metasiltstones with common resistant feldspathic fine metasandstone interbeds.
6. Weakly laminated resistant metasiltstones grading into feldspathic fine metasandstones. Some rocks calcareous.
7. Laminated calcareous fine metasiltstones with small-scale cross-bedding.
8. Laminated metasiltstones with interbedded less micaceous metasiltstones with minor scapolite increasing up the sequence.
9. Dark grey weakly laminated metasiltstones with common scapolite in parts.
10. Weakly laminated fine metasiltstones with thin interbeds of more micaceous metasiltstones (grading into quartz-micaschists) and common lenticular scapolite-rich beds. These lithologies grade laterally and vertically into calc-silicates.
11. Metasiltstones, scapolite absent.
12. Poorly bedded fine pale grey slightly feldspathic metasandstones and quartzites. Occasional fine to medium-grained metasandstones (to 1 m). Minor thin weakly laminated metasiltstone and rare quartz-micaschist interbeds. Rare thin medium-grained meta-arkoses.
13. Gradation from fine metasandstone to weakly laminated metasiltstone.
14. Quartz-micaschists and less micaceous metasiltstones.
15. Andalusite schists, quartz-micaschists .
16. Metasiltstones, minor micaschists and andalusite schists.
17. Calc-silicates grading laterally and vertically into scapolite-rich metasiltstones (refer to Figure 4 for more detail).
18. White ortho-quartzite.

Figure 3 (Description of lithologies continued).

Waterfall Creek (Hallett Cove Area) - Marino Group Stratotype (after Daily & Gostin[1], pers.comm. and Sprigg (1942)[1].

1. Moderately well laminated to ripple bedded grey-green to mauve coloured siltstones with thin interbeds of purple shales and fine sandstones. Purple clay galls a prominent feature, often associated with mud-cracked horizons.
2. Current-bedded and laminated red and green clay gall-bearing feldspathic sandstone with thin mud-cracked red and green shales.
3. Coarse cross-bedded arkose and sandstone with yellow limestone intraclasts and clay galls. Some mud cracks. Poor outcrop.
4. Olive green coloured calc-siltstones and medium-grained feldspathic sandstone. Poor outcrop.
5. Cross-bedded sandy limestone and calc-sandstone with granule and pebble bands; pebbles to 1 cm.
6. Current-bedded very fine-grained to granule-rich feldspathic sandstone.
7. Calcareous pebbly and granule-rich cross-bedded sandstone to limestone.
8. Thin grey oolitic limestones interbedded in coarse sandstone and thin lenticular fine-grained limestone. Coarse to pebbly calc.-sandstone with limestone clasts (to 5 cm), also quartz, feldspar, porphyry (pebbles to 1.5 cm). Minor purple silt partings.
9. Grey cross-bedded and current-bedded heavy mineral-bearing calcareous and non-calcareous fine to medium-grained sandstone with some clay galls. Some bedded calc-silts with oscillation ripples.
10. Tan to olive green coloured calc- fine siltstones, very well laminated in lower part. Current-bedded towards top with corresponding increase in grainsize to coarse silt or fine sand.
11. Pale brown fine to coarse and pebbly cross-bedded feldspathic sandstones and arkoses. Also fine sandstone with ripples and heavy mineral bands. Calcareous intervals, slightly oolitic in part.
12. Finely laminated olive-green shales.
13. Laminated olive-grey calc-siltstone with thin (to 3 cm) interbeds of fine calcareous and feldspathic sandstone.

---

[1]Divisions 1-17 after Daily and Milnes, pers. comm; 17-24 after Sprigg (1942).

Figure 3 (Description of lithologies continued)

14. Stromatolitic and sandy oolitic limestone and calc-sandstone with limestone clasts.
15. Olive-green to grey shales and micaceous calc-siltstones with minor sandstone interbeds to 30 cm thick. Sequence less laminated, coarser upwards.
16. Brown fine micaceous calcareous sandstone strongly channeled and slumped in the basal parts, coarsening upwards to red granule-bearing sandstones at the top.
17. Diamictite. Rocks above outcrop poorly, with large areas having no outcrop. The descriptions of the lithologies and the thicknesses given below are after Sprigg (1942). The section runs to the western limit of Waterfall Creek (i.e. Gulf St. Vincent). The section was supplemented with data from the youngest rocks which are exposed a few hundred metres to the NE and SW of the Waterfall Creek outlet. The following description of the diamictite is after Willoughby (1960).
The pale-coloured diamictite is described as being predominantly a fine siltstone which is flaggy near the base. Pebbles, exceptionally to 1.5 cm in size, consist of limestone, feldspar and quartz. Rare thin arkose bands are present.
18. Massive grey quartzite ("Seacliff Sandstone Member" of Thomson (1966)).
19. Thick bedded purple quartzites with interbeds of purple slates and siltstones, banded in parts.
20. Alternating purple slates and purple quartzites.
21. Grey quartzites.
22. Grey quartzite with some slaty bands. Frequent cross-bedding and laminations.
23. Alternate flaggy chocolate to grey quartzites and slates.
24. Sequence of alternating massive quartzites and flaggy quartzites with thin interbedded shales. The finer subdivision of this interval by Sprigg (1942) is not given here.

Stockyard Creek (near Delamere, western Fleurieu Peninsula).
(After Daily (1963) with minor additions after Leslie (1962)).

1. Dark grey calc-siltstones overlain by dark-coloured current-bedded siltstones and silty quartzites with interbeds of cleaner quartzite, especially near the top. Mud-cracks are present through the sequence.
2. Cross-bedded coarse to pebbly calcareous sandstone with clean and sandy marble lenses.

Figure 3 (Description of lithologies continued).

3. Laminated siltstone with minor cross-bedded grey silty quartzite interbeds in the upper parts. Lower part banded.
4. Massive dark grey pebbly quartzite.
5. Soft green to grey coloured siltstones and phyllites, coarser in the upper part. The phyllites are rich in magnetite, particularly in the lower levels. Thin sandstone beds (to 10 cm) occur near the top.
6. Uppermost unit of the Marino Group. Alternating thin flaggy and rippled clean quartzites, laminated siltstones. At least three massive clean quartzite bands are present, thicknesses ranging from 3 m to 9 m.

Figure 4

Detailed stratigraphic sections in the vicinity of the contact between the Marino Group and the Kanmantoo Group, Nairne-Mt. Barker Creek area. Sections (A to G) are located in Map 1. Gaps in columns indicate an absence of outcrop. Stratigraphic columns in inside pocket.

Section A. (Composite section, thicknesses approximate)

1. Scapolite-rich metasiltstones with minor micaschists.
2. Weakly laminated metasiltstones. Minor less micaceous metasiltstone interbeds.
3. Well laminated metasiltstones grading into quartz-micaschists with common scapolite-rich beds.
4. Well laminated metasiltstones.
5. Micaceous fine metasandstones and minor metasiltstones passing up into laminated medium-grained feldspathic metasandstones and meta-arkoses.

Section B.

1. Laminated fine metasiltstones and minor metashales, scapolite-rich in upper levels. Lamination decreases markedly down sequence.
2. Massive well layered calc-silicate with minor scapolite-rich fine metasiltstone and metashale interbeds.
3. Weakly laminated kaolinized metasiltstones with thin white, slightly feldspathic quartzite interbeds, to 20 cm thick near top.
4. Feldspathic metasiltstones with minor scapolite, hornblende. Extensively kaolinized.
5. Massive white orthoquartzite with thin fine metasandstone and metasiltstone interbeds, particularly common in the lower levels where the quartzites are well bedded in parts and weakly laminated.
6. Finely laminated metasiltstones with common scapolite-rich beds in lower levels where the rocks are highly kaolinized.

Figure 4 (description of lithologies continued)

7. Laminated feldspathic metasiltstones and fine metasandstones with resistant less micaceous metasandstone interbeds which are poorly laminated.

Section C.

1. Layered calc-silicate passing laterally and vertically into metasiltstones and quartz-micaschists.
2. Very micaceous metasiltstones to quartz-micaschists.
3. Layered calc-silicate.
4. Massive white orthoquartzite
5. Feldspathic metasandstones and minor metasiltstones, metaarkoses.

Section D.

1. Layered calc-silicate.
2. Weakly laminated very micaceous metasiltstones with minor less micaceous interbeds and quartz-micaschists containing occasional andalusite bands. Scapolite rapidly increases at the top.
3. Massive layered calc-silicate with some flaggy horizons containing minor metasiltstone interbeds which are most common near the top.
4. Weakly laminated calcareous metasiltstones with thin hornblende, scapolite-bearing beds (to 1 cm).
5. Weakly laminated fine metasandstones and thin metasiltstones which are well laminated.
6. Weakly laminated fine to medium-grained feldspathic metasandstone and meta-arkose with well laminated, more micaceous metasandstone and metasiltstone interbeds. Some small and medium scale cross-bedding.

Figure 4 (description of lithologies continued)

Section E

1. Layered calc-silicate
2. Weakly laminated metasiltstones with less micaceous interbeds.
3. Layered calc-silicates
4. Scapolite and hornblende-bearing metasiltstones with thin calc-silicate interbeds including a thin calc-silicate pebble bed (A405/BC49). Lens of pale grey marble with thin silty layers passing laterally into calc-silicate, 3.5 m from top.
5. Backstairs Passage Formation

Section F

1. Metasiltstones with scapolite, hornblende
2. Layered calc-silicate. Thin interbeds (to 30 cm) of hornblende, scapolite-bearing metasiltstones (grading to quartz-micaschists).
3. Glassy white orthoquartzite
4. Backstairs Passage Formation

Section G

1. Layered calc-silicate
2. Very micaceous metasiltstones and minor quartz-micaschists
3. Layered calc-silicate passing laterally into fine meta-sandstones and metasiltstones in the upper parts. Poor outcrop.
4. White orthoquartzite lensing out into calc-silicate
5. Backstairs Passage Formation.

Figure 5

Equal-area stereographic projection of poles to bedding (πS_o) (strata above the upper level of the Mt. Barker Quartzite indicated by crosses; below this level by dots), with statistical fold axis β_2 for the whole Nairne-Mt. Barker Creek area. F_2 fold axes determined from mesoscopic folds are indicated by open circles. F_2 lineations (l_2) on bedding (S_o) are indicated by solid circles.

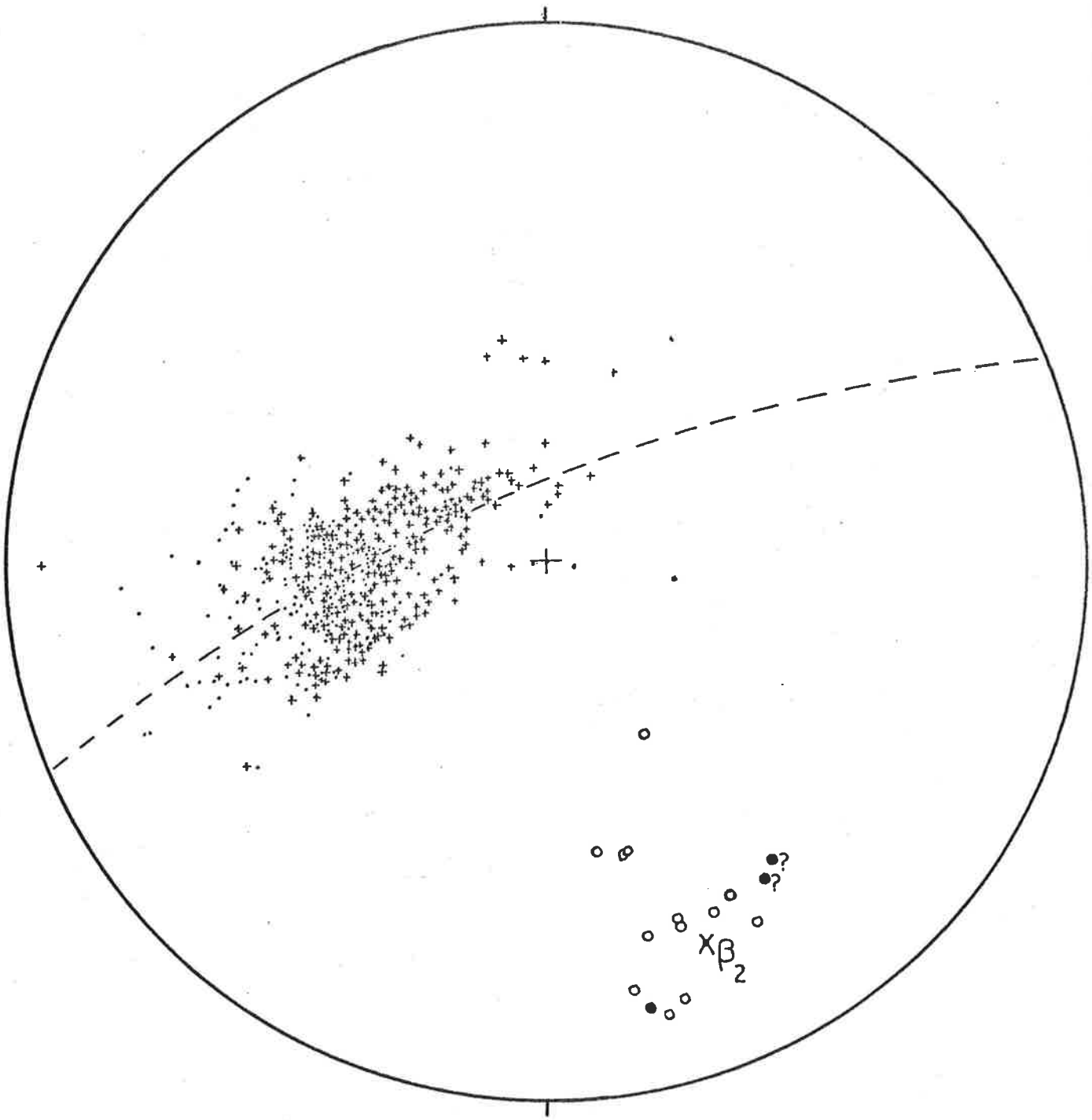

fig.5.

Figure 6

Stereographic projection showing:

a) F_3 crenulations on S_2 surfaces, defined as l_3. Well developed crenulations, generally paralleled by a biotite lineation (possibly l_2' in some cases) are indicated by solid squares. Open squares indicate an approximate orientation of l_3 owing to poor outcrop.

b) Orientation of biotite lineation l_2' on S_2 surfaces (crosses).

c) F_4 axes (open triangles) and lineations (solid triangles).

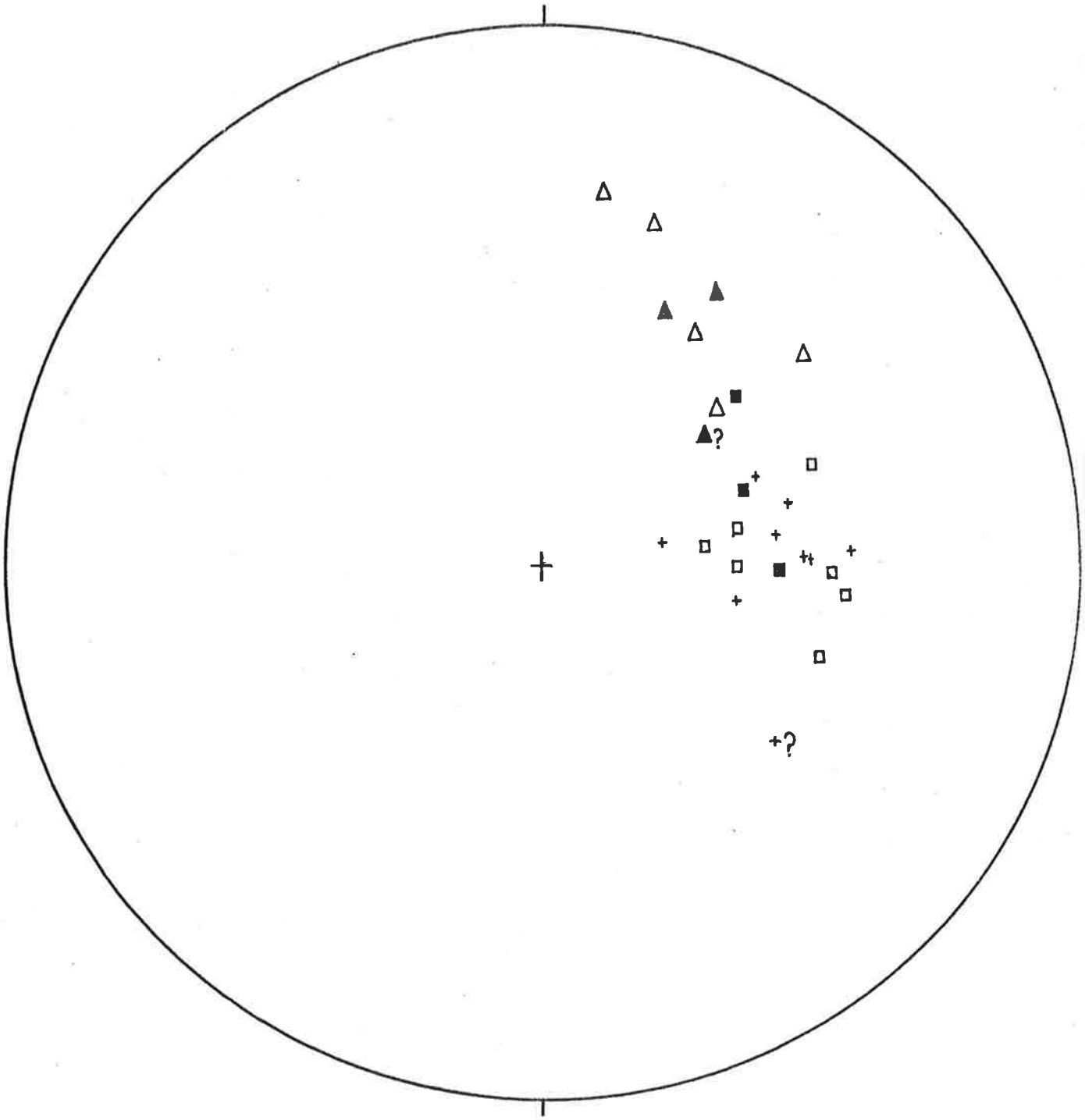

fig.6

Figure 7

Diagrammatic sketch of the major tectonic elements recognized in the Nairne-Mt. Barker Creek area.

S_0 = bedding

F_2 = axis of F_2 folds

l_2 = biotite lineation which parallels some F_2 axes

S_2 = axial plane schistosity of F_2 folds

l_2' = biotite lineation seen on S_2 and most S_0 surfaces

F_3 = axis of F_3 crenulations

S_3 = axial plane of F_3 crenulations

l_3 = lineation defined by crenulations seen on some S_2 surfaces.

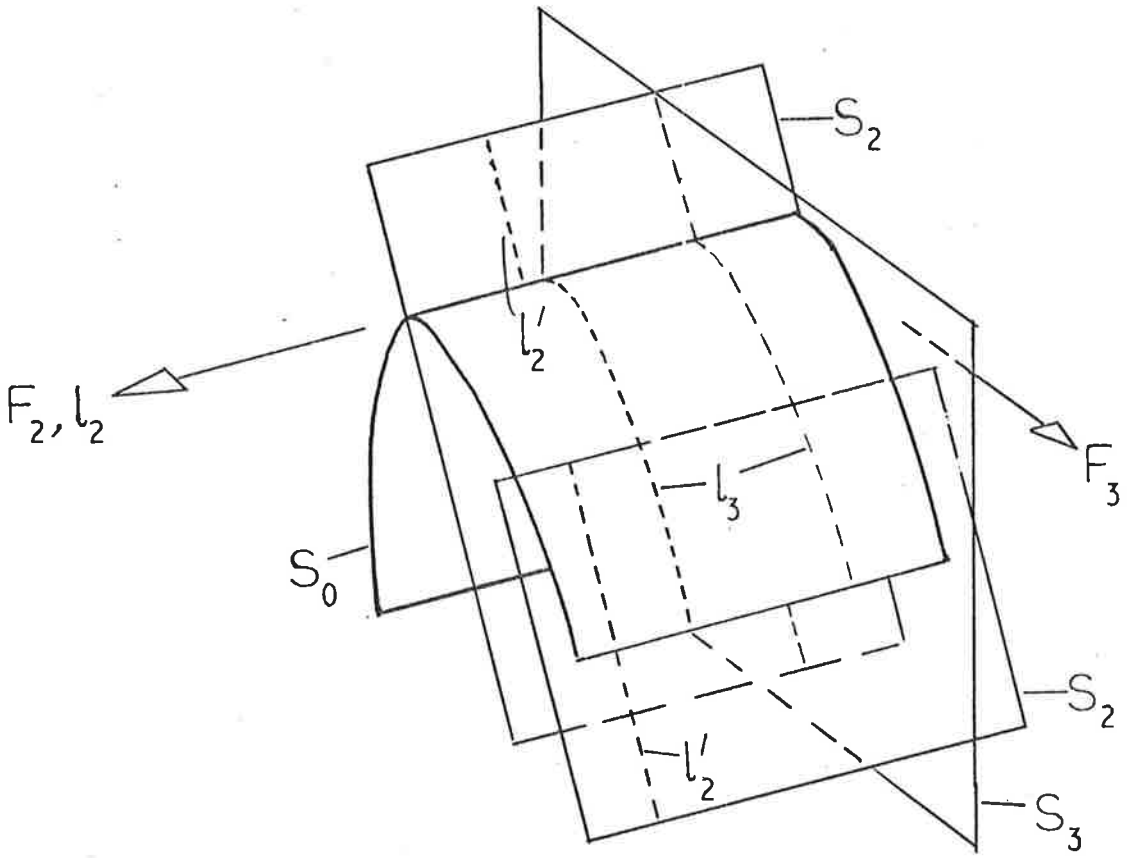

fig. 7

Figure 8

Distribution of metamorphic zones in the Mt. Lofty Ranges in the vicinity of the Nairne-Mt. Barker Creek area (after Offler and Fleming, 1968 and Fleming, 1971).

The Nairne-Mt. Barker Creek area is outlined by the dashed line.

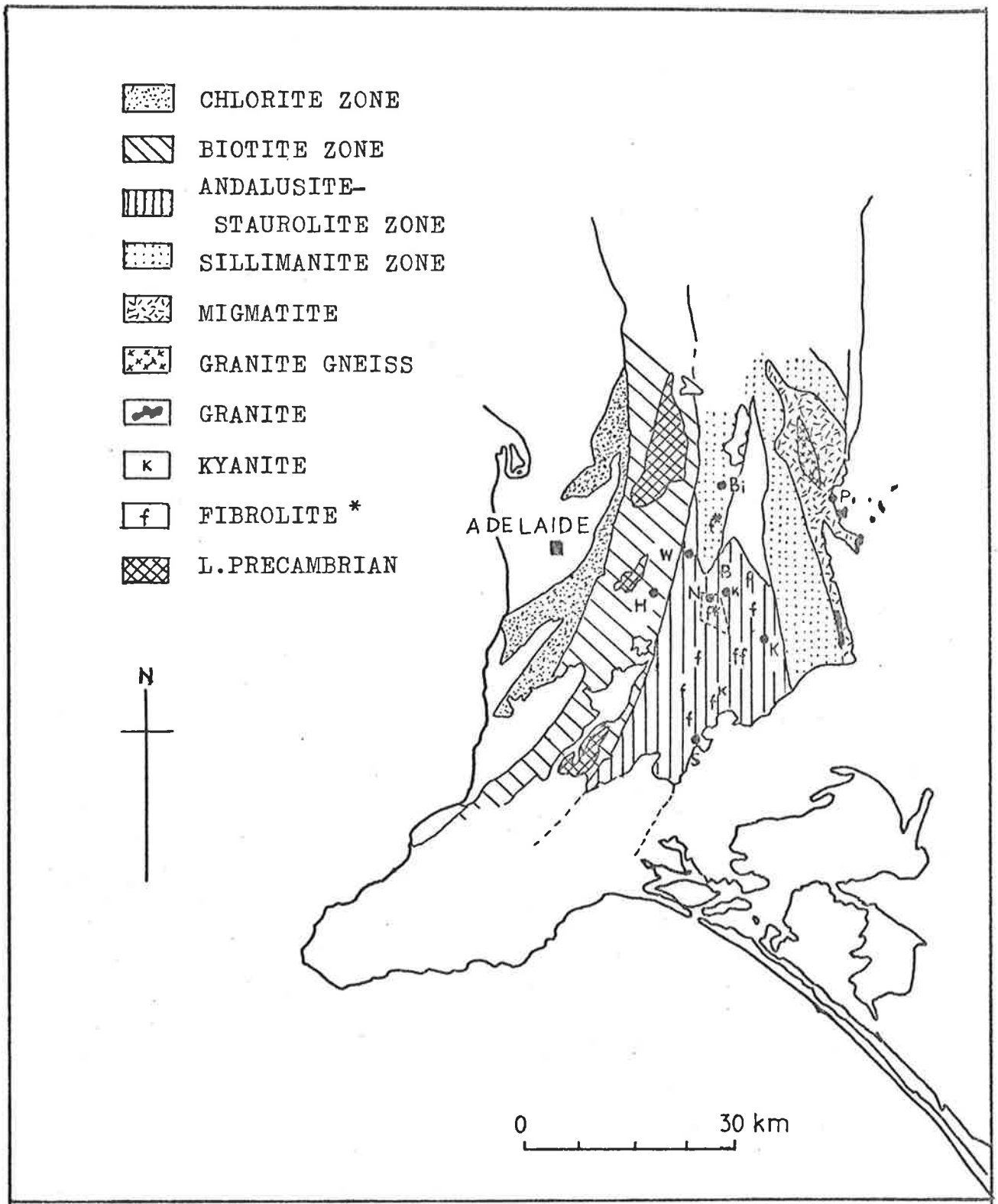

B	BRUKUNGA	N	NAIRNE
Bi	BIRDWOOD	P	PALMER
H	HAHNDORF	S	STRATHALBYN
K	KANMANTOO	W	WOODSIDE

* Fibrolite occurrence, this study.

fig.8

Figure 9

P-T diagram of equilibrium curves relevant to assessment of P-T conditions in the Nairne-Mt. Barker Creek area.

A. Phase diagram for Al_2SiO_5 equilibria after Richardson et al. (1969). That of Althaus (1967) is similar but with a lower slope for the andalusite-kyanite phase boundary.

B. Phase diagram for Al_2SiO_5 equilibria after Newton (1966).

C. Phase diagram for Al_2SiO_5 equilibria after Holdaway (1971).

1 Staurolite + quartz $\rightleftarrows$ Al silicate + garnet + H_2O (Hoschek, 1969).

2 Staurolite + muscovite + quartz $\rightleftarrows$ Al silicate + biotite + H_2O (Hoschek, 1969).

3 Chlorite + muscovite $\rightleftarrows$ staurolite + biotite + quartz + H_2O (Hoschek, 1969).
(a) $X_{H_2O} = 1$; (b) $X_{H_2O} = 0.5$ ($P_{H_2O} < P_S$)

4 Chloritoid + quartz $\rightleftarrows$ staurolite + garnet + H_2O (Hoschek, 1969).

5 Chloritoid + Al-Silicate $\rightleftarrows$ staurolite + quartz + H_2O (Hoschek, 1969).

6 Chloritoid + chlorite + muscovite $\rightleftarrows$ staurolite + biotite quartz + H_2O
Reaction curve lies between 4 and 5 (Hoschek, 1969).

7 Pyrophyllite $\rightleftarrows$ Al-silicate + quartz + H_2O (Althaus, 1969)

8 Muscovite + quartz $\rightleftarrows$ sillimanite + K-feldspar + H_2O (Evans, 1965).

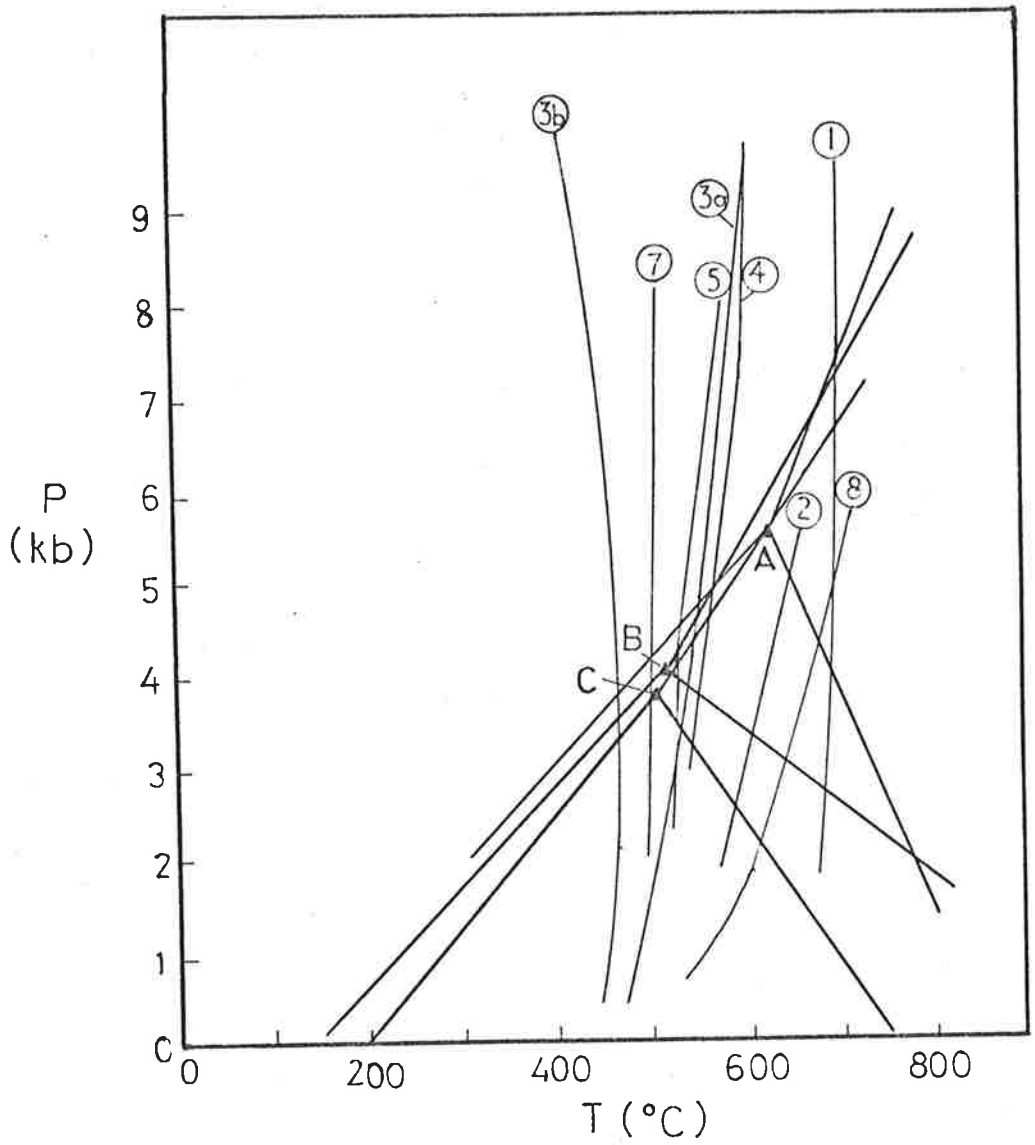

fig. 9

Figure 10

P-T diagram of phase boundaries relevant to assessment of the stability of cordierite in the Nairne-Mt. Barker Creek area.

A. Phase diagram for Al_2SiO_5 equilibria after Richardson, et al. (1969).

B. Phase diagram for Al_2SiO_5 equilibria after Holdaway (1971).

1 Low temperature margin of stability field of Mg-cordierite, hydrous conditions (Schreyer and Yoder, 1964).

2 Upper pressure limit of stability field of Mg-cordierite in the system K_2O-MgO-SiO_2-Al_2O_3-H_2O. (Schreyer and Seifert, 1969).

3 Upper stability field of Fe-cordierite (conditions of QFM). (Richardson, 1968).

4 Conservative estimate of the upper stability of cordierite in natural pelites (Richardson, 1968).

5 and 6 delineate amphibole + Mg-cordierite + kyanite + quartz field from high-Mg-cordierite + quartz field and amphibole + kyanite + quartz field respectively. (Green and Vernon, 1974).

Cross-hatched areas show approximate P-T conditions which prevailed in the Nairne-Mt. Barker Creek area in relation to the two Al_2SiO_5 phase diagrams (A and B).

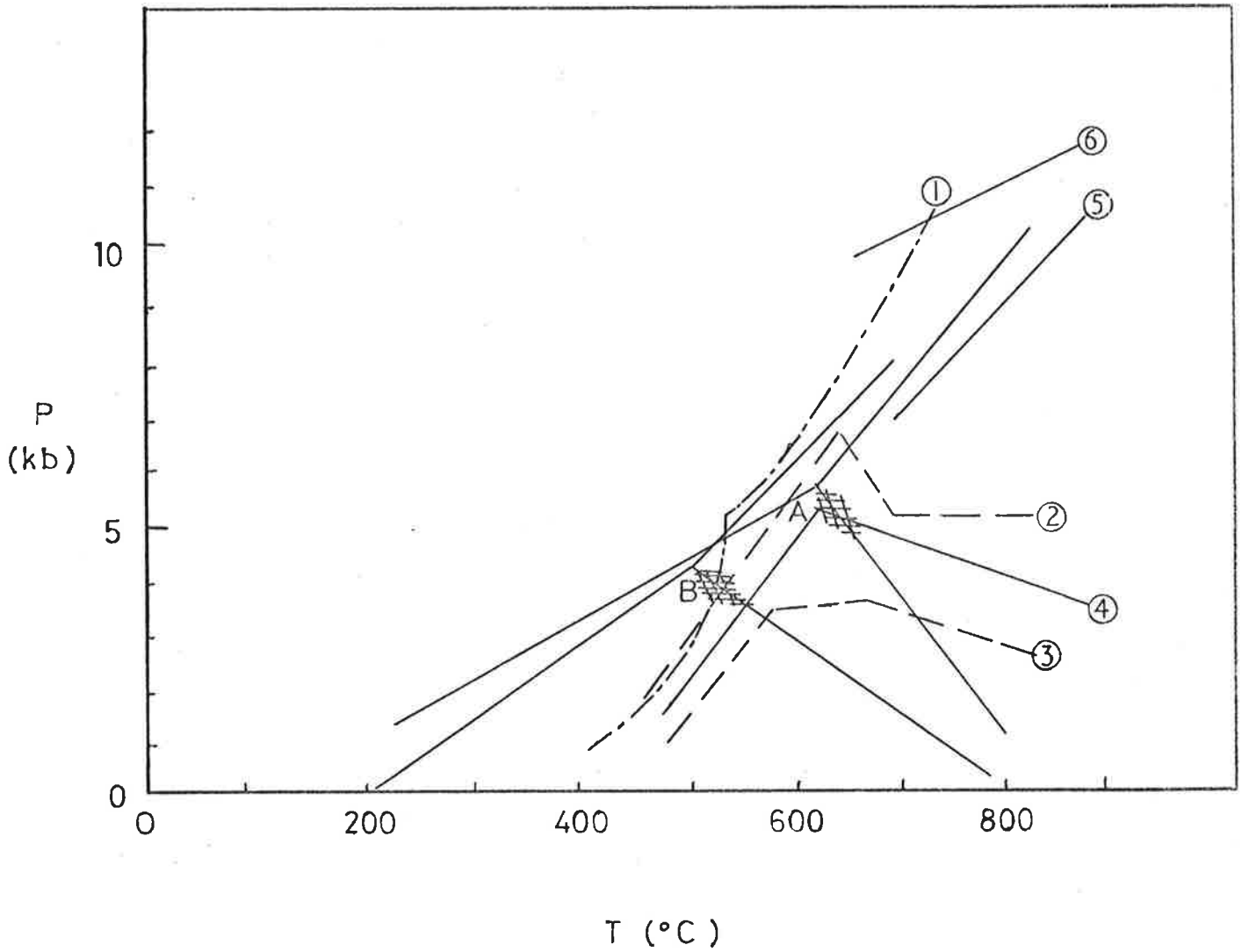

fig.10

Figure 11A.

Average distribution coefficient $K_{D_{Mg}}^{G\text{-}Bi}$ (= 0.199) for rocks A405/E2A, M24, E4B, E4E plotted on Mg-distribution diagram.

X_{Mg} = $Mg/Mg+Fe_{TOT}$. K_D determined for garnet rims only.

Figure 11B.

Relation between atomic ratio of Ca in garnet and $Mg/Mg+Fe_{TOT}$ ratio (X_{Mg}) in garnet and biotite. c = data from garnet core; r = data from garnet rim.

Rock A405/E2A = ● ; M24 = ■ ; E4B = o; E4E = x.

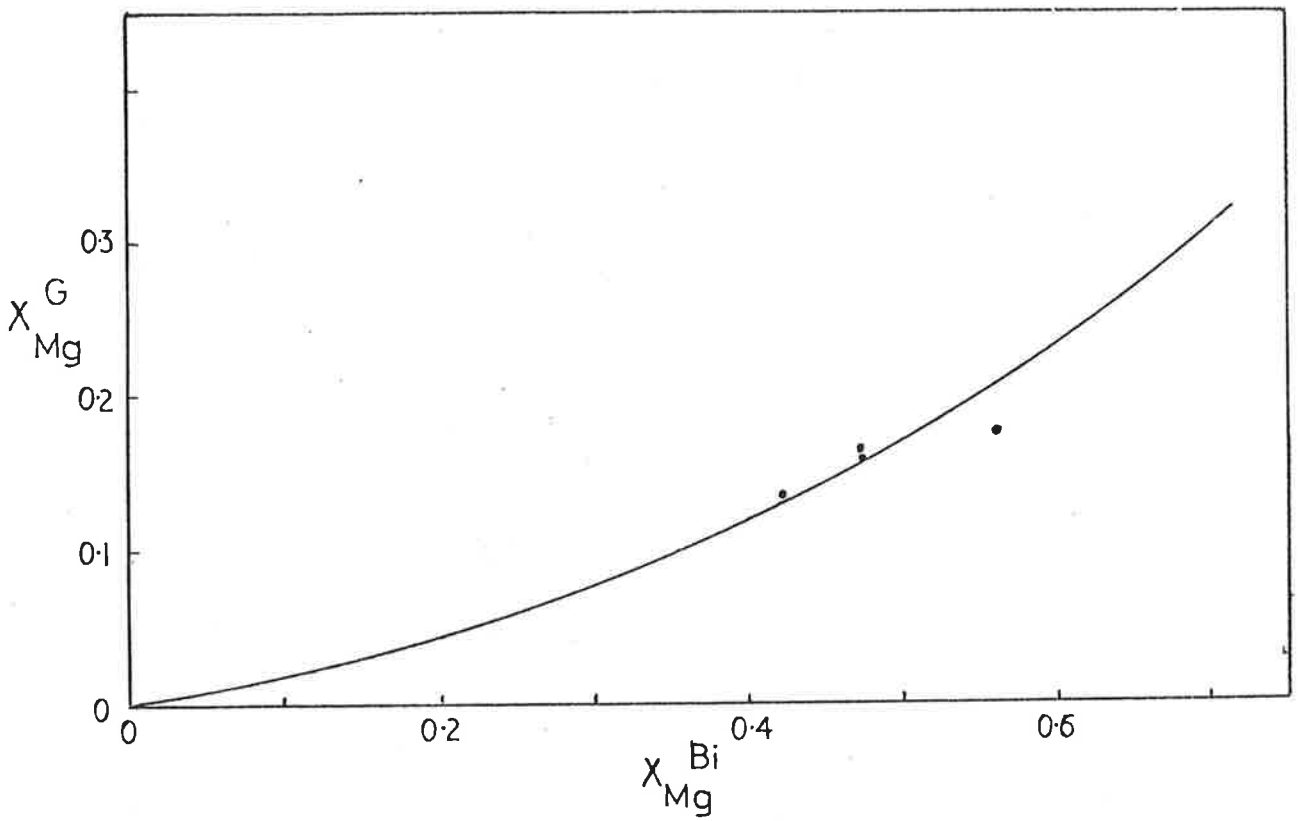

fig.11A

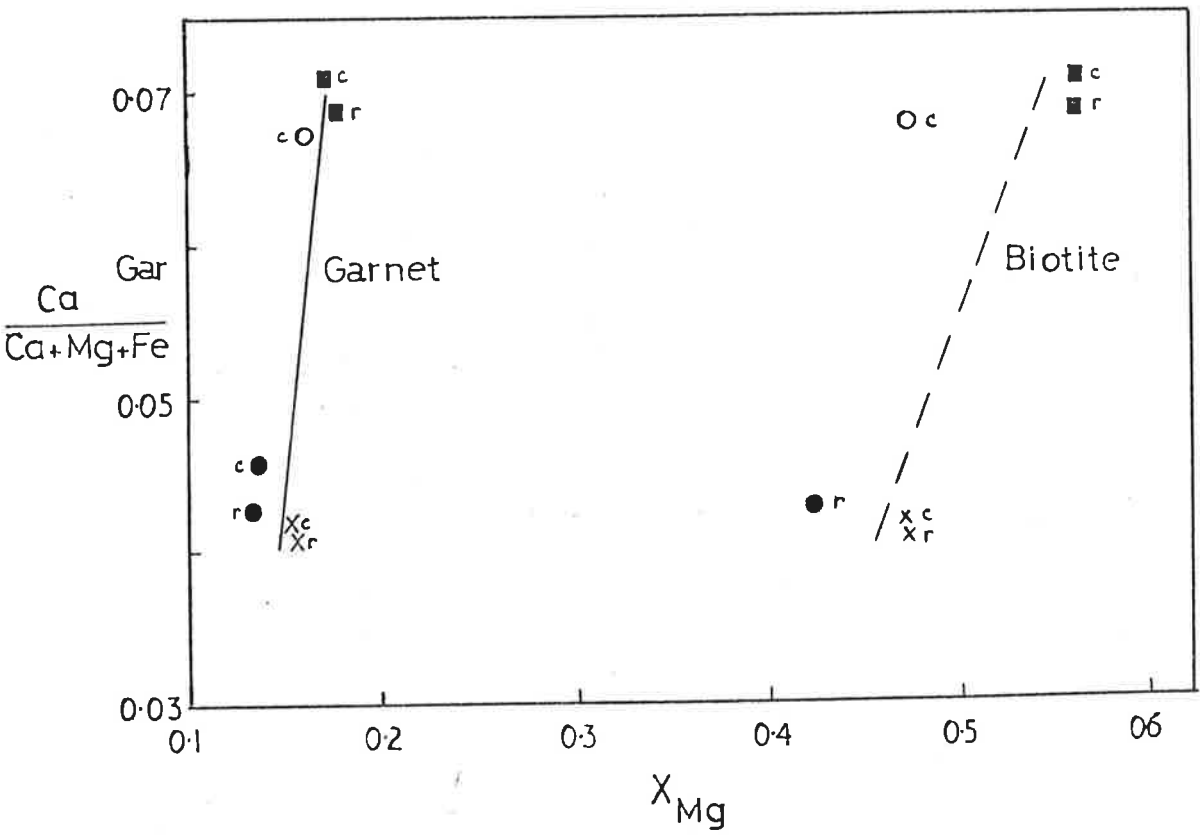

fig.11B

Figure 12A

Relation between Mn content of garnet (expressed as X_{Mn} = Mn/Mn+Mg+Fe_{TOT}) and Mg/Mg+Fe_{TOT} (= X_{Mg}) in garnet and biotite. C = data from garnet core; r = data from rim.

Figure 12B

Plot of $X_{Mg}^{G}/1-X_{Mg}^{G}$ against $X_{Mg}^{Bi}/1-X_{Mg}^{Bi}$

X_{Mg} = Mg/Mg+Fe_{TOT}+Mn. Points scatter about a line of slope = 0.148 (= Av. K_D). For ideal mixtures points should fall on a line with slope = Av. K_D.

A405/E2A = ● ; M24 = ■ ; E4B = o; E4E = x.

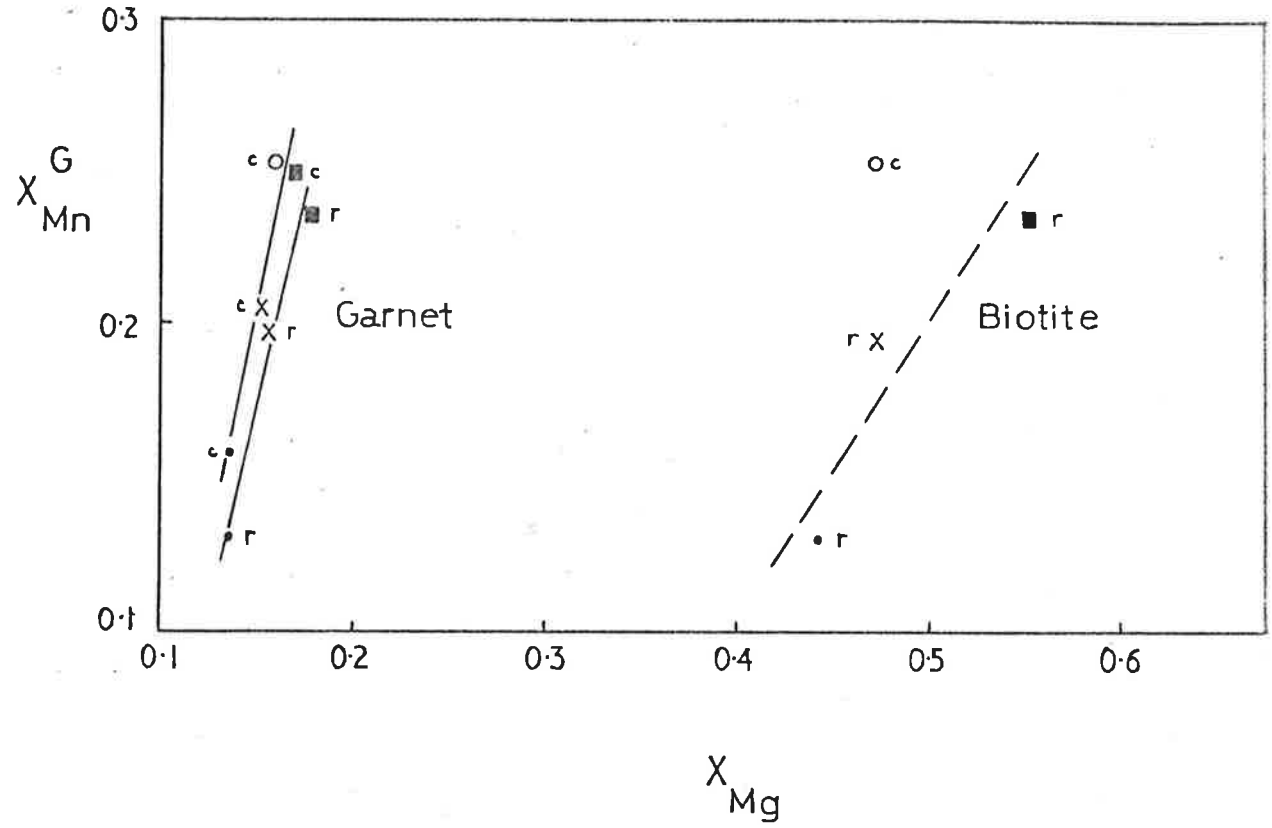

fig.12 A

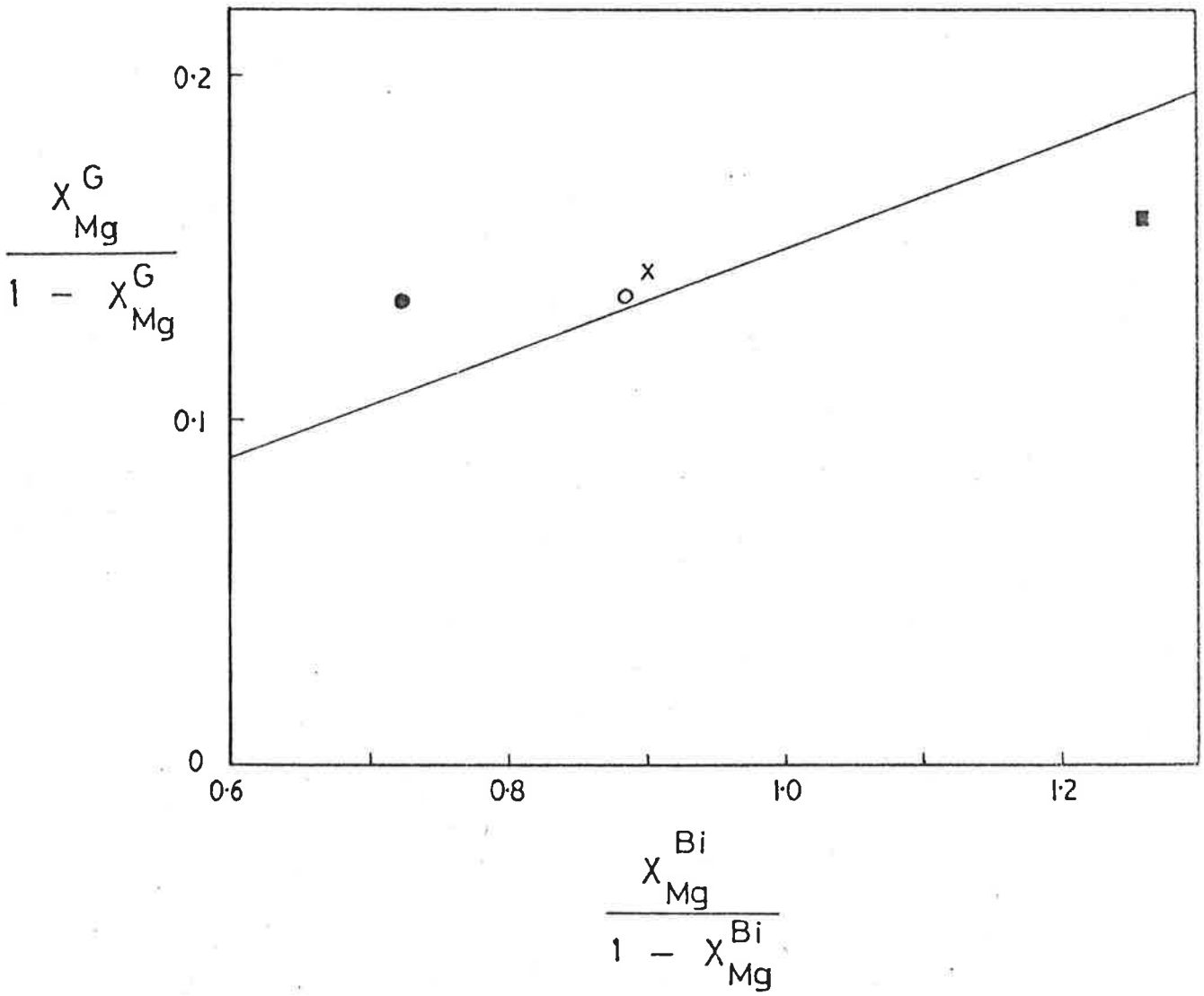

fig.12B

Figure 13.

Isotherms of the distribution of Mg between coexisting garnet and biotite (after Perchuk, 1967).

X_{Mg} = $Mg/Mg+Fe_{TOT}+Mn$. Data from garnet rims only.

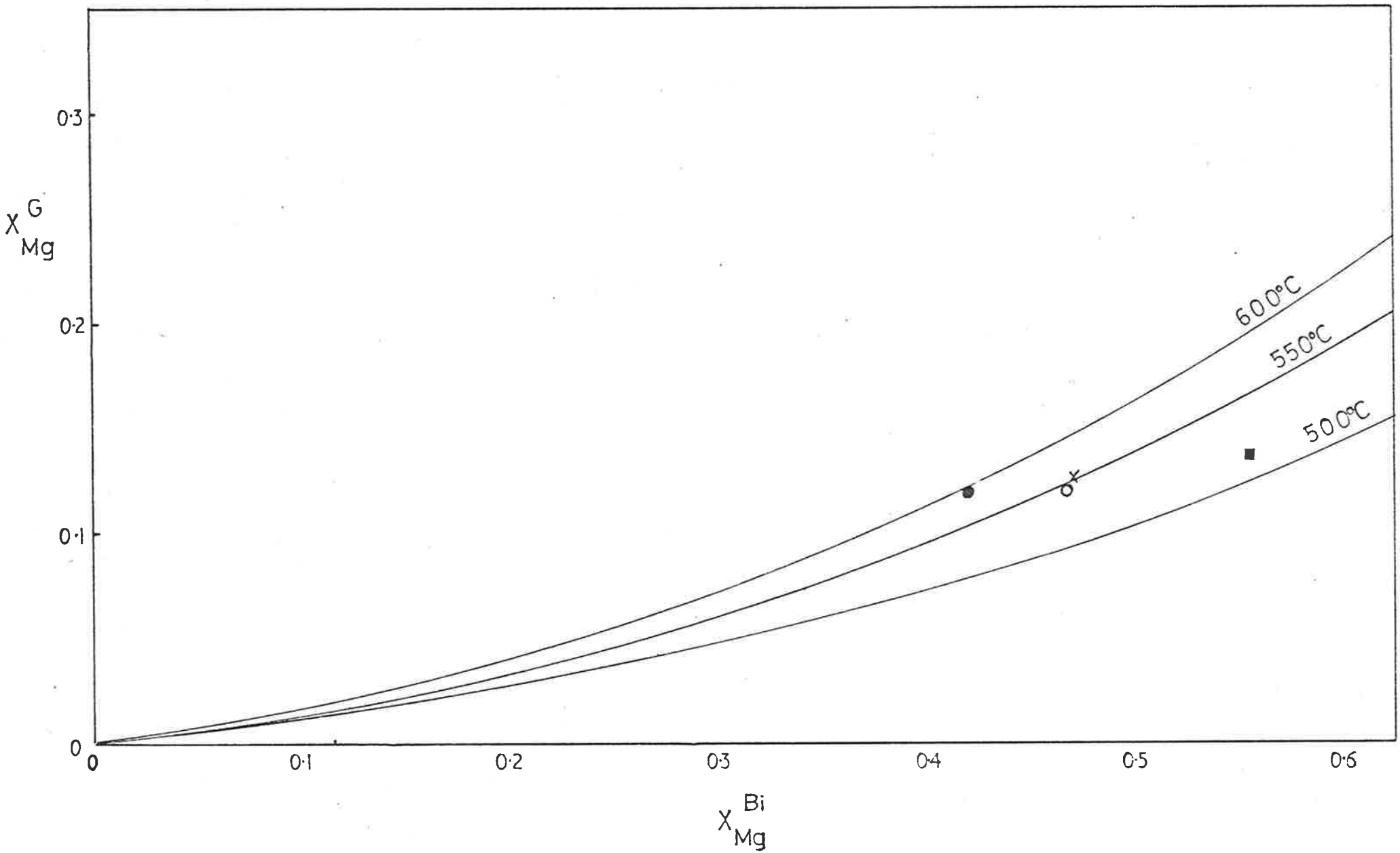

fig.13

Figure 14A

Plot of $X_{Mg}^{St}/1-X_{Mg}^{St}$ against $X_{Mg}^{Bi}/1-X_{Mg}^{Bi}$.

Staurolite-biotite pairs from 3-phase assemblages plot close to a line of slope = Av.K_D (0.262). Mineral pairs from 4-phase assemblages (denoted (4)) do not plot near this line.

Figure 14B

Relation between rock oxidation ratio and rock total Fe(as Fe_2O_3) for rocks in the Nairne-Mt. Barker Creek area (metasediments).

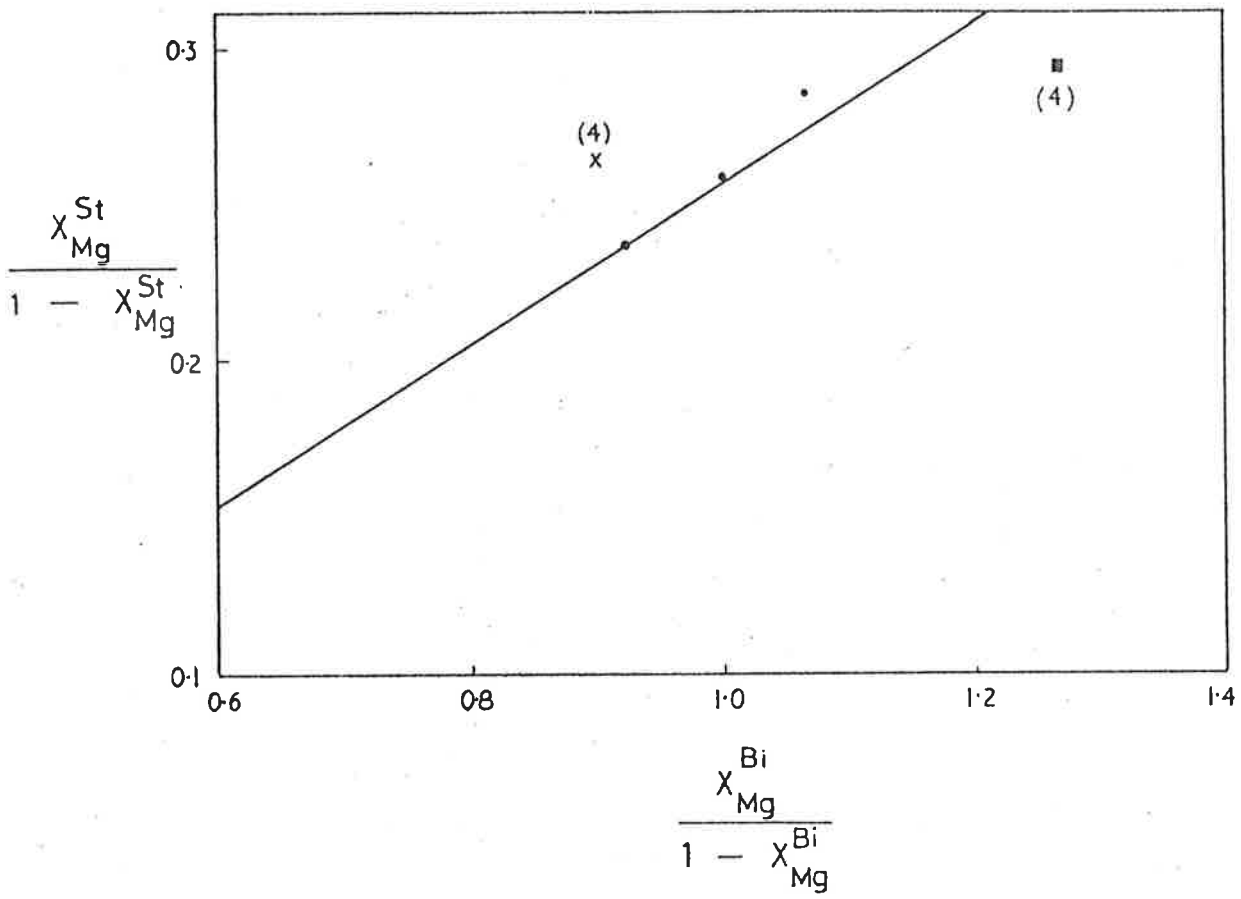

fig.14A

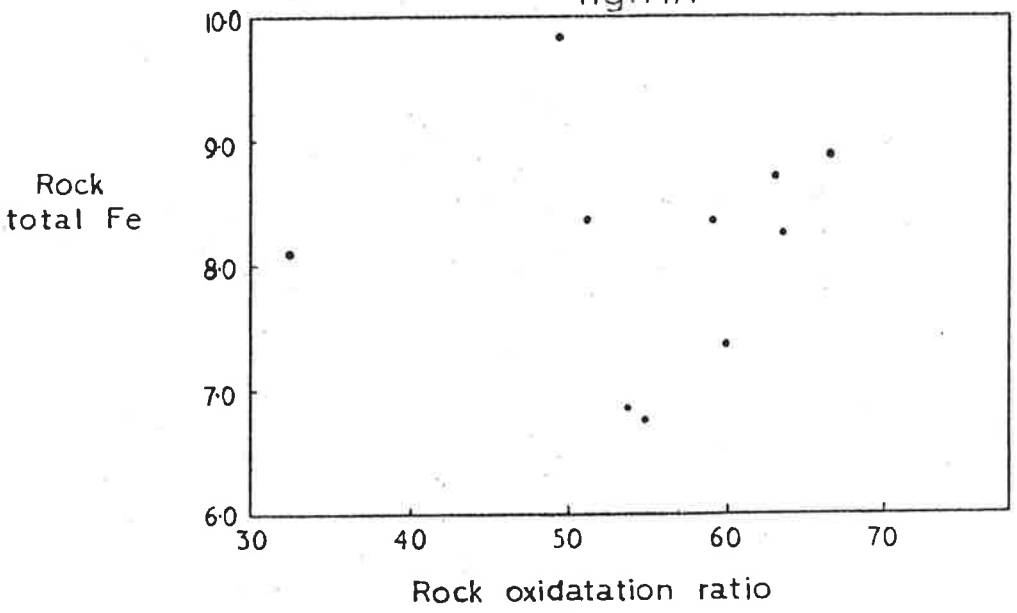

fig.14B

Figure 15.

Relation between rock oxidation ratio and $Mg/Mg+Fe_{TOT}$ of garnet, biotite and staurolite. Also shown is the relation between this ratio and $Mg/Mg+Fe^{2+}$ of three biotites (⊡) in which Fe^{2+} was determined by analysis.

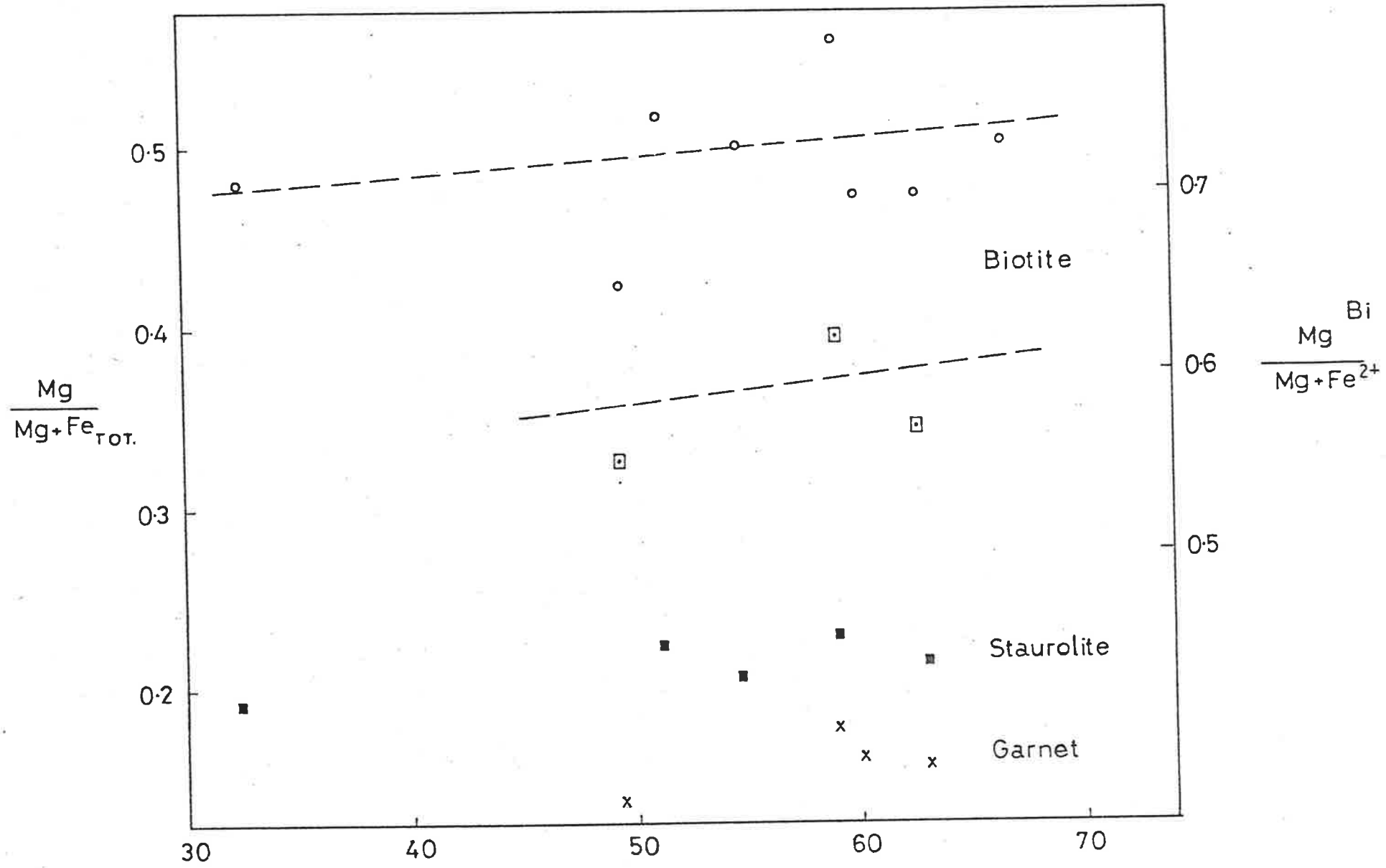
0·5
0·4
0·3
0·2
Mg / Mg+Fe TOT.
0·7
0·6
0·5
Mg Bi / Mg+Fe2+
Biotite
Staurolite
Garnet
30
40
50
60
70
Rock oxidation ratio

fig.15

Figure 16

Relation between rock oxidation ratio and rock $Mg/Mg+Fe^{2+}$ (crosses) and rock $Mg/Mg+Fe_{TOT}$ (circles).

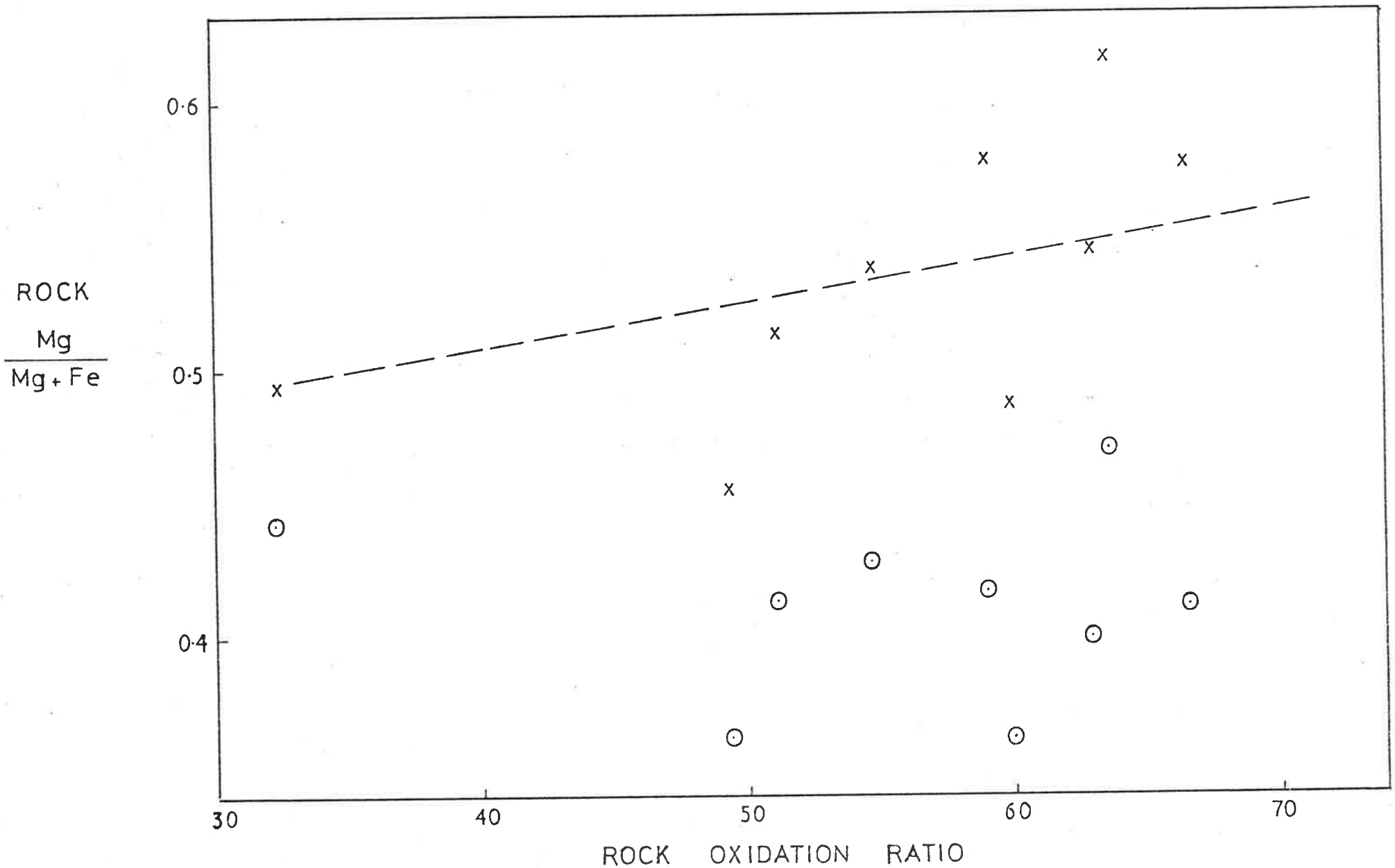

fig.16

Figure 17A

Relation between rock oxidation ratio and rock total Fe (as wt.% Fe_2O_3) for rocks from the Marino Group stratotype.

Figure 17B

Relation between rock oxidation ratio and rock MnO (as wt.%) for the metasediments of the Nairne-Mt. Barker Creek area.

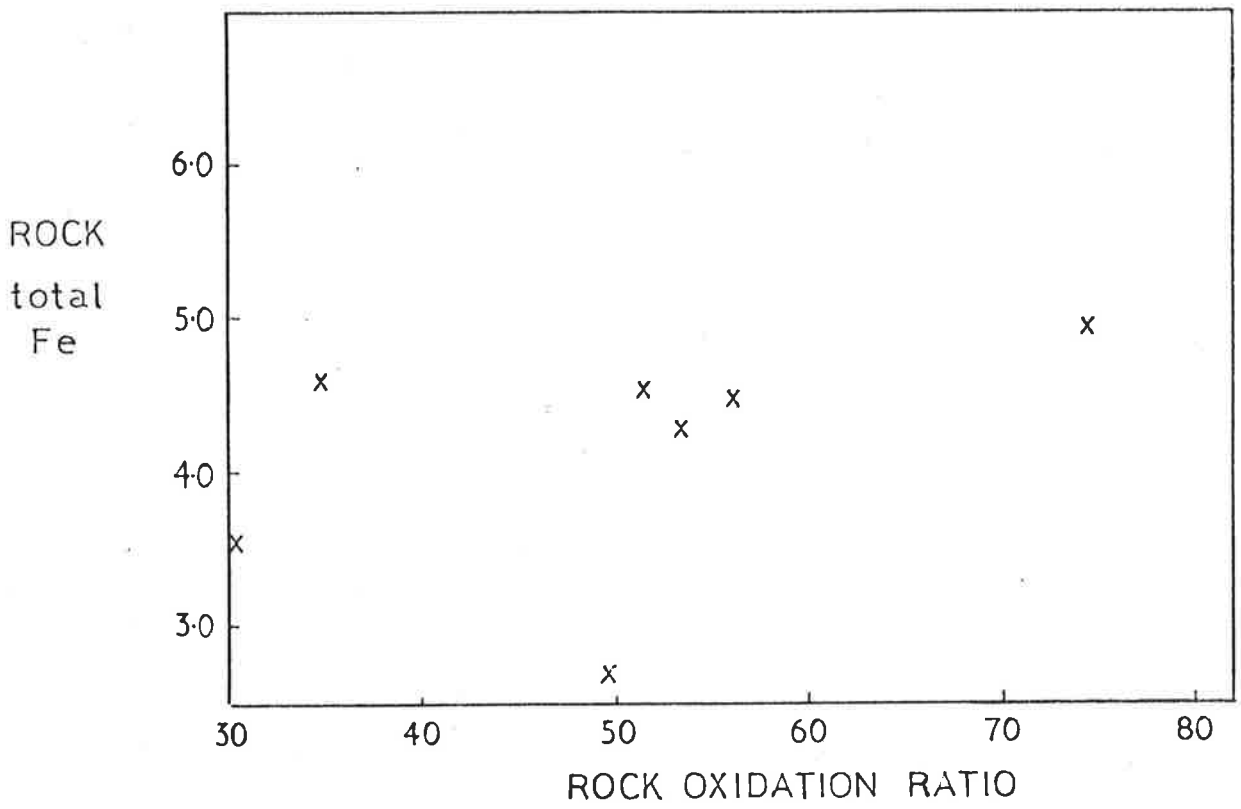

fig.17A

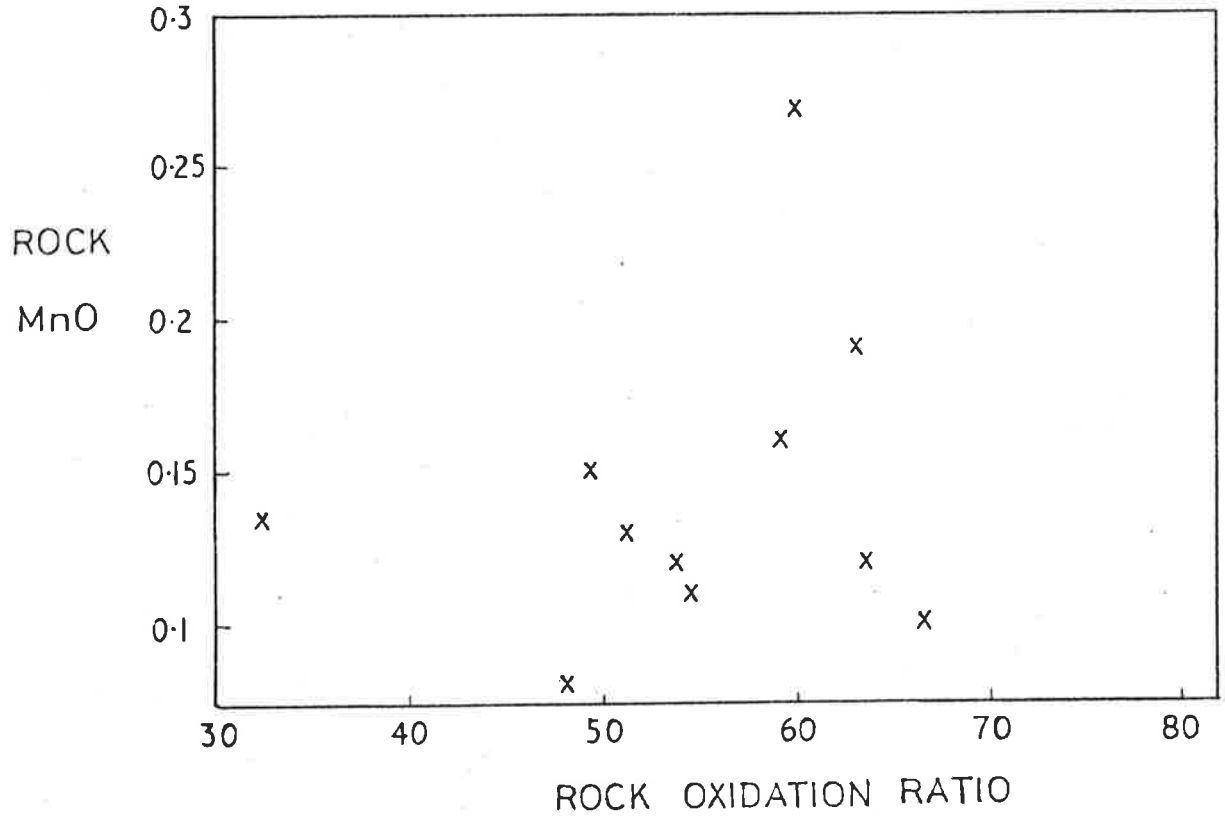

fig.17B

Figure 18A

Relation between rock oxidation ratio and rock MnO (wt.%) for rocks from the Marino Group stratotype.

Figure 18B

Relation between rock oxidation ratio and biotite oxidation ratio (rocks A405/E4E, E4B, M24).

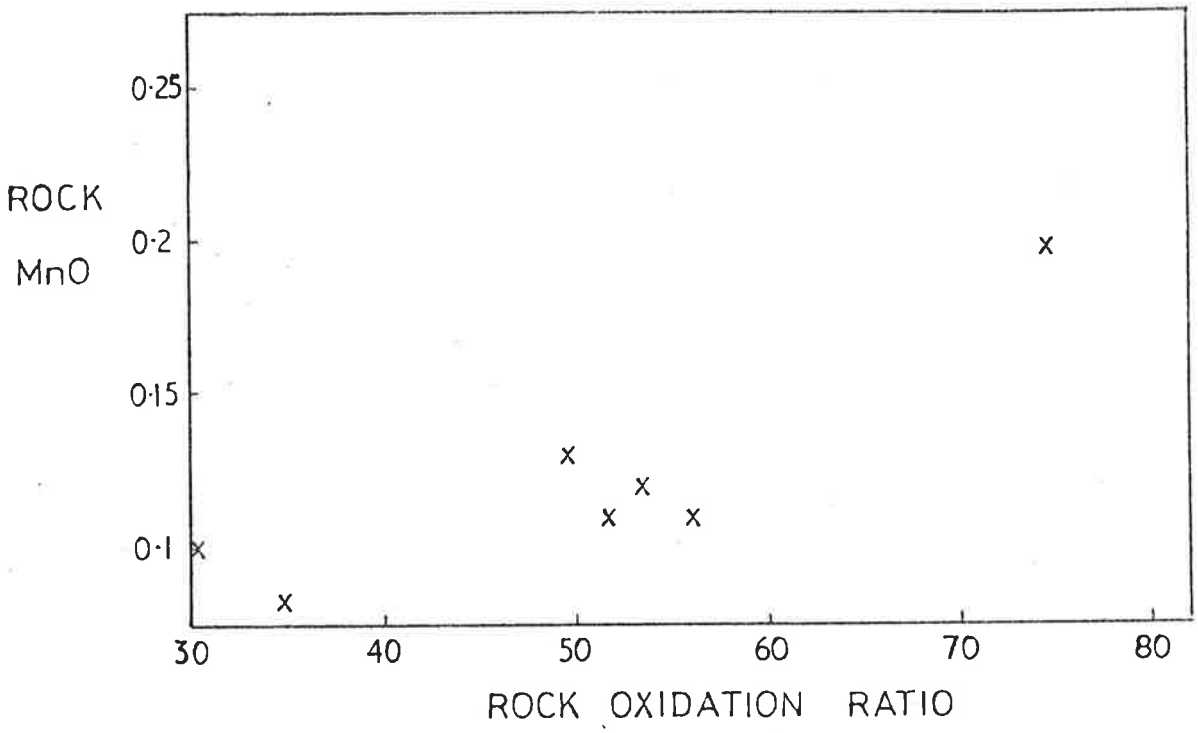

fig.18 A

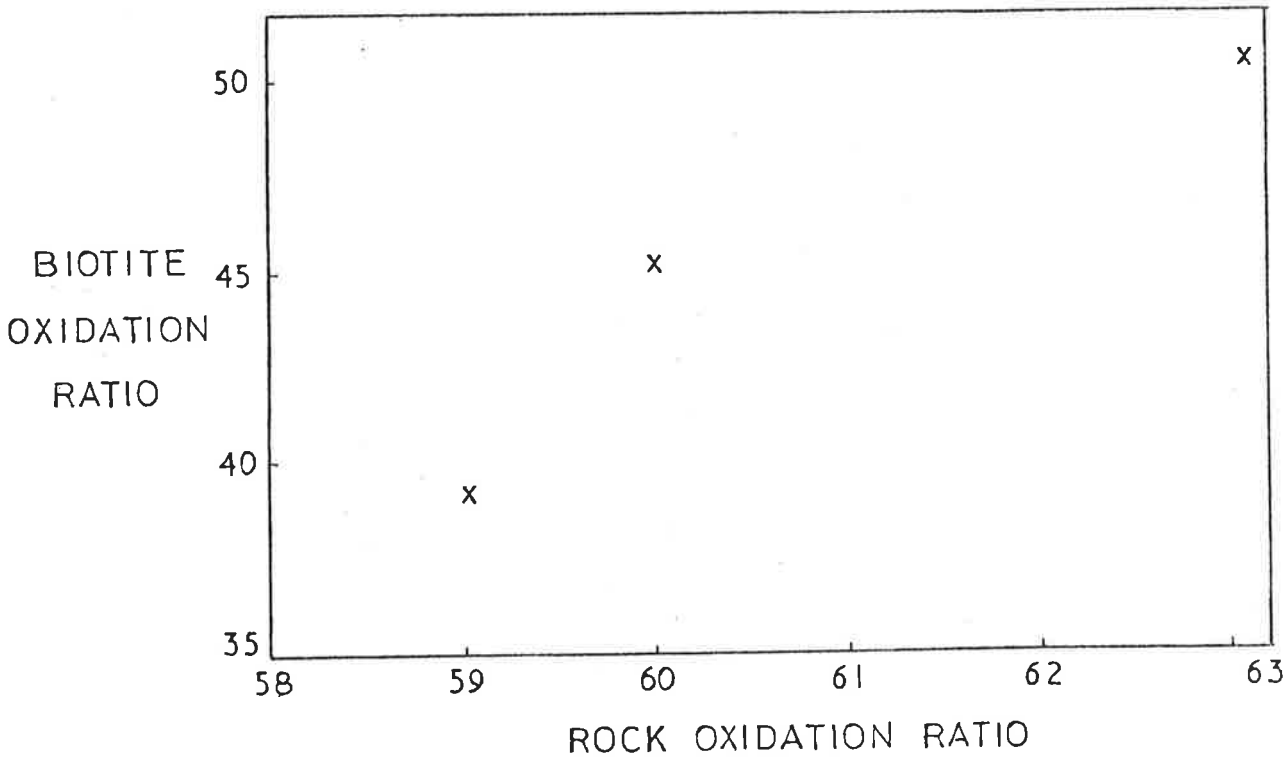

fig.18B

Figure 19A

Relation between Mn content of garnet (as atomic Mn/Mn+Fe) and rock oxidation ratio. 'C' = garnet core; 'r' = garnet rim.

Figure 19B

Relation between garnet Mn content (as ionic Mn) and rock MnO (wt.%). 'C' = garnet core; 'r' = garnet rim.

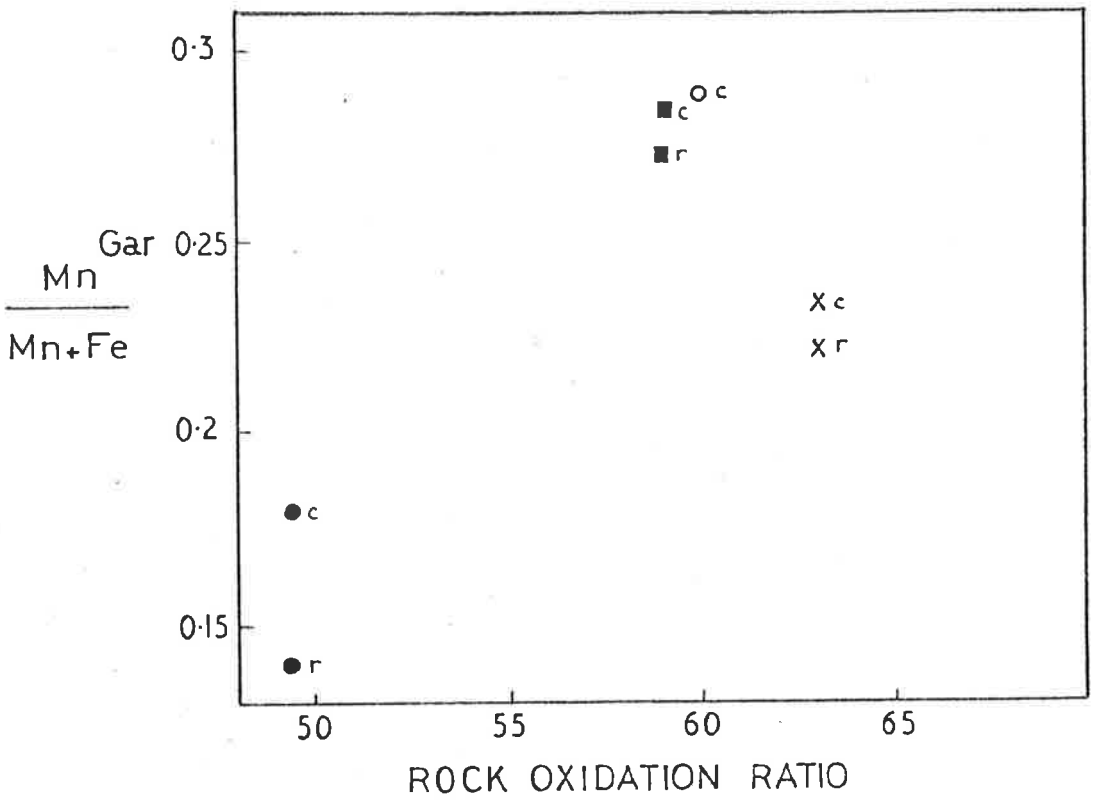

fig.19A

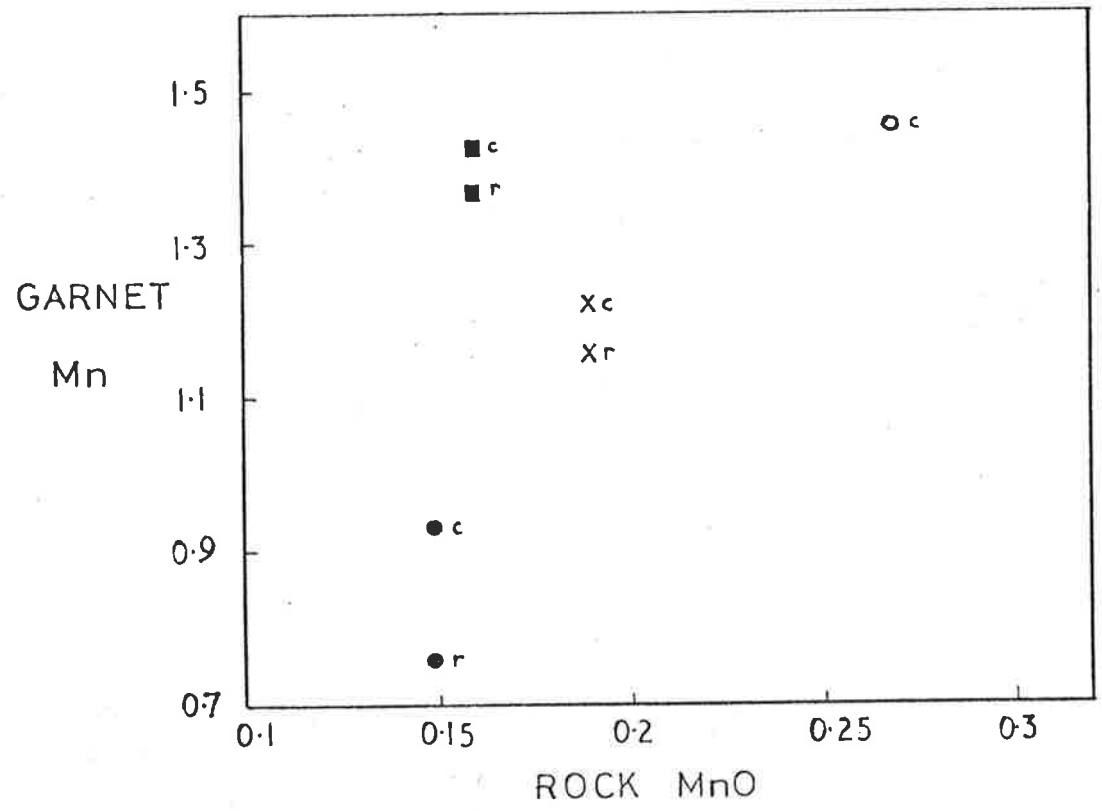

fig.19B

Figure 20A

Relation between biotite Mn content (as ionic Mn x 100) and rock MnO (wt.%).

⊗ garnet-bearing assemblages; * garnet in only trace amounts.

Figure 20B

Relation between the composition of calciferous amphiboles and metamorphic grade (after Harry, 1950, Fig. 1).

⊗ Hornblende from metadolerite;

x Hornblende from calc-silicate;

⊠ Hornblende from hornblende-rich quartzite.

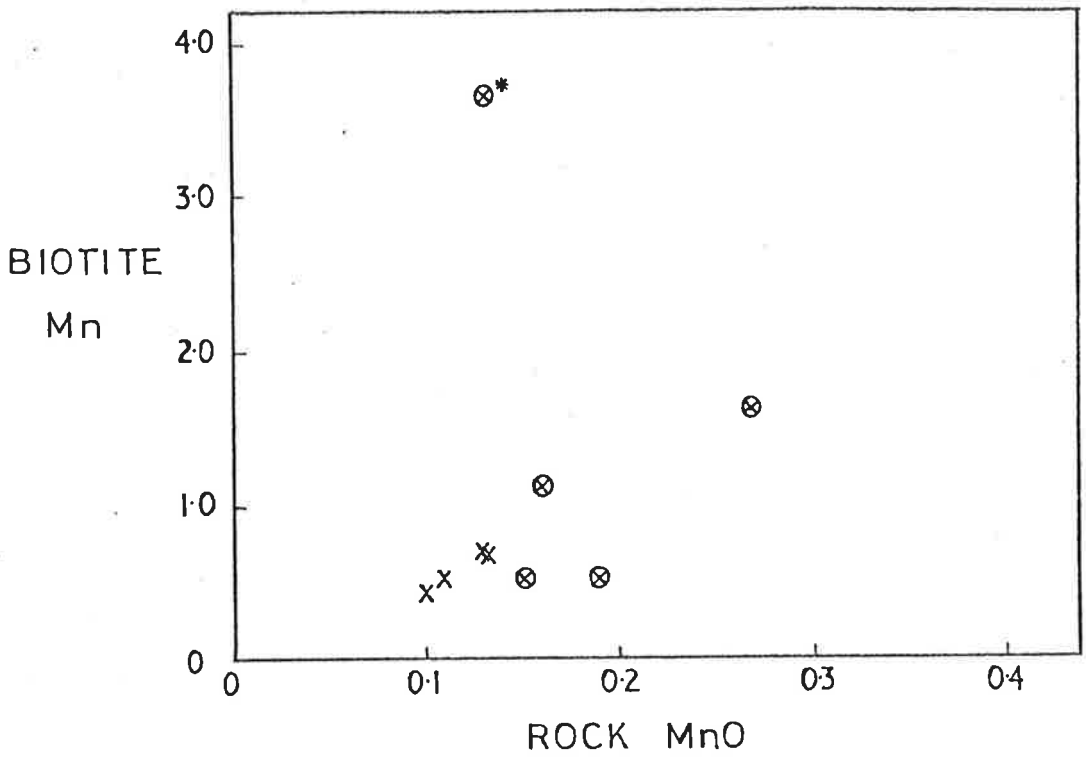

fig. 20A

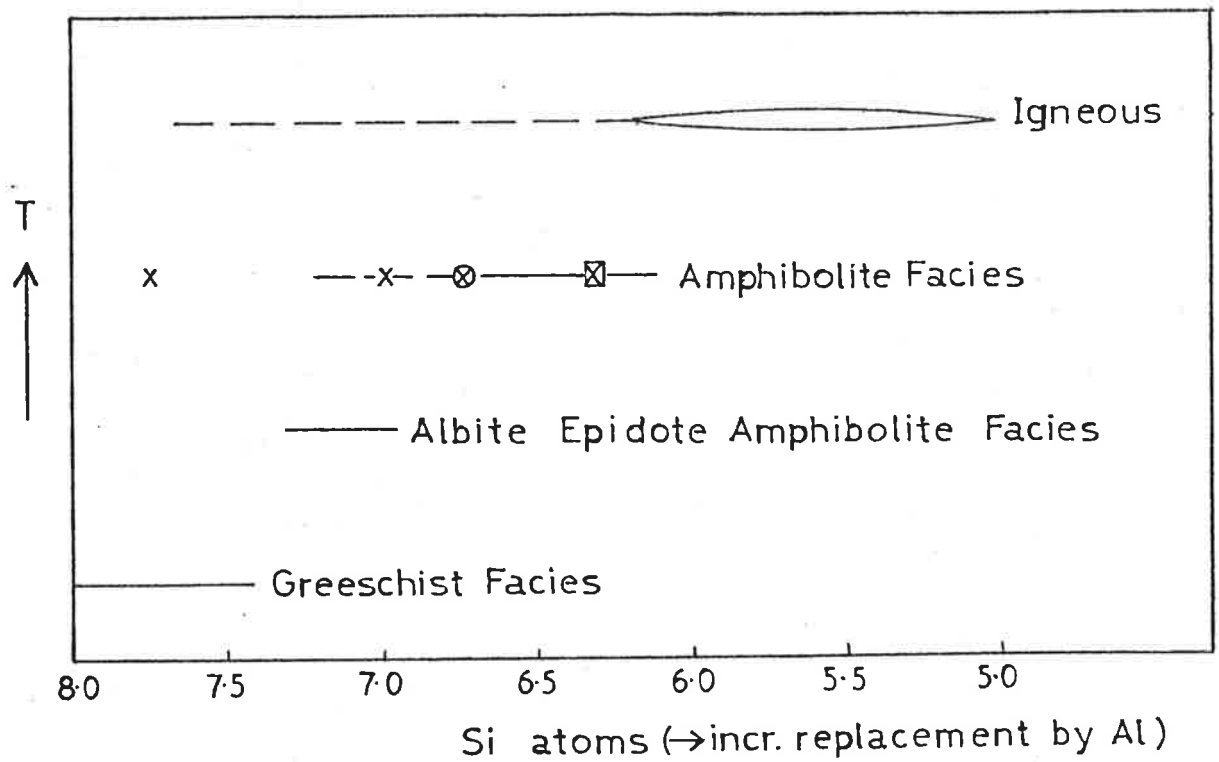

fig. 20B

Figure 21

Distribution diagram for Mg partitioned between garnet and biotite (in rocks A405/E4E,E4B,M24). The average distribution coefficient $K_{D_{Mg}}^{G\text{-}Bi}$ (= 0.147) is plotted.

X_{Mg} = $Mg/Mg+Fe^{2+}$. K_D determined for garnet rims only.

A405/E4E = x; E4B = 0; M24 = ■

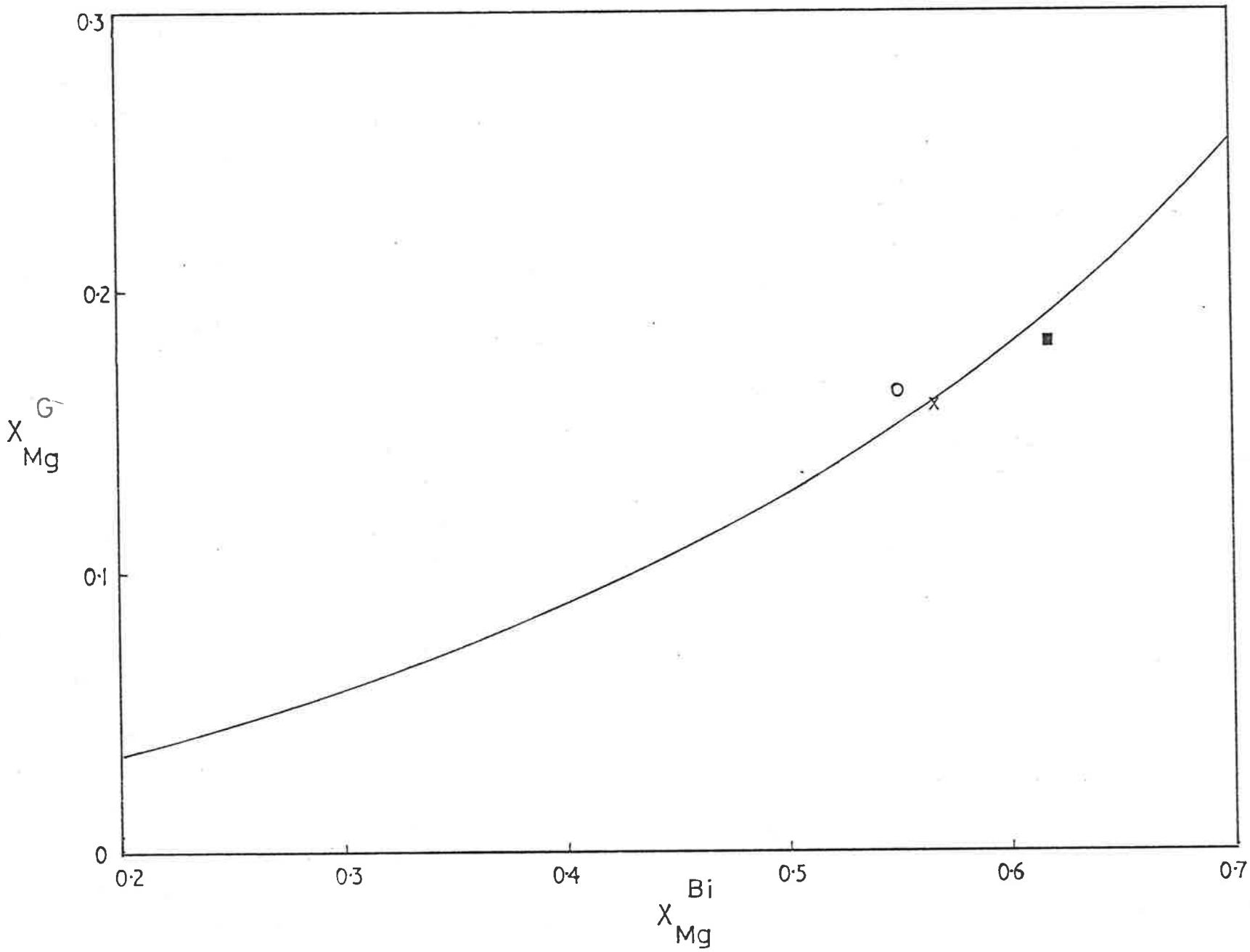

fig. 21

Figure 22

Variations in Al_2O_3(wt.%) and total $FeO+Fe_2O_3$(wt.%) contents of muscovites. Fields outlined are for:

muscovites from : A-Blueschist Facies;

B-Chlorite and Biotite Zones;

C-Almandine Zone;

D-Staurolite and higher zones

(After Butler, 1967, Fig. 4).

For Nairne-Mount Barker Creek muscovites:

x = coarse muscovite plates;

⊗ = matrix muscovite.

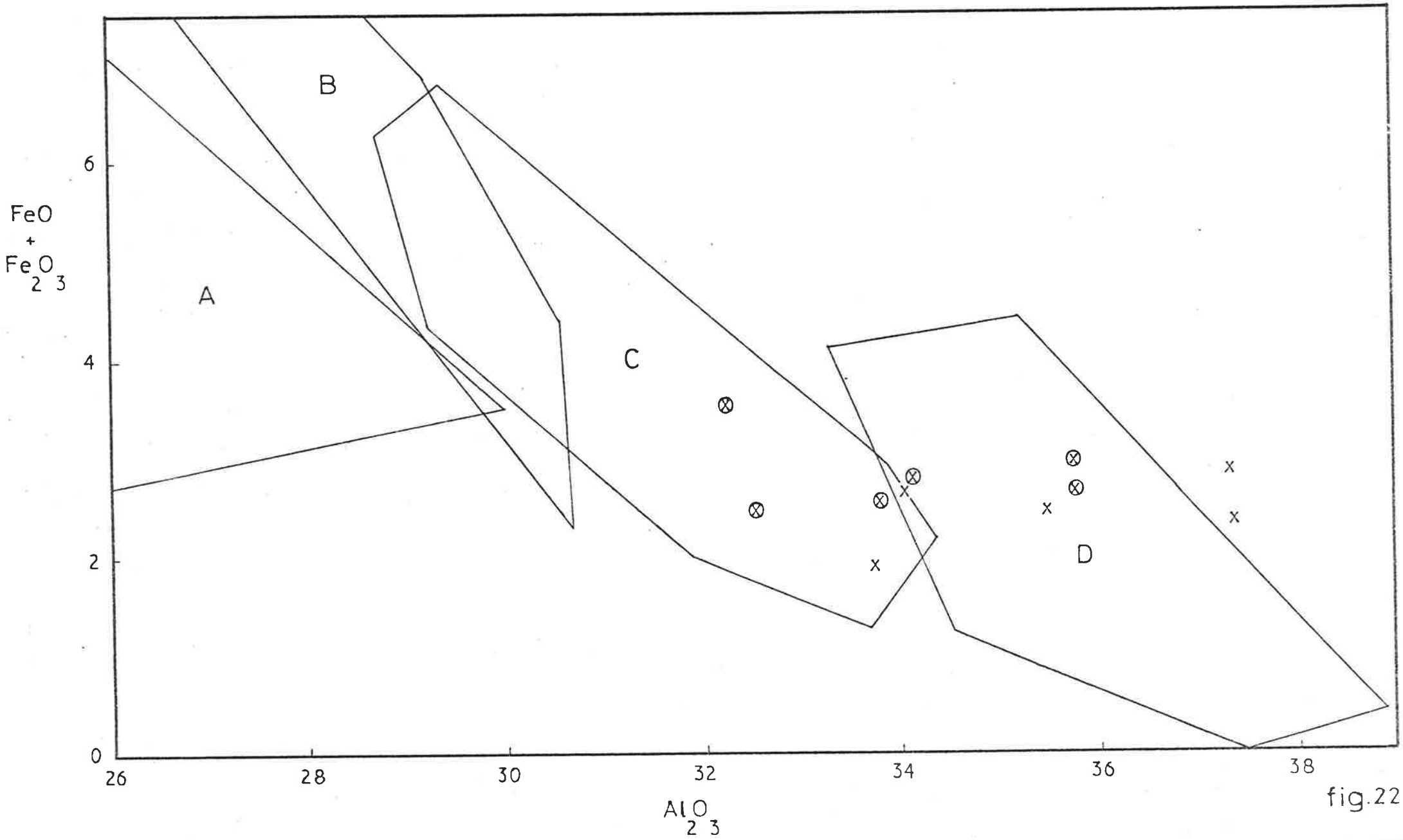

fig.22

Figure 23A

Effect of garnet Mn (as $Mn/Mn+Mg+Fe_{TOT}$) on $K_{D_{Mg}}^{G\text{-}Bi}$

⊗ K_D calculated using Fe^{2+} only

x K_D using Fe_{TOT}

Rock A405/E4E = x; E4B = o; M24 = ■ ; E2A = ●

Figure 23B

Distribution diagram for Mn partitioned between garnet and biotite (rocks A405/M24, E2A,E4B,E4E).

The average distribution coefficient $K_{D_{Mn}}^{G\text{-}Bi}$ (= 81.93) is plotted.

$X_{Mn} = {}^{Mn}/_{Mn+Fe_{TOT}+Mg}$

⊗ Data from garnet core; x data from garnet rim.

Rock A405/E4E = x; E4B = o; M24 = ■ ; E2A = ●

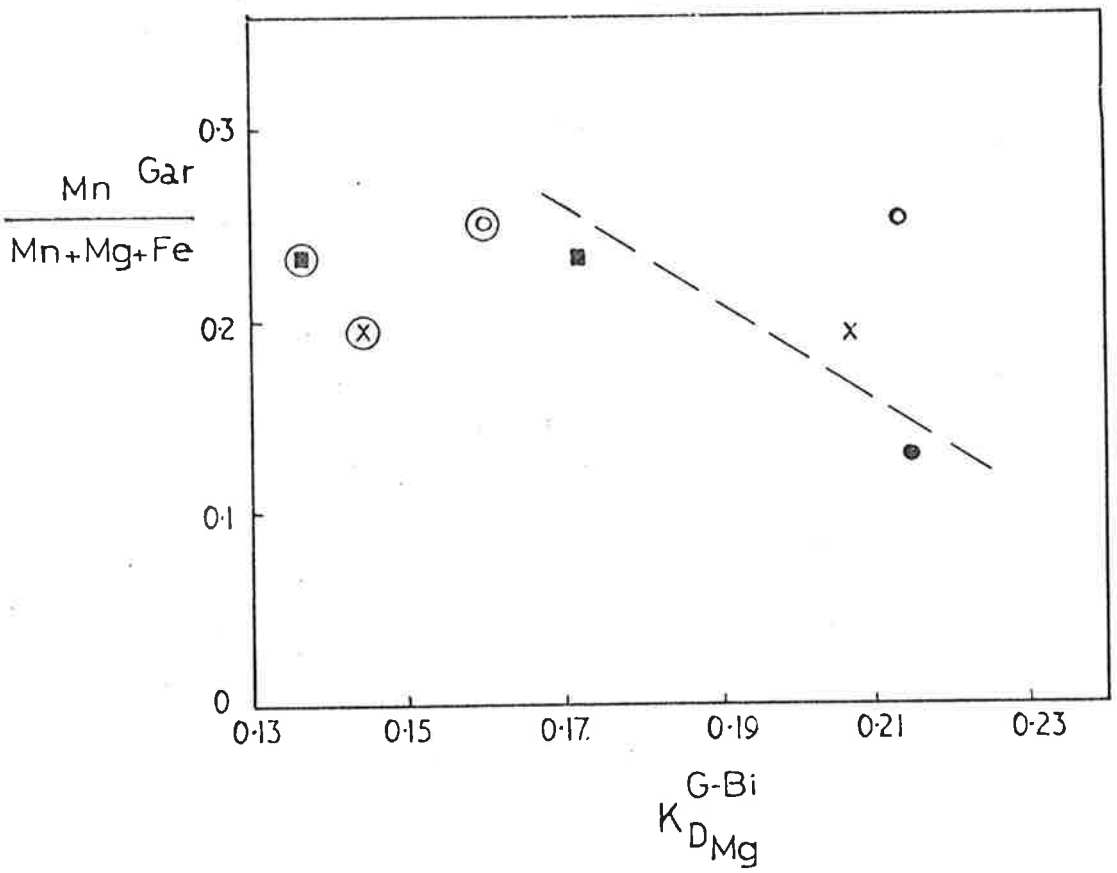

fig. 23A

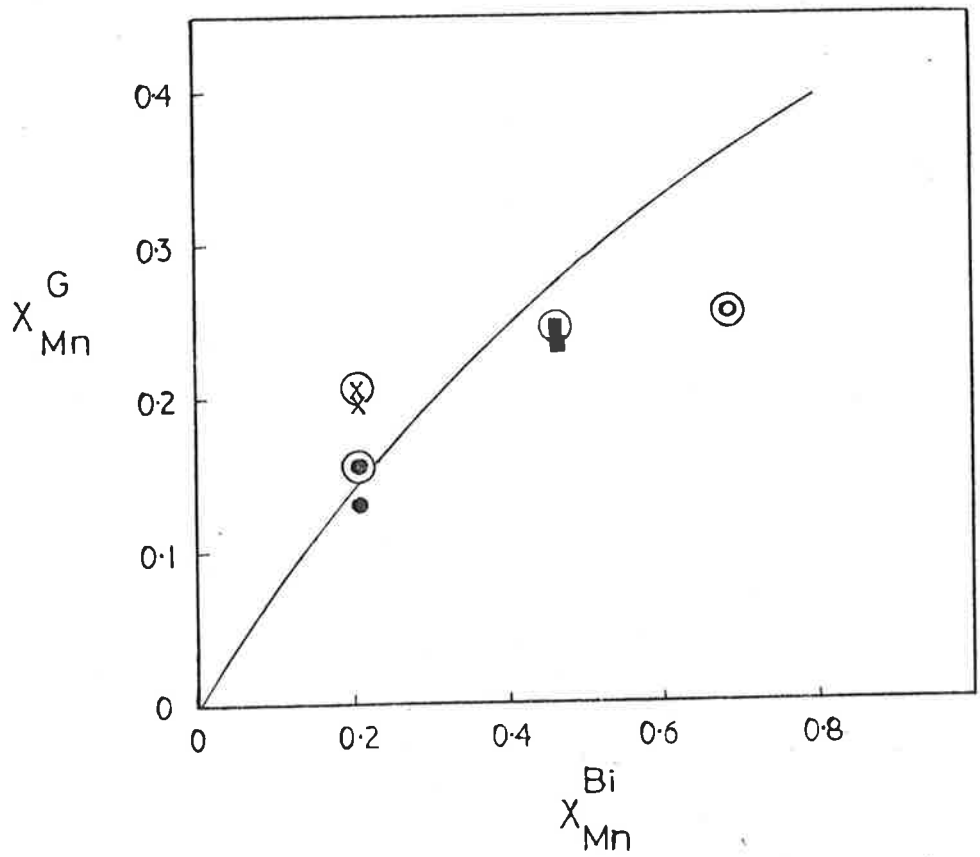

fig. 23B

Figure 24A

Distribution diagram for Mg partitioned between garnet and biotite. The average distribution coefficient $K_{D_{Mg}}^{G\text{-}Bi}$ (= 0.148) is plotted.

$$X_{Mg}^{Bi} = Mg/Mg+Fe_{TOT}+Mn; \quad X_{Mg}^{G} = Mg/Mg+Fe_{TOT}+Mn+Ca$$

Rock A405/E4E = x; E4B = o; M24 = ■ ; E2A = ● ; c = data from garnet core.

Figure 24B

Distribution diagram for Mg partitioned between staurolite and biotite. The average distribution coefficient

$K_{D_{Mg}}^{St\text{-}Bi}$ (= 0.262) is plotted.

$X_{Mg} = Mg/Mg+Fe_{TOT}$

⊗ = staurolite-biotite pairs from 3-phase assemblages.

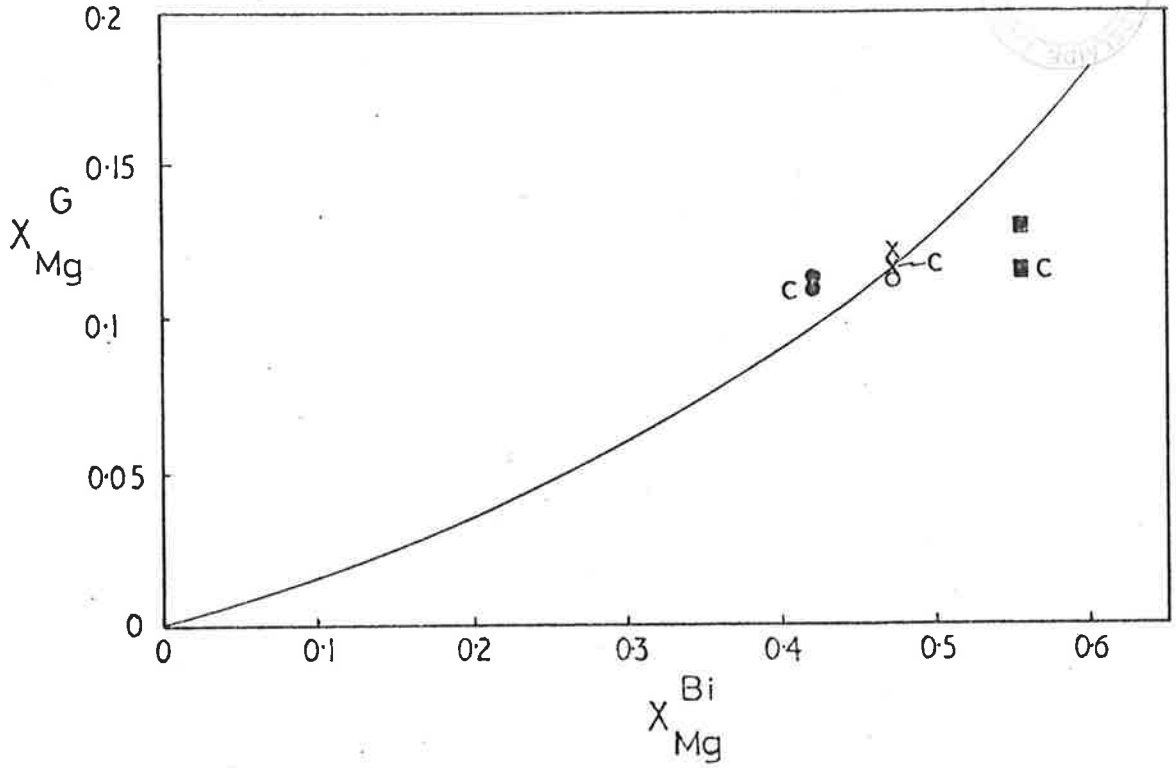

fig. 24A

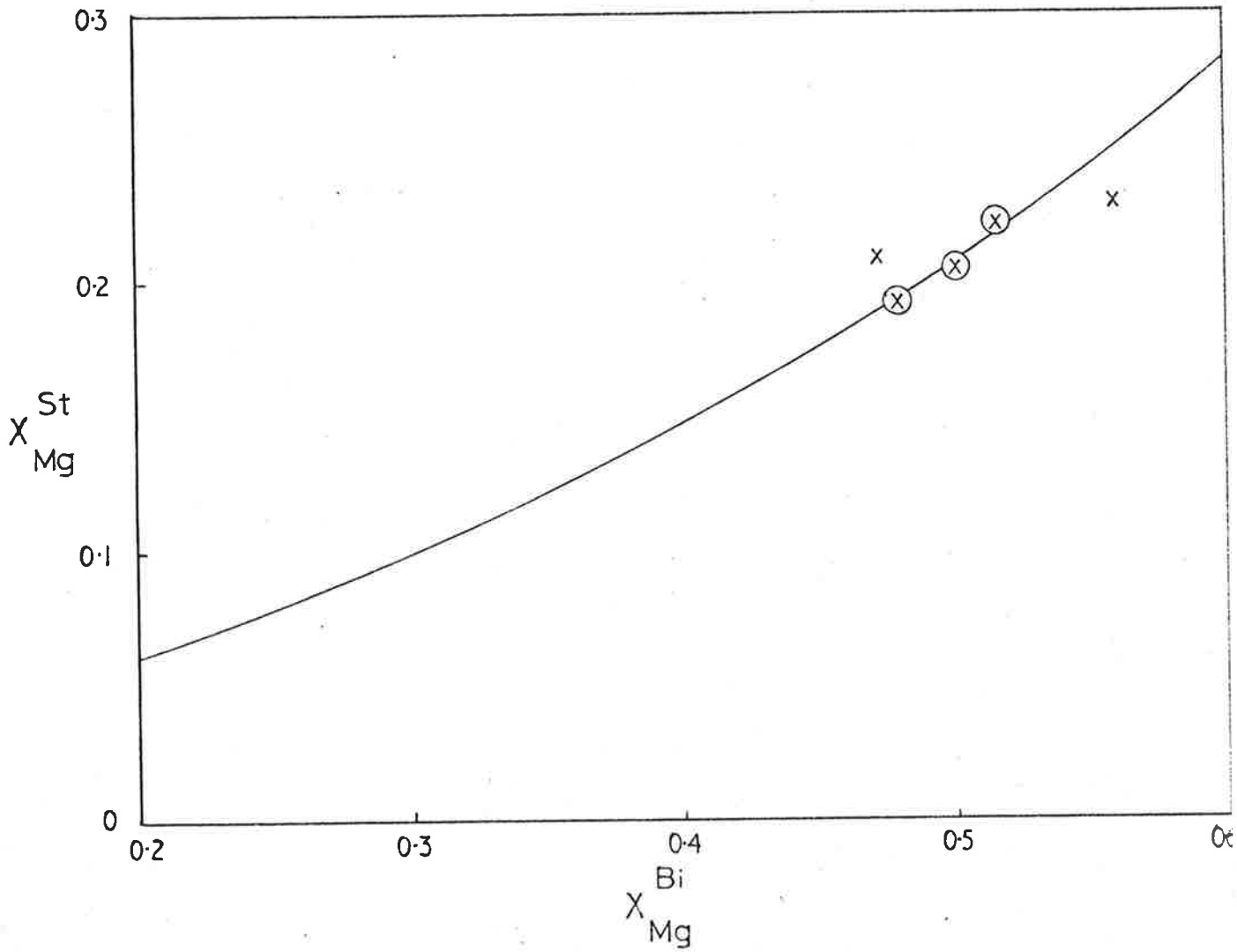

fig. 24B

Figure 25A

Relation between rock Mg/Mg+Fe and biotite Mg/Mg+Fe using Fe_{TOT} and Fe^{2+}

x using Fe_{TOT}; ⓧ biotites from 4-phase assemblages;

☒ using Fe^{2+}.

Figure 25B

Relation between rock $Mg/Mg+Fe_{TOT}$ and $Mg/Mg+Fe_{TOT}$ in garnet and staurolite.

⊙ = X_{Mg} in garnet; X = X_{Mg} in staurolite.

Rock A405/E4B - asterisk.

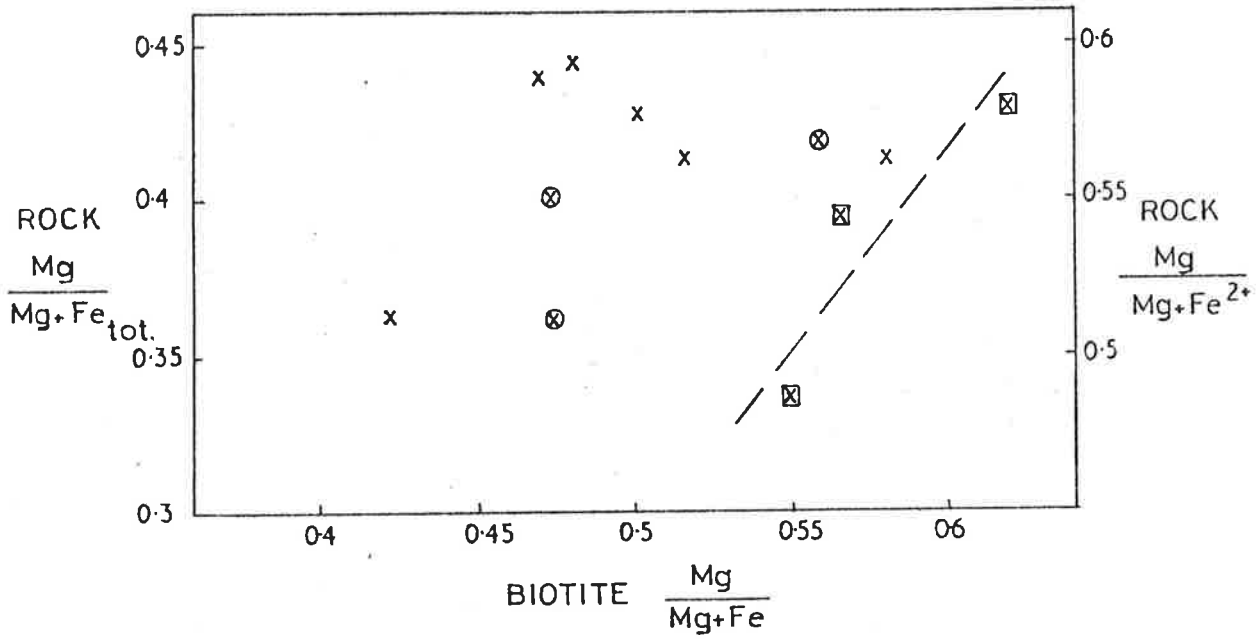

fig. 25A

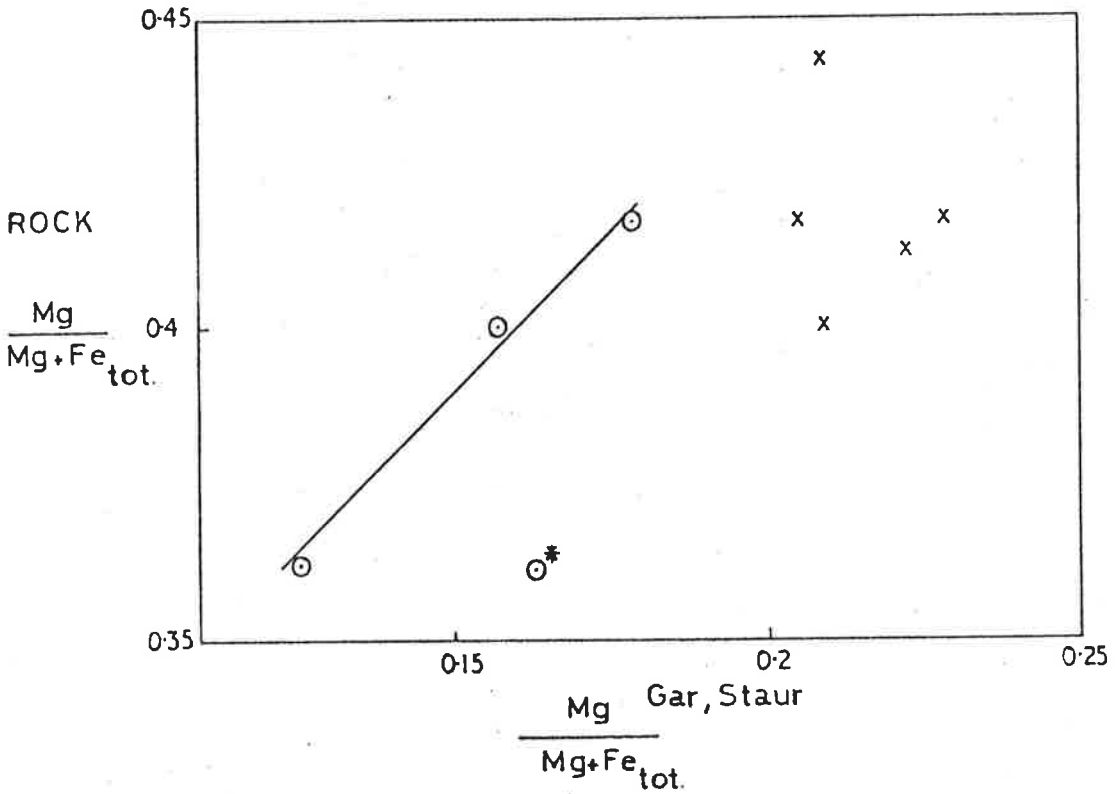

fig. 25B

Figure 26

$Mg/Mg+Fe_{TOT}$ trends in coexisting minerals. This ratio increases in the order almandine garnet → staurolite → muscovite → biotite.

garnet = ⊙ ; staurolite = x; biotite = ■ ; matrix muscovite = ▲ ; coarse muscovite porphyroblasts = △

1 = Rock A405/BC37a; 2 = BC34a; 3 = M24; 4 = BC38; 5 = E4E; 6 = M21'; 7 = E2A; 8 = E4B.

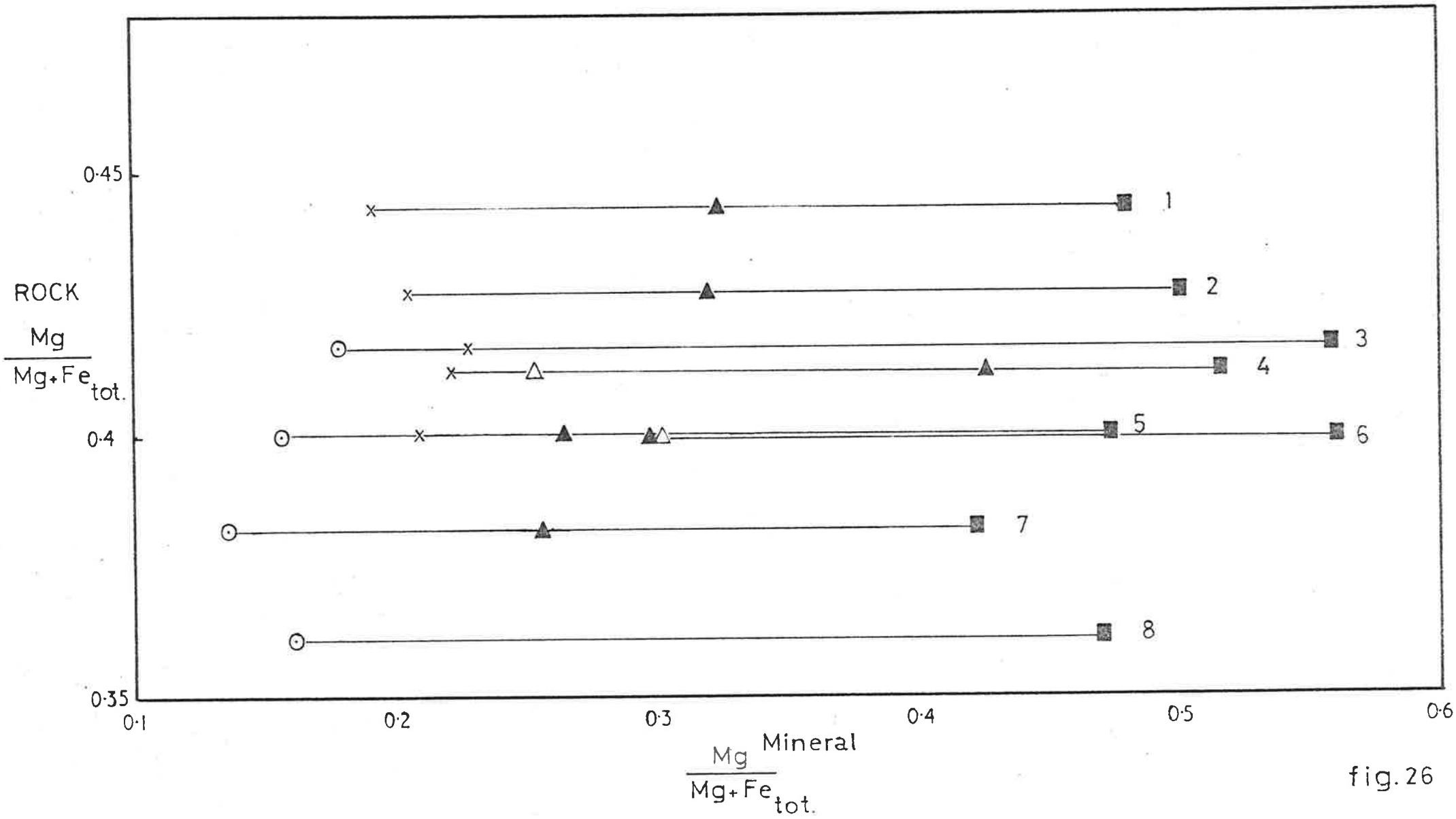
0·45
0·4
0·35
ROCK
Mg / Mg+Fe tot.
0·1
0·2
0·3
0·4
0·5
0·6
Mg / Mg+Fe tot. Mineral
1
2
3
4
5
6
7
8

fig. 26

Figure 27

Relation between $K_{D_{Mg}}^{G\text{-}Bi}$ and garnet Ca content

(as Ca/Ca + Fe + Mg + Mn)

Rock A405/E4E = x; E4B = o; M24 = ■ ; E2A = ●

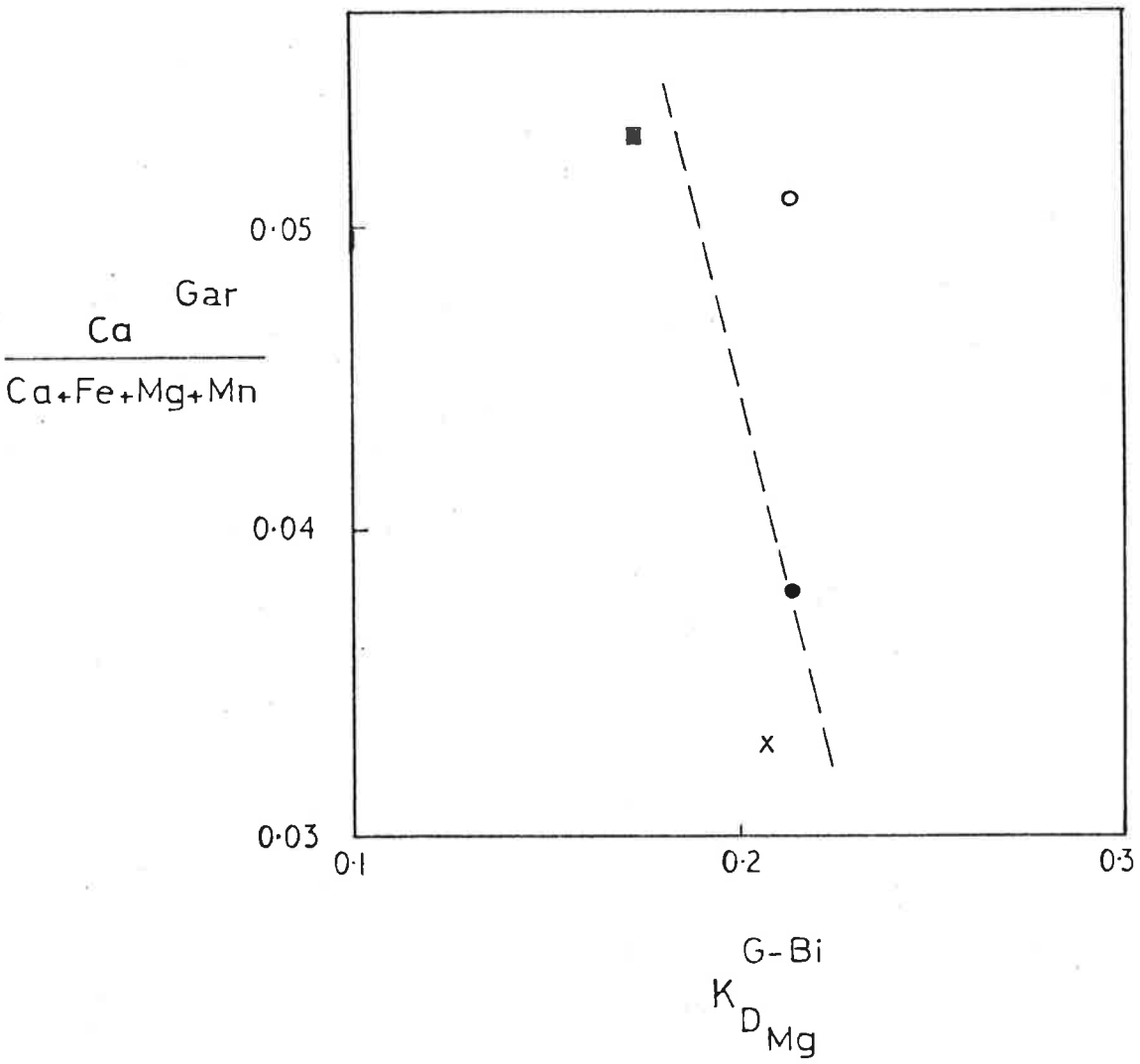

fig. 27

Figure 28

Plot of transformed K_D against assumed temperature of formation of rocks (after Saxena, 1969).

Rock	Transformed K_D	T(^{o}C)
A. High Amphibolite	-0.1954	500
B. Epidote-Amphibolite and Staurolite Zone	-0.4800	400

(Saxena, 1969, p.266)

For Nairne-Barker Creek rocks; solid lines - K_D (transformed) computed using Fe_{TOT}; broken lines - K_D (transformed) computed with Fe^{2+}

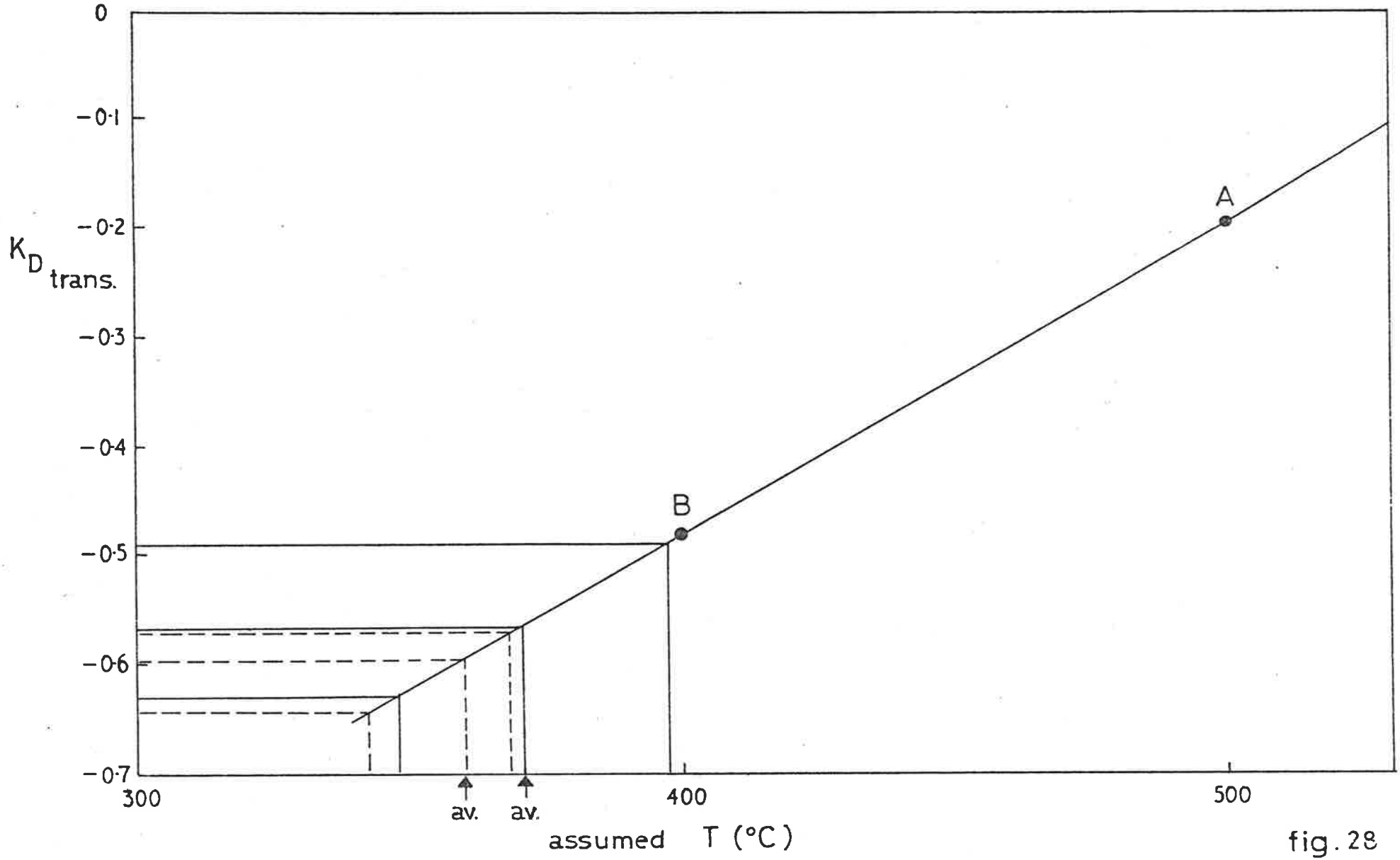

fig. 28

Figure 29A.

Relation between Ca atomic ratio in garnet and Mn/Mn+Mg+Fe in garnet and biotite.

Garnet = ● ; Biotite = x.

Figure 29B.

Relation between Ca atomic ratio in garnet and $K_{D_{Mn}}^{G\text{-}Bi}$. A405/E4E = x; E2A = ● ; E4B = 0; M24 = ■ .

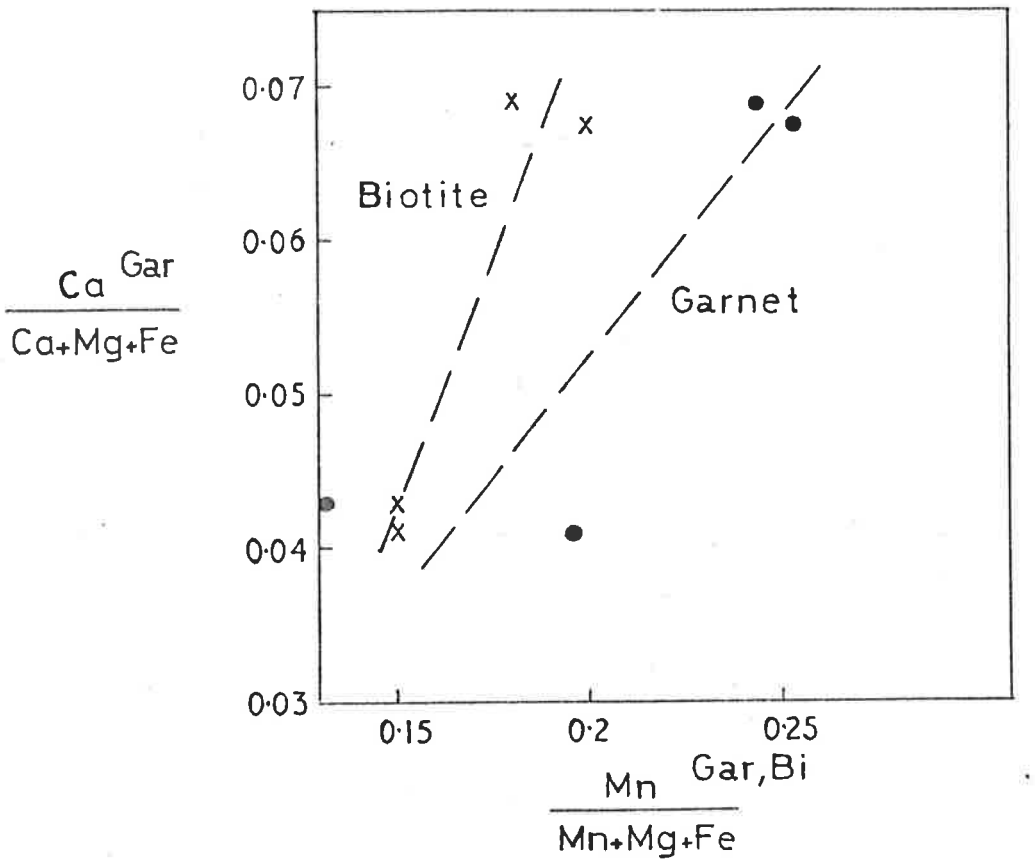

fig. 29A

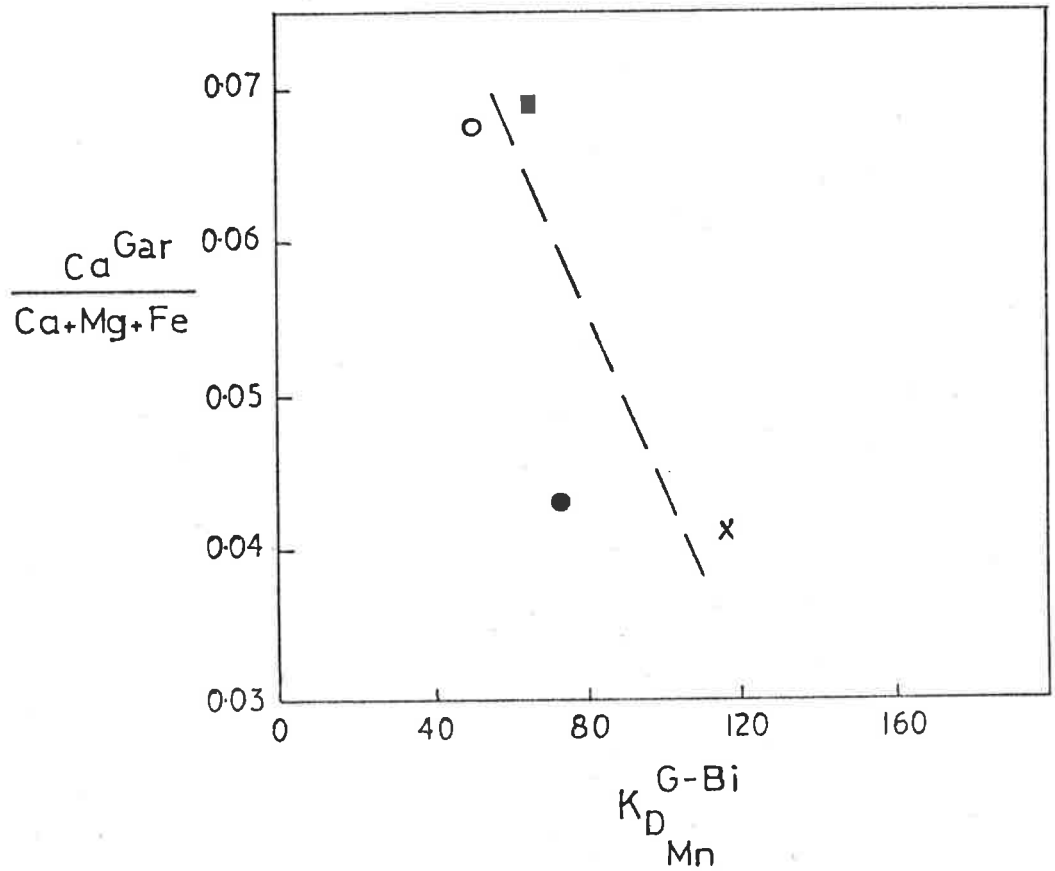

fig. 29B

Figure 30

AFM diagram showing most assemblages found in metapelites in the Nairne-Mt. Barker Creek area. The anomalous 2-phase assemblages (garnet + biotite) are not shown.

Whole rock compositions are indicated by:

⊗ = 4-phase assemblages

⊠ = 3-phase assemblage (garnet + biotite + [andalusite, fibrolite]).

x = 3-phase assemblages (staurolite + biotite + [andalusite, fibrolite]).

⊠ = 2-phase assemblages (biotite + [andalusite, fibrolite]).

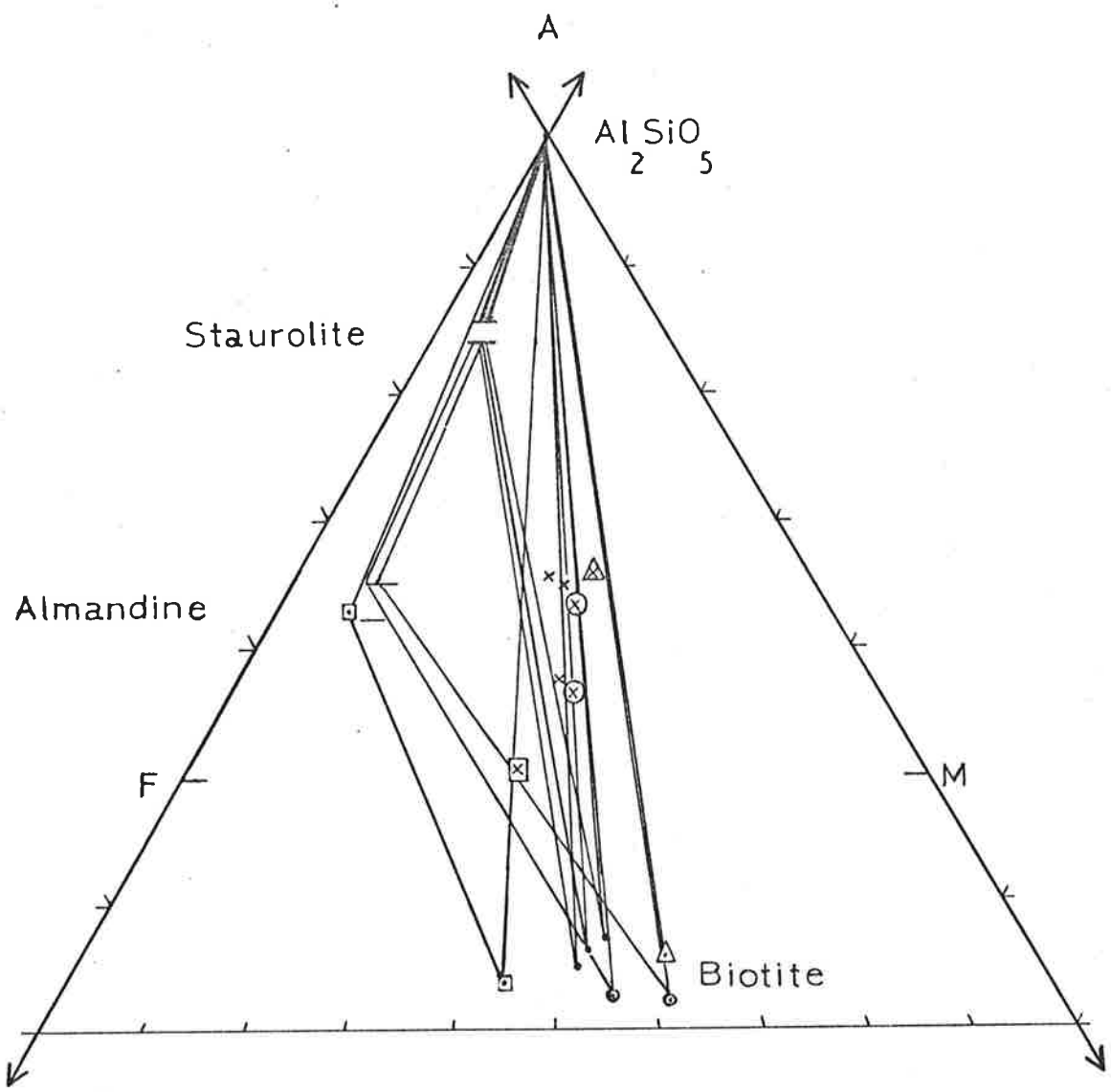

fig. 30

Figure 31.

AFM plot of 3-phase assemblages from metapelites.

(i) Al_2SiO_5 minerals + staurolite + biotite (rocks A405/BC38, BC37a, BC34a). A405/Bc34a contains only traces of fibrolite as the Al_2SiO_5 phase. Whole rocks:

▲= A405/BC38; Ⓐ = A405/BC37a; ▲ = A405/BC34a

(ii) Al_2SiO_5 minerals + almandine garnet + biotite

▣ = whole rock composition of A405/E2A.

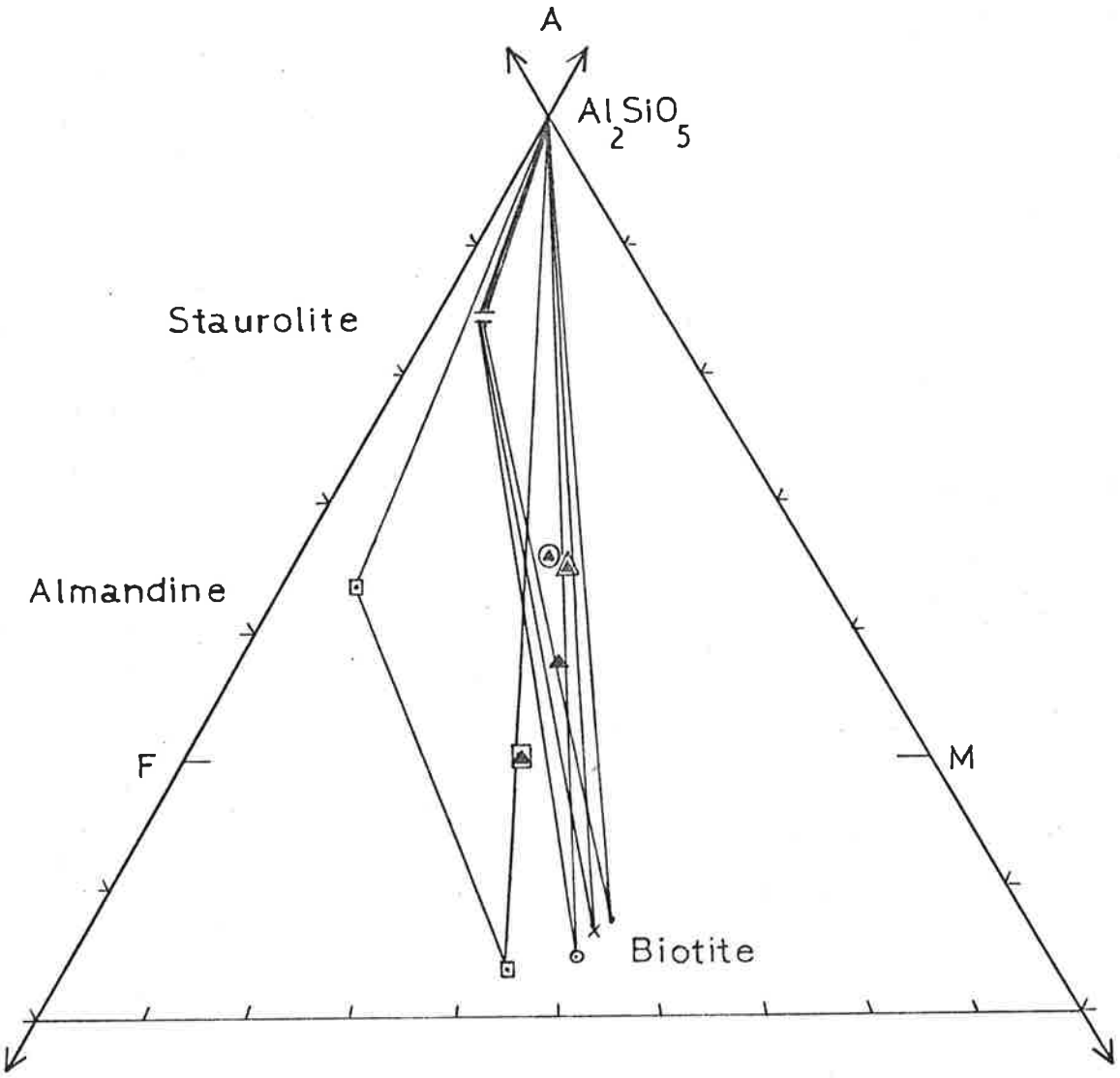

fig. 31

Figure 32.

AFM plot of 4-phase assemblages from metapelites. Al_2SiO_5 minerals + almandine garnet + staurolite + biotite (rocks A405/M24,E4E).

▲ = rock composition, A405/M24; Ⓐ = rock composition, A405/E4E.

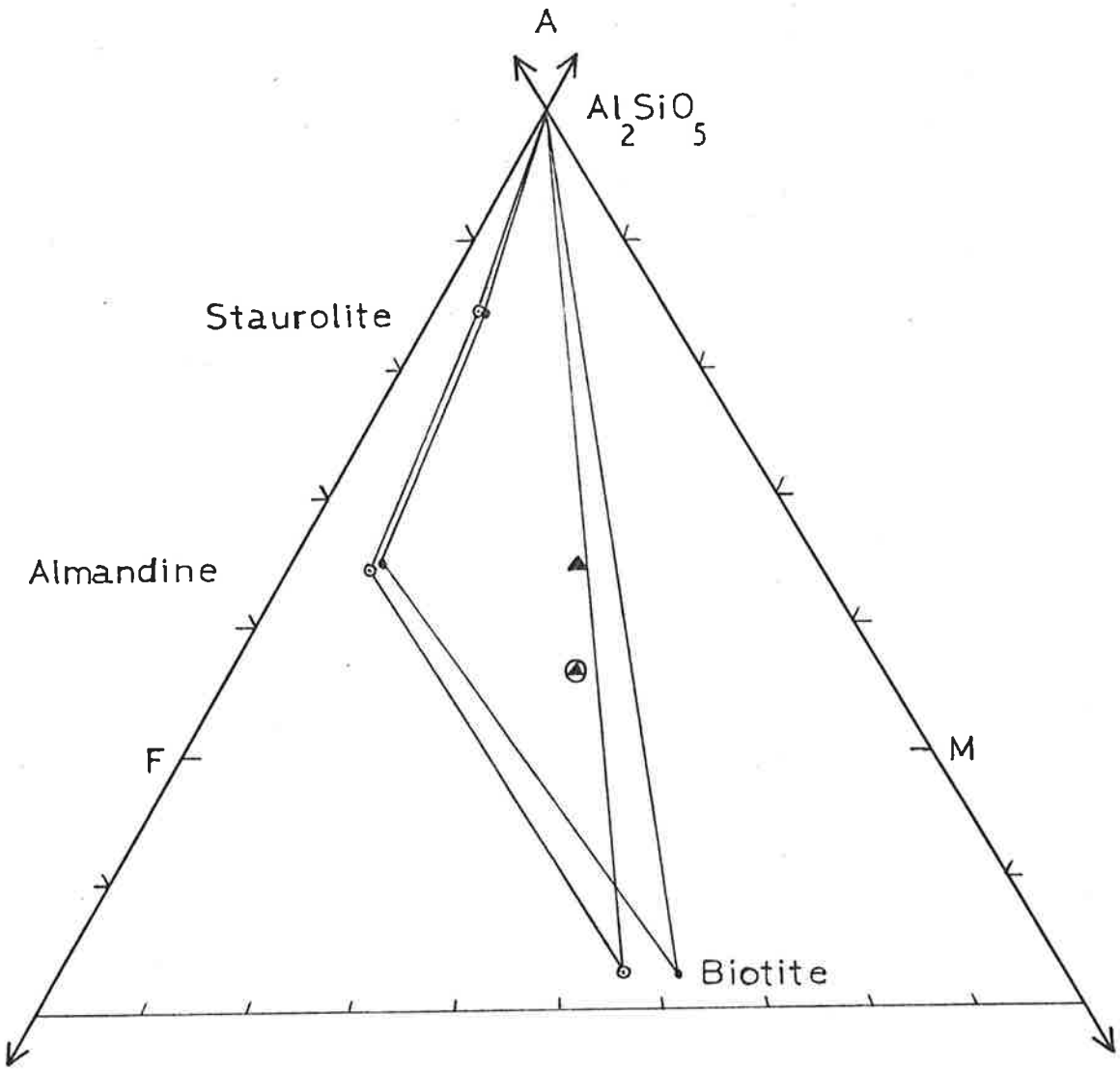

fig. 32

Figures 33.

AFM plot of 2-phase assemblages from metapelites.

(i) Al_2SiO_5 minerals + biotite (A405/M21')

◉ = whole rock composition

(ii) Almandine garnet + biotite (A405/E4B,F10)

▲ = whole rock composition A405/E4B

◭ = " " " " corrected for magnetite

▣ = whole rock composition A405/F10

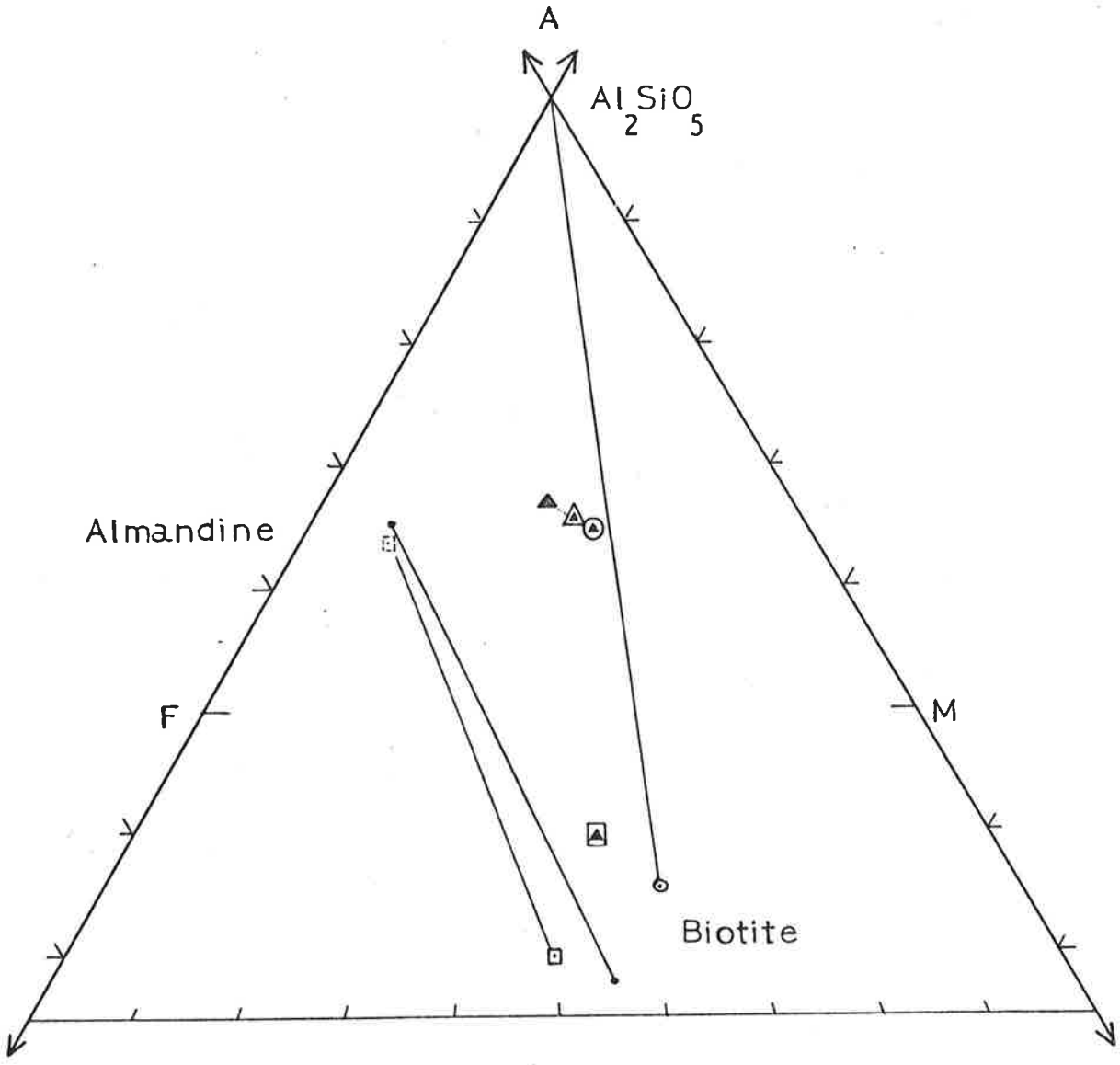

fig. 33

Figure 34.

AFM plot of assemblages with garnet, co-ordinates of garnet and rock being determined by including MnO with FeO.

Whole rock : ▣ = A405/E2A; ▲ = A405/M24; Ⓐ = A405/E4E; ◬ = A405/E4B.

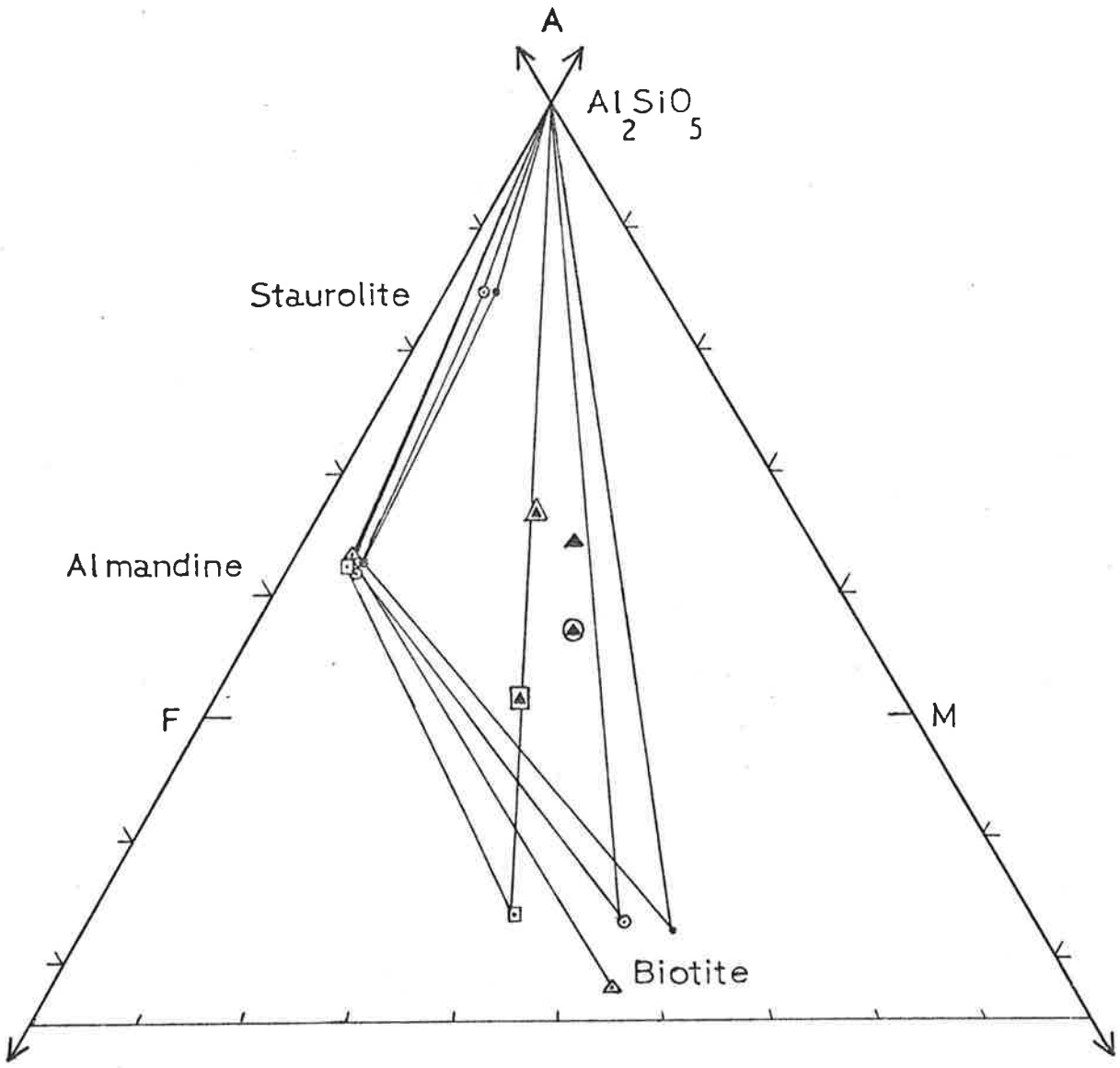

fig. 34

Figure 35.

ACF plot of Ca-rich rocks in the Nairne-Mt. Barker Creek area.

(i) Metadolerite; Hornblende + plagioclase (bytownite). (Rock A405/E9S.) ▲ = whole rock composition.

(ii) Calc-silicates; (a) Hornblende + plagioclase + epidote + quartz (Rock A405/BC45.) ◎ = whole rock composition.

(b) Hornblende + plagioclase + scapolite + diopside (Rock A405/MCS2C). ◉ = whole rock composition.

(iii) Hornblende rich quartzite; Hornblende + plagioclase + quartz (Rock A405/BC40) ■ = whole rock composition.

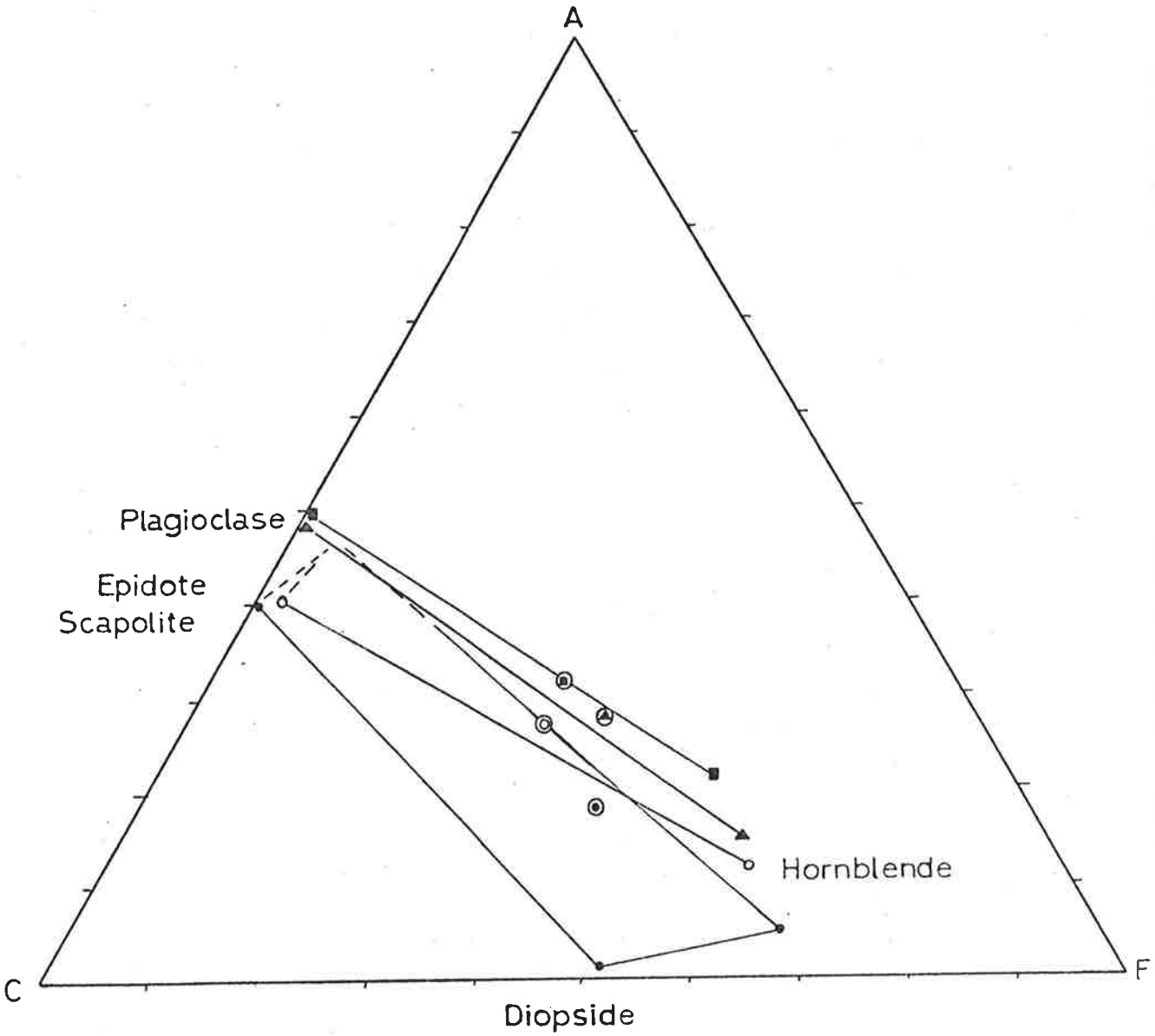

fig.35

Plate 1

(a) Fine metasiltstones grading into phyllites (from left to right). Unit 2, Member b, Torrens Group.
Length of hammer handle 25 cm.

(b) Non-laminated metasiltstones and phyllites in Unit 2, Member b, Torrens Group. Note refraction of the well developed cleavage near the hammer.

(c) Lamination in metasiltstones; Unit 2, Member b, Torrens Group.

(d) Boudinaged metasiltstone bed in more micaceous strata of Unit 2, Member b, Torrens Group.

Plate 2

(a) Well developed kinks in phyllites and fine metasandstones. Unit 2, Member b, Torrens Group. Length of hammer handle 25 cm.

(b) Small-scale faulting in kaolinized, well laminated fine metasiltstones typical of Unit 2, Member c (Torrens Group). Pen (length 10.5 cm) on fault.

(c) Fine lamination in kaolinized fine metasiltstones. Note the minute fractures and thin dark lenses. Unit 2, Member c, Torrens Group. Pen 10.5 cm.

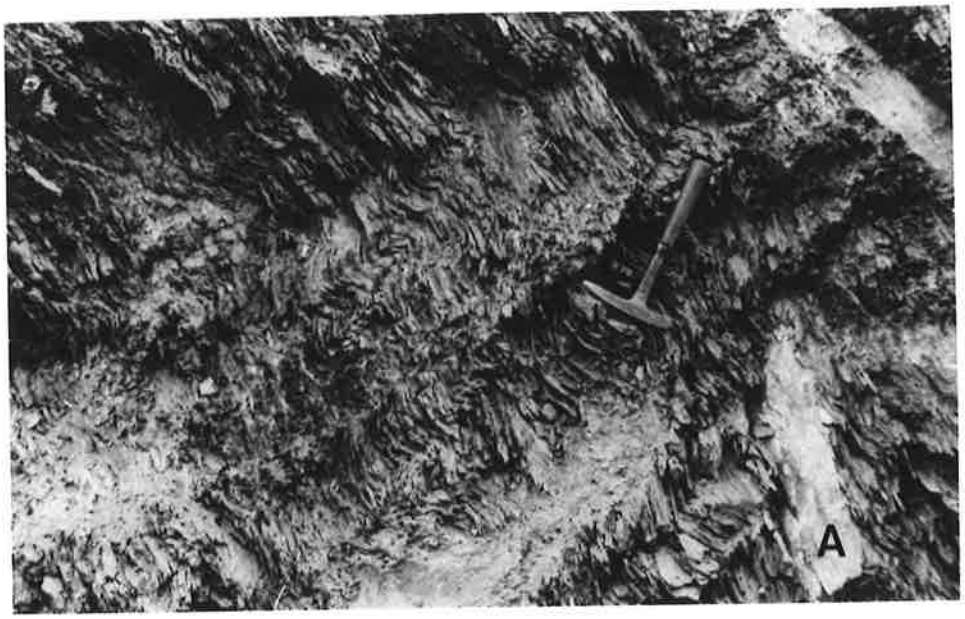
A


B

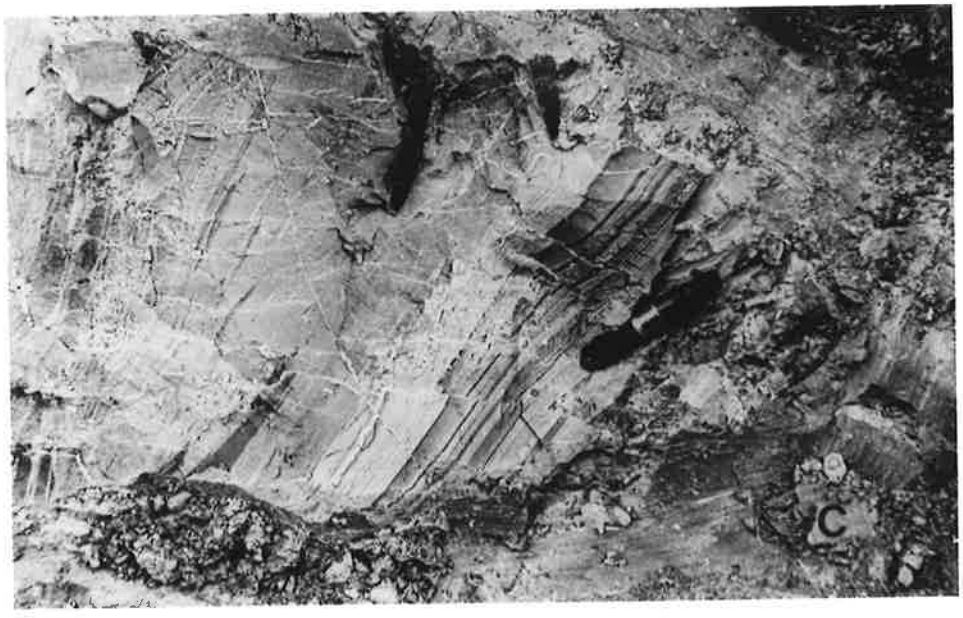
C

Plate 3

(a) Poorly laminated very fine metasandstones and meta-siltstones. Interval possibly equivalent to the basal portion of Unit 5, Torrens Group. Length of hammer handle 25 cm.

(b) Laminated interval in strata shown in (a).

(c) Pale grey fine to medium-grained feldspathic metasandstone unit within a sequence of metasiltstones. Unit 4, Member c, Torrens Group.


A


B

Plate 4

(a) Boudinaged competent metasandstone unit in metasiltstones. Unit 4, Member c, Torrens Group. Length of hammer handle 25 cm.

(b) Flaggy laminated scapolite-bearing metasiltstones. Unit 4, Member b, Torrens Group.


A

Plate 5

(a) Poorly laminated metasiltstones. Unit 4, Member b, Torrens Group. Length of hammer handle 25 cm.

(b) Metasiltstones grading vertically into micaschists. Unit 4, Member b, Torrens Group.

(c) Boudinaged quartzitic metasandstone bed enclosed by very micaceous metasiltstones and micaschists. Unit 4, Member b, Torrens Group.

(d) Actinolite and scapolite rich bed in scapolite and actinolite-bearing metasiltstones. Unit 4, Member b, Torrens Group.


A


B


C


D

Plate 6

(a) Flaggy interval in laminated metasiltstones. Unit 4, Member b, Torrens Group. Length of hammer handle 25 cm.

(b) Equal proportions of black carbonaceous very fine metasiltstones or metashales and paler coloured weakly laminated metasiltstones. Unit 4, Member a, Torrens Group.

(c) Well bedded dark grey laminated scapolite-bearing metasiltstones. Unit 4, Member a, Torrens Group.

Plate 7

(a) Weakly laminated very micaceous metasiltstones adjacent to hammer and to right. Unit 4, Member a, Torrens Group. Length of hammer handle 25 cm.

(b) Thin fine sand lenses in laminated metasiltstones. The lenticular form may be partly due to boudinage. Paler laminae are very fine sands. Unit 4, Member a, Torrens Group.

(c) Variable mica content of metasiltstones, rocks passing from fine quartz-micaschists into resistant metasiltstones which are flaggy in parts. Unit 4, Member a, Torrens Group. Length of pen 10.5 cm.


A


B


C

Plate 8

(a) Low angle cross-bedding in laminated metasiltstones. Note very pale weathered scapolite-rich unit on left. Unit 4, Member a, Torrens Group. Length of hammer handle 25 cm.

(b) Interbedded weakly laminated pale grey scapolite-rich beds in well laminated, well bedded darker grey meta-siltstones which are typically less weathered. Unit 4, Member a, Torrens Group.

(c) Fine to coarse metasandstone and meta-arkose beds inter-bedded with very fine metasandstones grading into meta-siltstones. Unit 3, Torrens Group.

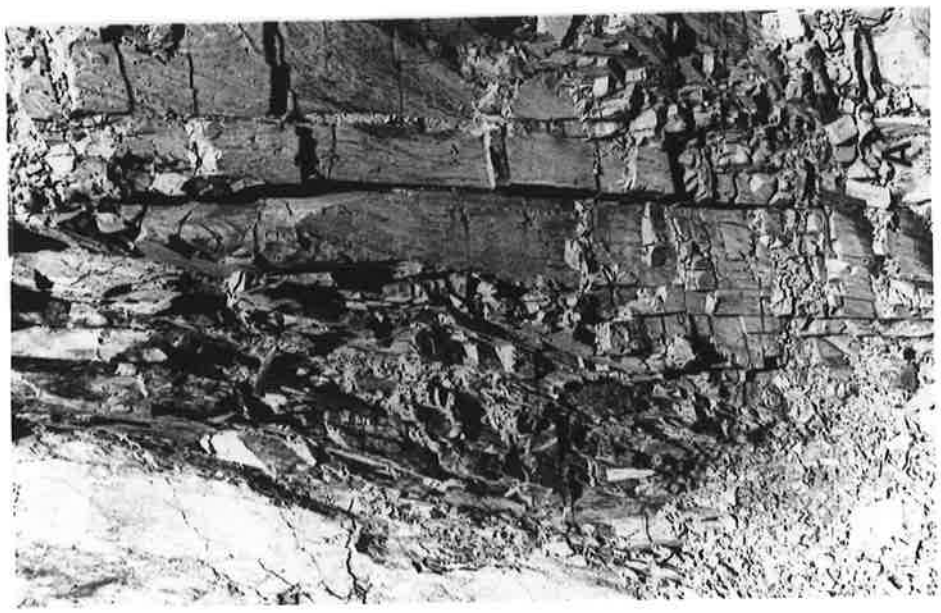

Plate 9

(a) Interbedded fine to medium-grained metasandstone units in a sequence of metasiltstones with occasional thin fine metasandstone beds and laminae. Unit 3, Torrens Group. Length of hammer handle 25 cm.

(b) Laminated metasiltstones at locality D2 (Fig. 2). Resistant flaggy horizons are present. In some thin horizons, metasiltstones grade into fine quartz-micaschists (e.g. by hammer head). Unit 4, Torrens Group.

(c) Well laminated fine metasandstones grading into metasiltstones with flaggy horizons. Locality D3 (Fig. 2). Unit 4, Torrens Group (Scale: depth of trench 4 m).

(d) Flaggy and phyllitic metasiltstones. Locality D5 (Fig. 2). Unit 4, Torrens Group.


A


B


C


D

Plate 10

(a) Fold in kaolinized metasiltstones with scapolite-rich beds. An interbed of black carbonaceous rock can be seen in the centre of the frame. Unit 4, Torrens Group. Length of hammer handle 25 cm.

(b) Highly contorted interbedded schists and metasiltstones near locality B5 (Fig. 2). Unit 4, Torrens Group.

(c) Minor folds in very micaceous metasiltstones and mica-schists. Locality B5 (Fig. 2).

(d) Minor fault in metasiltstone and fine metasandstone strata of Unit 4, Torrens Group. Locality D4 (Fig. 2).


A


B


C

Plate 11

(a) Small-scale low angle cross-bedding in finely laminated metasiltstones (directly above hammer). Locality B3 (Fig. 2). Unit 5, Member a, Torrens Group. Length of hammer handle 25 cm.

(b) Fine to medium-grained metasandstone lenses in finely laminated metasiltstones. The pale laminae are very fine sands. Locality B3 (Fig. 2). Unit 5, Member a, Torrens Group.

(c) Opalized zone in altered metasiltstones. Locality B4 (Fig. 2). Unit 5, Torrens Group.

(d) Altered, ferruginous metasiltstones in the zones of opal formation. Locality B4 (Fig. 2).


B

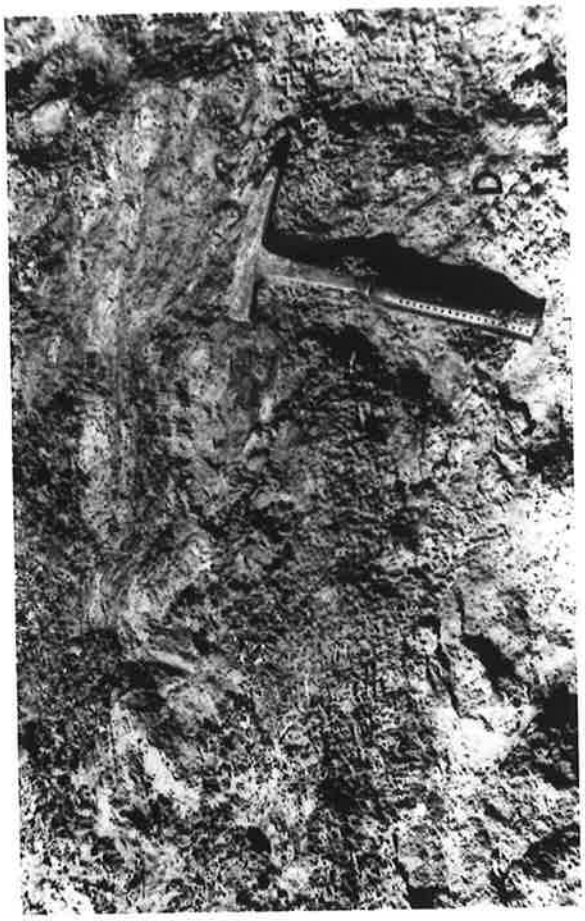
D


A


C

Plate 12

(a) Minor fault with associated brecciation in laminated metasiltstones at locality B2 (Fig. 2). Unit 5, Member a, Torrens Group. Length of hammer handle 25 cm.

(b) Kaolinized well laminated fine metasandstones and metasiltstones. Note deformation about coarse metasandstone lens (immediately to left of hammer handle). Unit 5, Member a, Torrens Group.

(c) Kaolinized fine metasandstones with flaggy intervals. Unit 5, Member c, Torrens Group.

(d) Laminated metasiltstones and thin fine to coarse metasandstones. Basal strata of the Sturt Group.


D

Plate 13

(a) Coarse metasandstone lens in laminated fine scapolite-bearing metasandstones and minor metasiltstones. Unit 1, Belair Sub-Group. Length of hammer handle 25 cm.

(b) Minor fault in interbedded coarse metasandstones and fine metasandstones. Hammer in fault. Strata to left are steep to overturned. Unit 3, Belair Sub-Group.


A


B

Plate 14

(a) Rounded quartzite boulder in kaolinized Sturt Tillite (to right of pen). Locality B11a (Fig. 2). Length of pen 10.5 cm.

(b) Subrounded quartz pebbles in kaolinized metasiltstones and fine metasandstones. Sturt Tillite. Locality B11a (Fig. 2). Length of hammer handle 25 cm.

(c) Kaolinized feldspathic metasiltstones of the Tapley Hill Formation. Note the protruding joints and beds which are ferruginous and more resistant. Locality B12a (Fig. 2).

(d) Extensively kaolinized well laminated scapolite-rich metasiltstones of the Tapley Hill Formation. Locality B12a (Fig. 2).

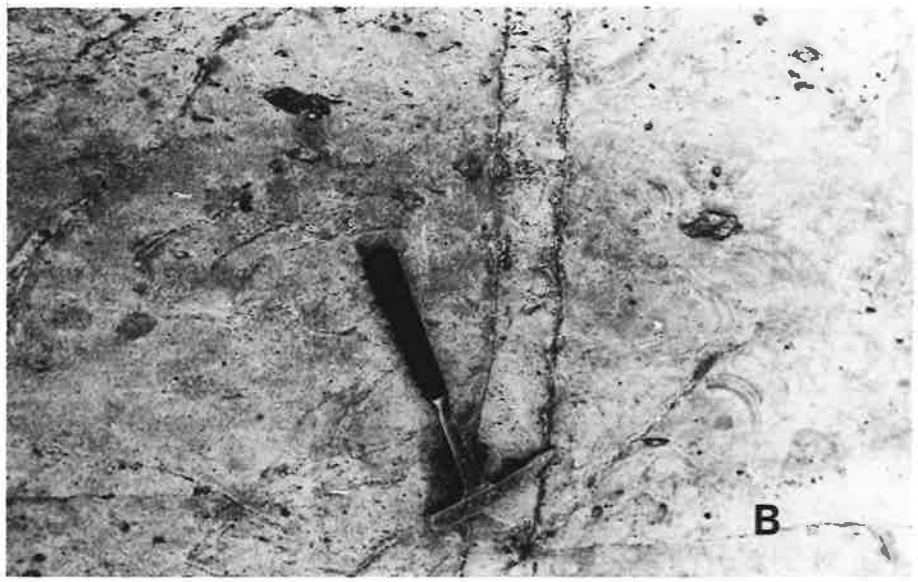
B

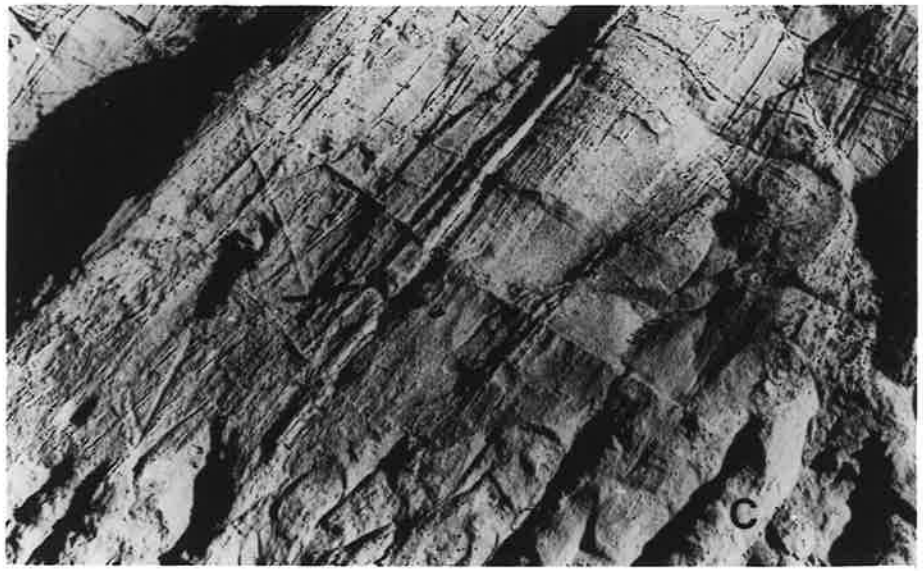
C


D

Plate 15

(a) Complex intertonguing of scapolite-rich metasiltstones and metashales with scapolite-deficient rocks. Unit 1, Marino Group.

(b) Weakly laminated metasiltstones near the top of Unit 1, Marino Group. Low angle cross-bedding can be seen in the strata, far right. Length of hammer handle 25 cm.

(c) Andalusite-rich interbed in quartz-micaschist. Unit 2, Marino Group.

(d) Thinly interbedded andalusite-rich quartz-micaschist and micaschist. Note typical quartz-biotite segregations developed in a less micaceous bed. Shape and orientation of the segregations is controlled by bedding (S_o) and schistosity (S_2). Unit 2, Marino Group.


A


B


C

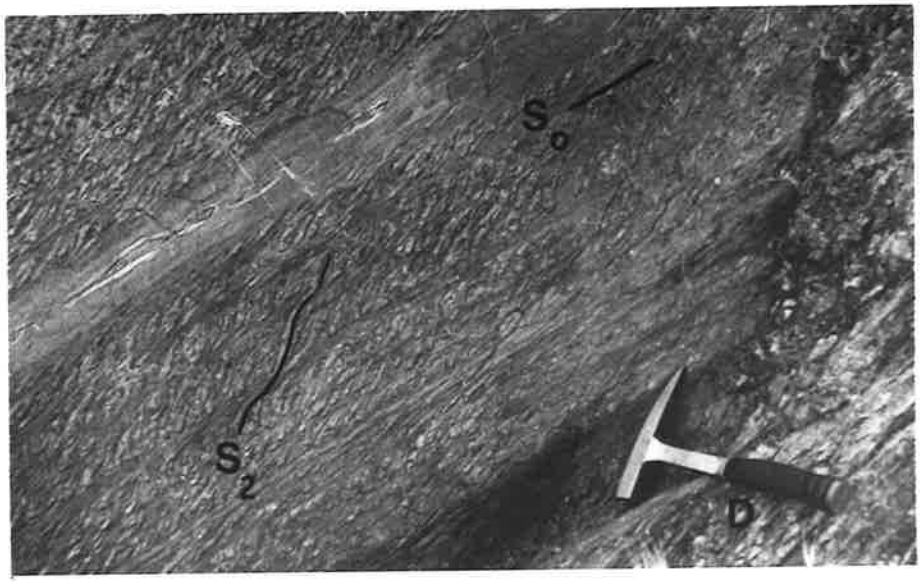
S_0
S_2
D

Plate 16

(a) Small F_2 folds in andalusite schist and quartz-micaschist. The schistosity S_2 is axial plane to the folds. Length of hammer handle 25 cm.

(b) Strongly aligned post-schistosity crenulations (with axial planes S_3) seen on a well developed S_2 surface. Unit 2, Marino Group.

(c) Crenulations on a schistosity surface, emanating from porphyroblasts. Scale: 20 cent coin.

(d) Thick resistant metasiltstone and fine metasandstone beds characteristic of interval (ii), Member (a), Unit 3, Marino Group.

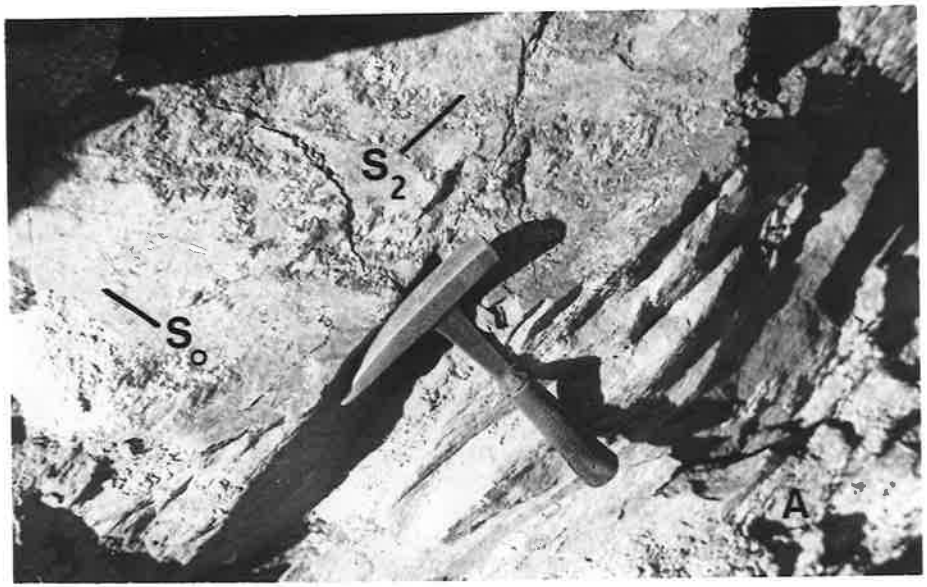
S_2
S_o
A

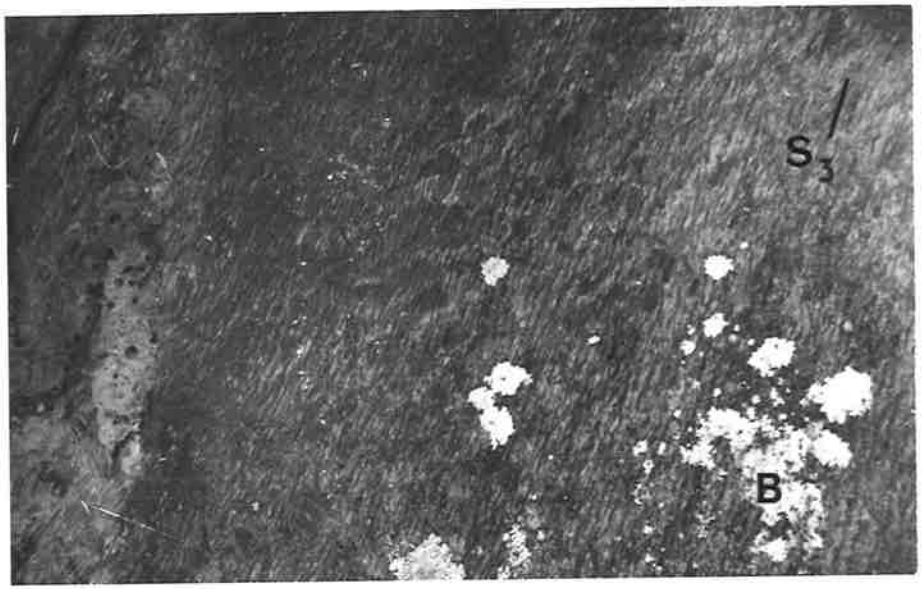
S_3
B


C


D

Plate 17

(a) Interbedded micaceous metasiltstones and minor thin quartz-micaschists in Member a, Unit 3, Marino Group. A quartz-biotite segregation can be seen in the top right (arrow). Length of hammer handle 25 cm.

(b) Resistant beds of metasiltstone grading into micaceous fine metasandstone in the upper levels of Member a, Unit 3, Marino Group. Thin, more micaceous layers occur which are characteristically more deeply eroded (by hammer's head).

(c) Very micaceous metasiltstones grading into quartz-micaschists in Member b, Unit 3, Marino Group.

(d) Interbedded quartz-micaschists and micaschists in Member d, Unit 3, Marino Group.


A


C


D

Plate 18

(a) Flaggy strata consisting of interbedded metasiltstones and quartz-micaschists which are common in Member e, Unit 3, Marino Group.

(b) Lens of Mt. Barker Quartzite (Q) in the foreground truncated above (left) by the Nairne Fault. Layered calc-silicates, minor metasiltstones and a lenticular pale grey marble (outlined) occur immediately above and are interpreted as being within the Carrickalinga Head Formation. Below the quartzite are layered calc-silicates of Unit 4. In the background the Mt. Barker Quartzite (Q) reappears again but is displaced by a cross-fault. View looking south from locality 104, Mt. Barker Creek.

(c) Well bedded lower levels of the Mt. Barker Quartzite. The conformable contact with the kaolinized metasiltstones of Unit 4 (right) is marked by an arrow. Scale bar = 60 cm. Exposure at northern extremity of Mt. Barker.


A

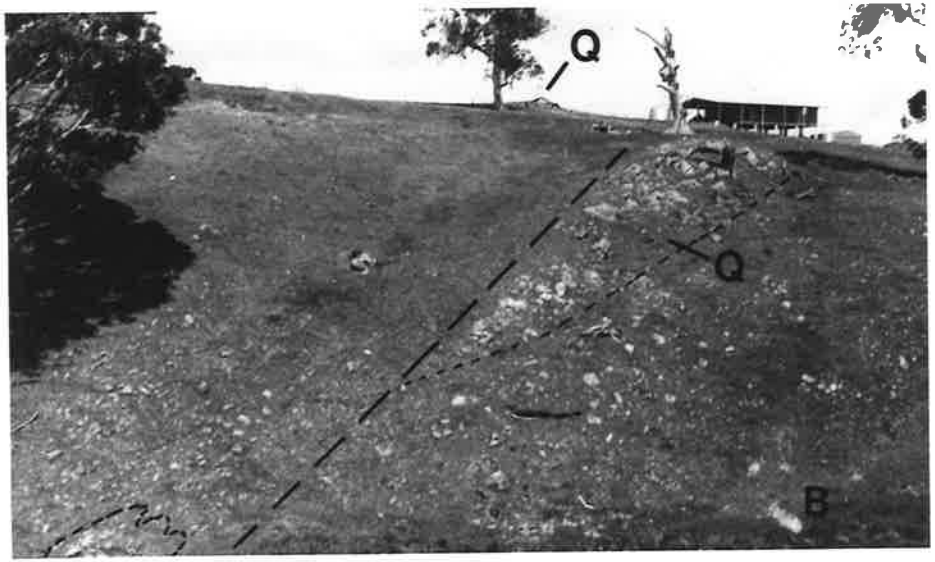
Q
Q
B

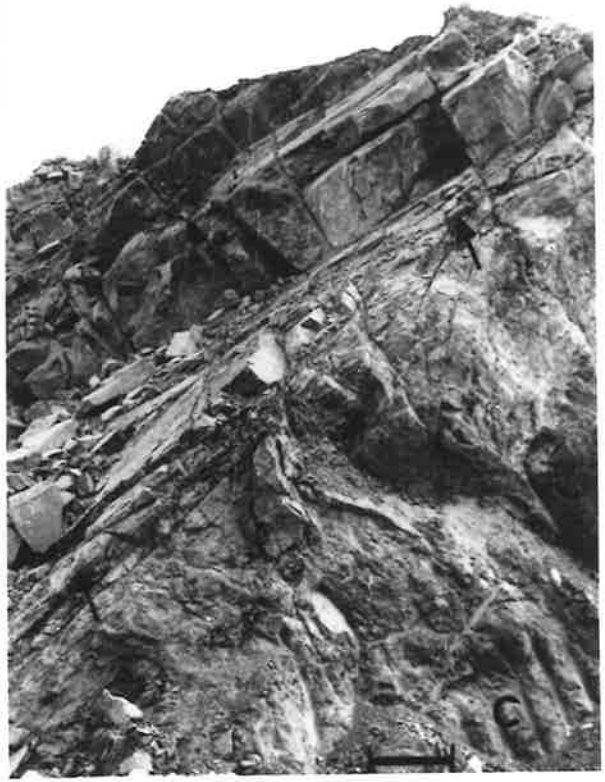
C

Plate 19

(a) Conformable contact (arrow) between massive Mt. Barker Quartzite and kaolinized scapolite-bearing metasiltstones of Unit 4. Exposure at northern extremity of Mt. Barker. Length of hammer handle 22 cm.

(b) Laminated horizons in the Mt. Barker Quartzite. Length of hammer handle 22 cm.

(c) Fault zone (outlined) of the Nairne Fault marking the contact between the kaolinized Carrickalinga Head Formation (left) and the Mt. Barker Quartzite (right). The quartzite is sharply truncated at the western margin of the fault zone which has the orientation: strike 350°, dip 58°E. Bedding in the Mt. Barker Quartzite at (1) has strike 340°, dip 35°E; at (2) it strikes 14°, dipping 10°E. Adjacent to the fault, bedding is dragged downwards, steepening considerably, the sense of drag being indicated by the dotted line. The eastern margin of the fault zone is indistinct due to extreme weathering of the rock. Within the fault zone are angular blocks of Mt. Barker Quartzite, the largest being indicated by an arrow. Ferruginous Tertiary conglomerates can be seen in the top left-hand corner of the photograph.


A


B


C

Plate 20

(a) Steeply dipping truncated upper surface (F) of the Mt. Barker Quartzite (left) and shallow-dipping kaolinized laminated metasiltstones and metashales of the Carrickalinga Head Formation (right). The latter are dragged upwards (dotted line), steepening suddenly adjacent to the fault which marks the contact between the two formations. The detail at the contact is obscured by extreme weathering and loose rubble. A minor fault (f) in the Carrickalinga Head Formation can be seen in the far right of the photo. South-East freeway excavations, northern extremity of Mt. Barker. Height of low vertical face on right is 2 m.

(b) Resistant metasandstone beds near the base of the Backstairs Passage Formation in Mt. Barker Creek.

(c) Cross-bedded micaceous metasandstones in the basal member of the Backstairs Passage Formation. Length of hammer handle 25 cm.

(d) Flaggy interval in the Backstairs Passage Formation. Length of bar 32 cm.

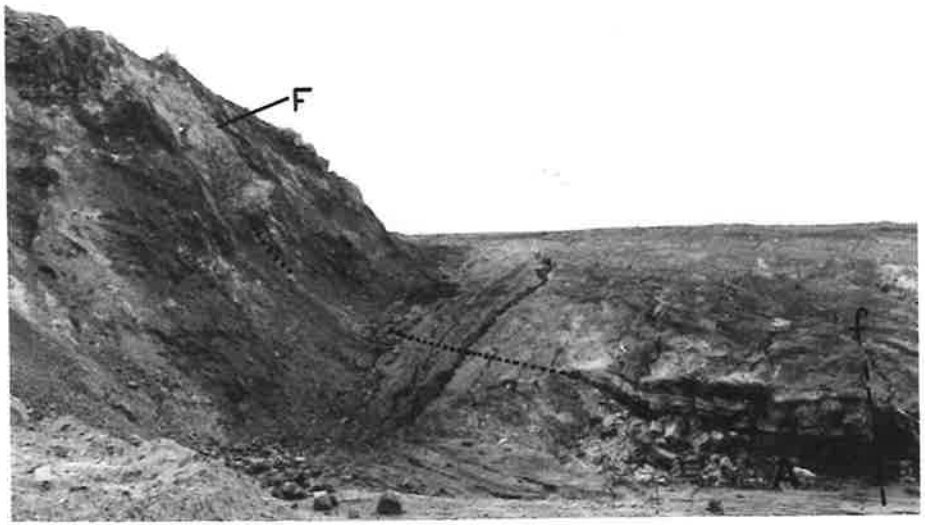
F


B


C


D

Plate 21

(a) Slumping at the base of a thick feldspathic metasandstone unit in the Backstairs Passage Formation. A more pelitic horizon occurs immediately to the left. Length of bar 32 cm.

(b) Eastern limit of a truncated quartzite of the Saddleworth Formation. The sharp margin is a possible fault surface, strike 320°, dip 80°E. Length of hammer handle 22 cm.

(c) Small probable F_2 mesoscopic fold in andalusite schist. The axial plane schistosity is shown by the dashed line. Upper levels of the Saddleworth Formation near Mt. Charles East. Length of hammer handle 22 cm.


A


B


C

Plate 22

(a) Hinge zone of F_2 microfold. Section perpendicular to l_2 and almost in plane of S_3. A405/E4. Field of view 14 mm.

(b) Relict sedimentary grains in metasiltstone. A405/E12A. Field of view 3.9 mm.

(c) Relict clay-rich lens in a metasiltstone. A405/E12C. Field of view 3.9 mm.

(d) Discontinuous network of biotite crystals defining the schistosity in a metasiltstone in which recrystallization has produced an entirely crystalloblastic texture. Polars crossed. A405/A6. Field of view 3.1 mm.

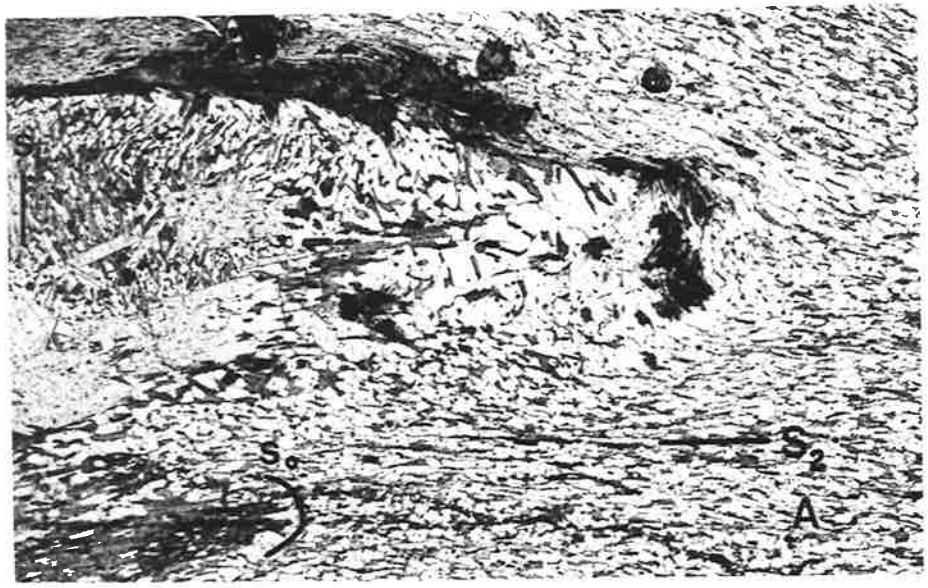
S_2
S_0
A

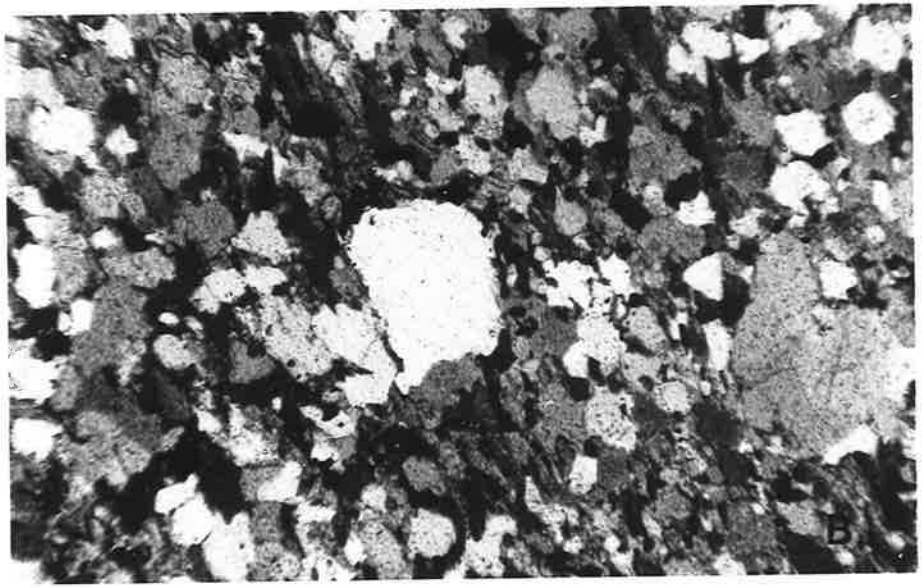
B

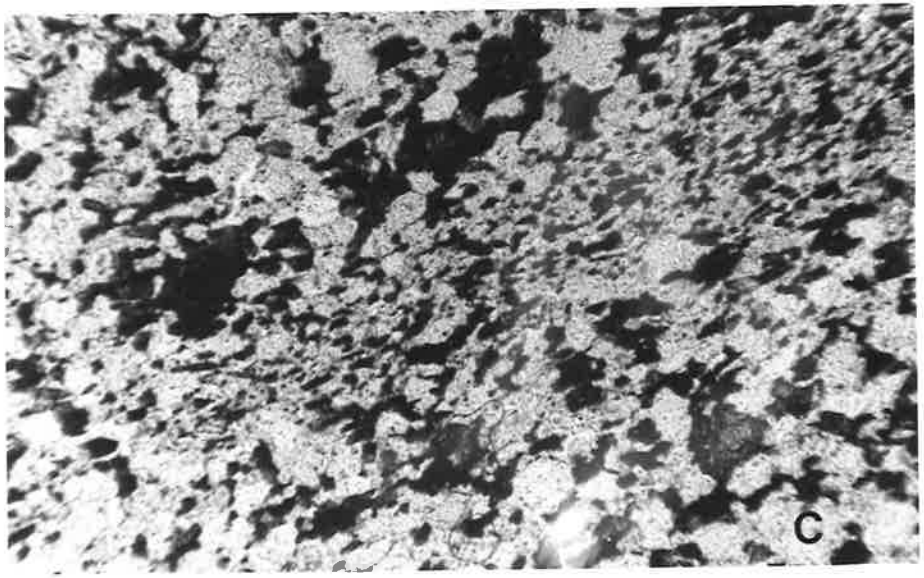
C


D

Plate 23

(a) Zoned zircon crystal in metasiltstone. Polars crossed. A405/A6. Field of view 1.25 mm.

(b) Syn-S_2 andalusite elongate in the S_2 plane. Note accentuation of sedimentary layering by metamorphic segregation. Section perpendicular to l_2. A405/H8b. Field of view 12.5 mm.

(c) Recrystallized pre-S_2 aggregate of quartz and biotite. S_2 is strongly deformed around this aggregate to form an augen structure. Section perpendicular to S_2 and l_3. Weak F_3 crenulations are visible. A405/E4E(2). Field of view 12.5 mm.

(d) Augen composed of quartz and biotite in S_2. Grainsize is noticeably finer than that of the enclosing matrix. Note layering which has probably been accentuated by segregation during metamorphism. Section perpendicular to S_2 and S_3, l_3. A405/E6(2). Field of view 14 mm.

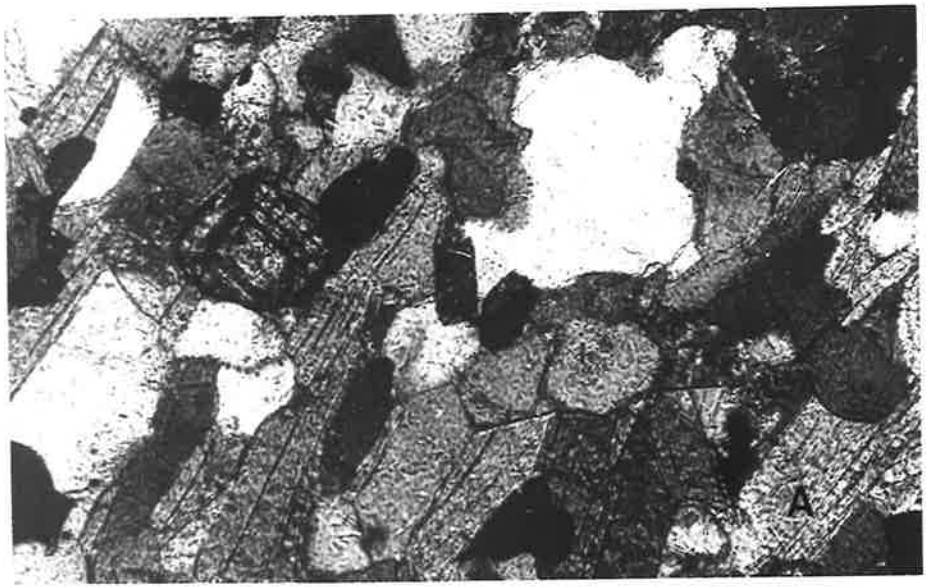
A


S2
B

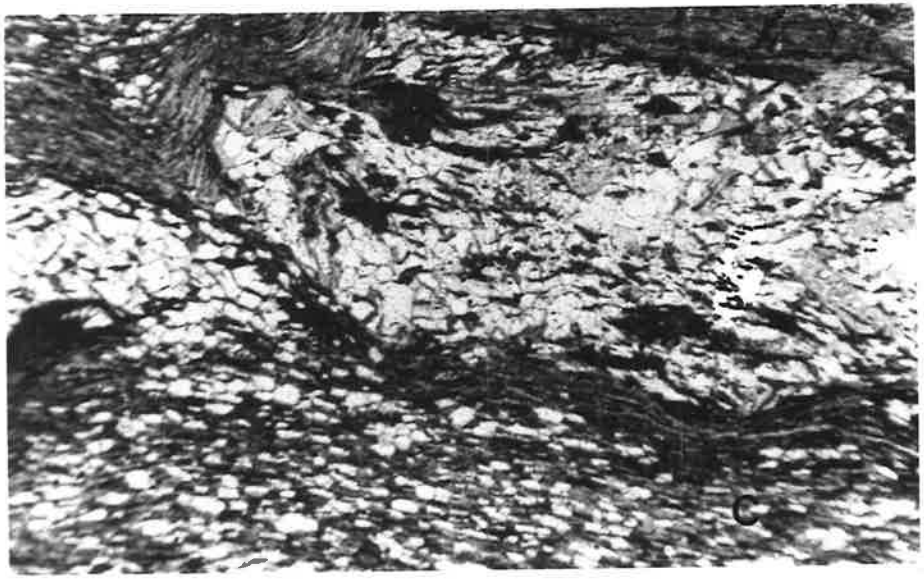
C

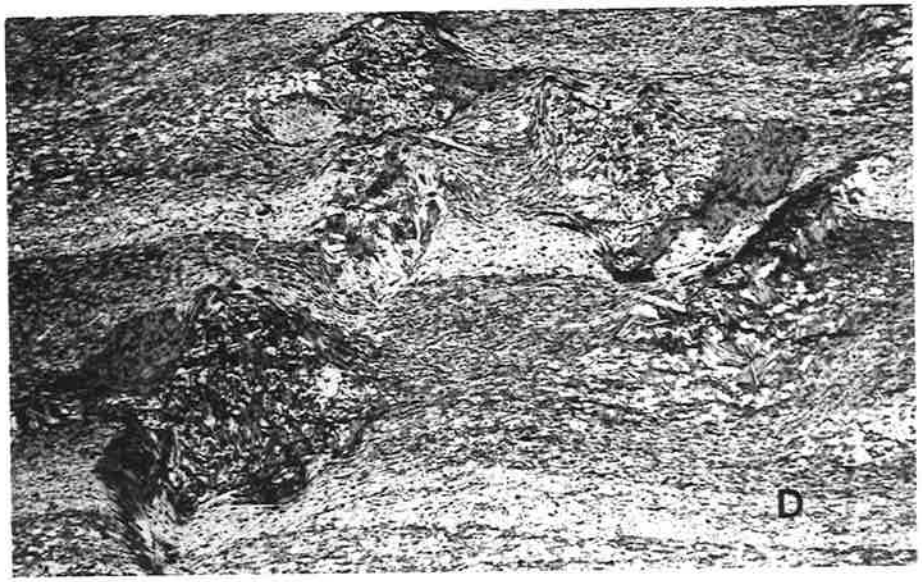
D

Plate 24

(a) Pressure shadow developed in the S_2 plane about pre-S_2 matrix. Section approximately perpendicular to l_2 and in S_3 plane. A405/E6(1). Field of view 14 mm.

(b) Close view of augen in S_2 composed of quartz and biotite. The fine biotites are aligned almost at 90^o to S_2 and define S_1. Randomly oriented post-S_2 coarse muscovite plates, presumably related to the breakdown of andalusite, cut across the earlier matrix. Section perpendicular to S_2, in plane of S_3, l_3. A405/BC44. Field of view 3.9 mm.

(c) Pre-S_2 poikiloblastic andalusite containing embayments of fine quartz-biotite aggregate which is possibly also pre-S_2. Here the biotites are aligned and parallel the orientation of quartz and minor biotite inclusions within the andalusite which are discordant with S_2. Section perpendicular to S_2, l_2. A405/E2A. Field of view 3.9 mm.

(d) Pre-S_2 andalusite porphyroblast. Only a minor pressure shadow has formed in S_2. Section parallel to l_2, perpendicular to S_2. A405/BC27(2). Field of view 14 mm.

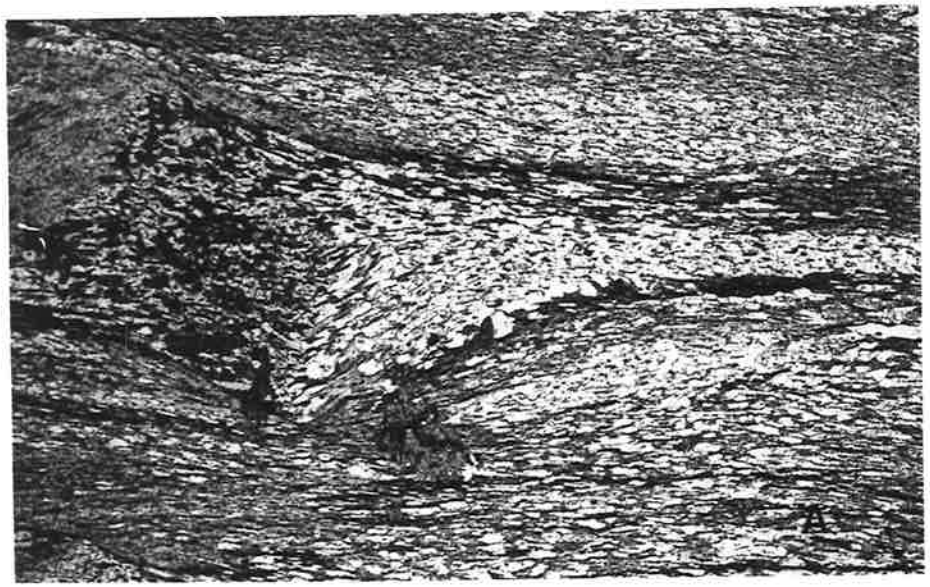
A

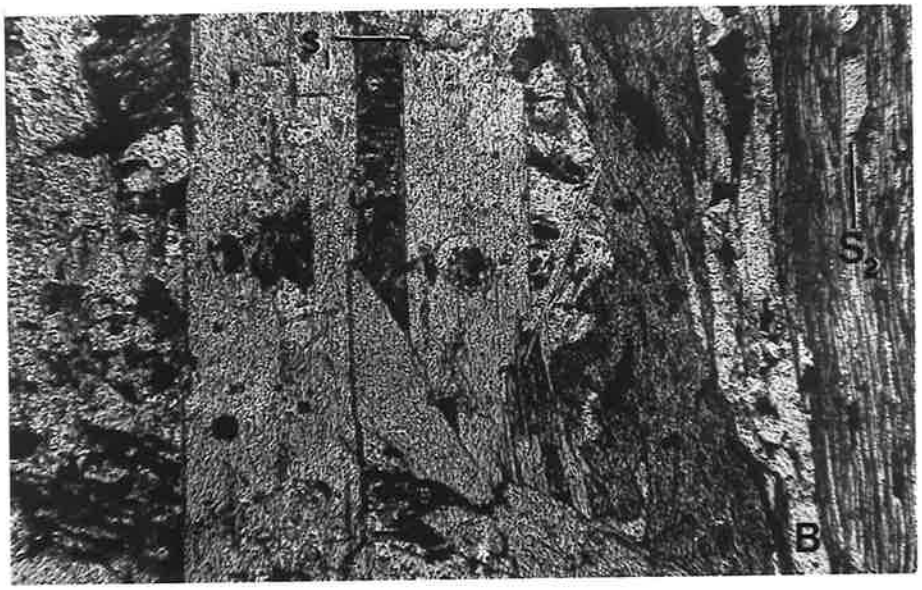
S1
S2
B

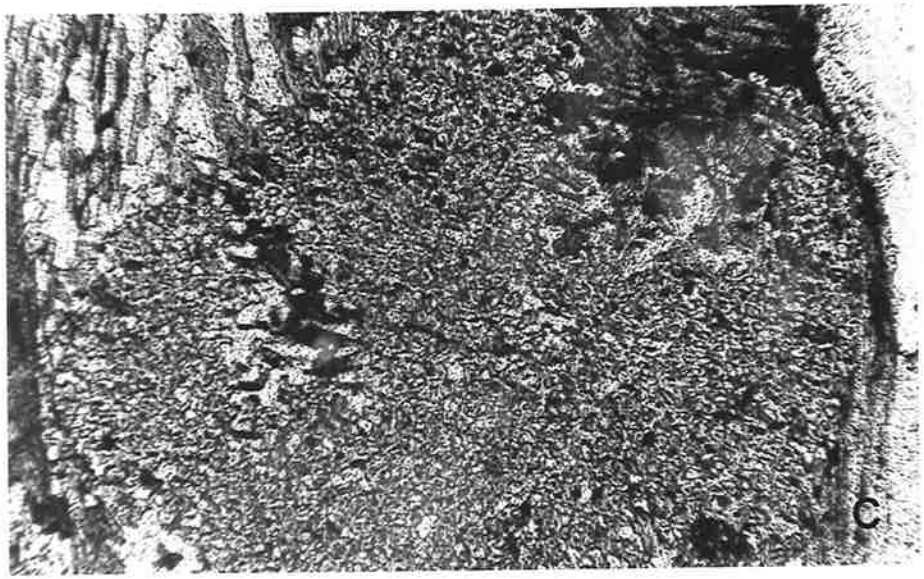
C

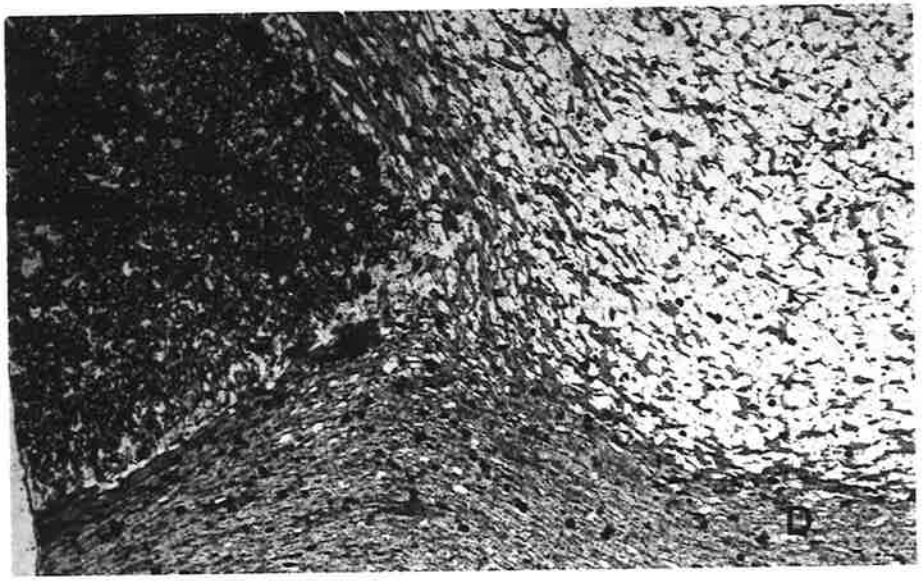
D

Plate 25

(a) Quartz-rich pressure shadow zone developed in S_2 around an aggregate of finer quartz and minor biotite which encloses a ragged poikiloblastic andalusite crystal. Quartz inclusions in the andalusite tend to define an earlier schistosity (S_1) and the andalusite is slightly elongate in this direction. Section perpendicular to S_2. A405/BC37. Field of view 14 mm.

(b) Poikiloblastic andalusites within quartz-biotite augen in S_2. The andalusites define a slightly sigmoidal pattern (S_1). Andalusite crystals in close proximity to each other are in optical continuity and may originally have formed larger crystals. Decomposition to fibrolite by indirect paths involving the replacement of andalusite by biotite and muscovite is evident. Biotites within the augen tend to align almost at right angles to S_2 and at a definite angle to S_1 and presumably formed syn-S_3. Some weak F_3 crenulations are visible. Section perpendicular to S_3. A405/BC27(4). Field of view 14 mm.

(c) Poikiloblastic andalusite in a recrystallized quartz-biotite matrix. Biotites are aligned in S_2. The fine inclusions in the porphyroblast are elongate along the long dimension of the crystal (which is some 30^{o} to S_0) and are assumed to represent S_1. Section perpendicular to S_2 and 1_3. A405/MD5. Field of view 3.1 mm.

(d) Pre-S_2 poikiloblastic andalusites. Fine quartz, opaque mineral inclusions define S_1 which is discordant with S_2. Andalusites are elongate in S_1 and opaques form bands in this direction. Individual opaques are also elongate in S_1. Section perpendicular to S_2. A405/MD5. Field of view 6.5 mm.

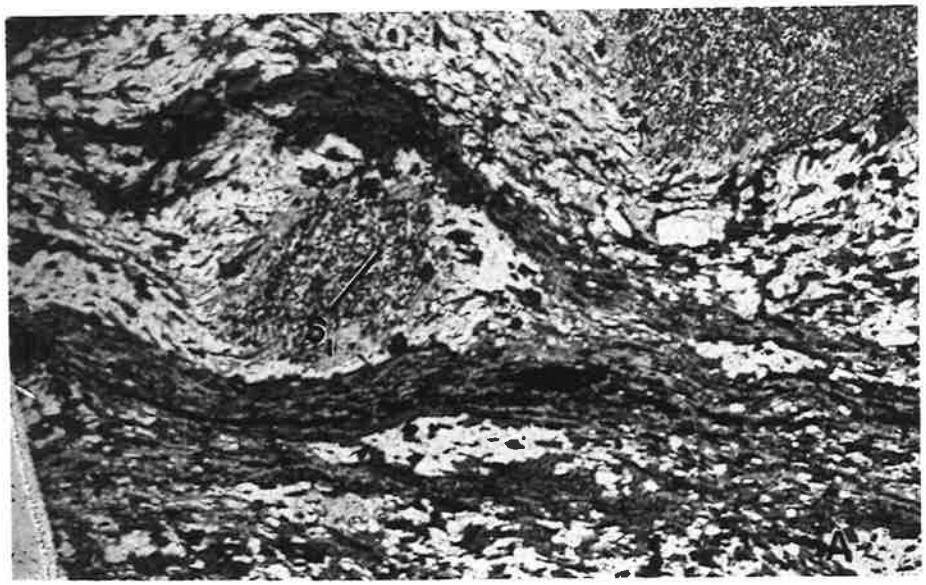
S1
A


S1
S2
B


S2
S1
C


S2
B

Plate 26

(a) Poikiloblastic andalusites elongate in S_1 which locally parallels S_0 (S_2 is also sub-parallel to S_0) whereas in an adjacent portion of the rock (Plate 25(b)), S_1 is obviously inclined to S_0. Note partial development of F_3 crenulations in S_2. Section perpendicular to S_2 and l_3. A405/BC27(4). Field of view 12.5 mm.

(b) Elongate poikiloblastic andalusite with equidimensional quartz inclusions. Large pressure shadow regions have formed where S_2 is strongly deformed about this pre-existing crystal which is elongate in S_0 and has not undergone rotation. Biotites in the pressure shadow are still aligned in S_2. A large idioblastic almandine cuts across S_2 and may be later than this schistosity. Section perpendicular to l_2, S_2. A405/E2A. Field of view 14 mm.

(c) Poikiloblastic andalusite as in (b). Note rotation of these porphyroblasts from their original orientation along S_0. Some F_2 microfolds of S_0 can just be distinguished . Section perpendicular to l_2. A405/E2A. Field of view 14 mm.

(d) Multistage andalusite. Cores containing very fine inclusions are often easily distinguished from rims with much coarser and commonly more elongate inclusions. A405/MD5. Field of view 5 mm.

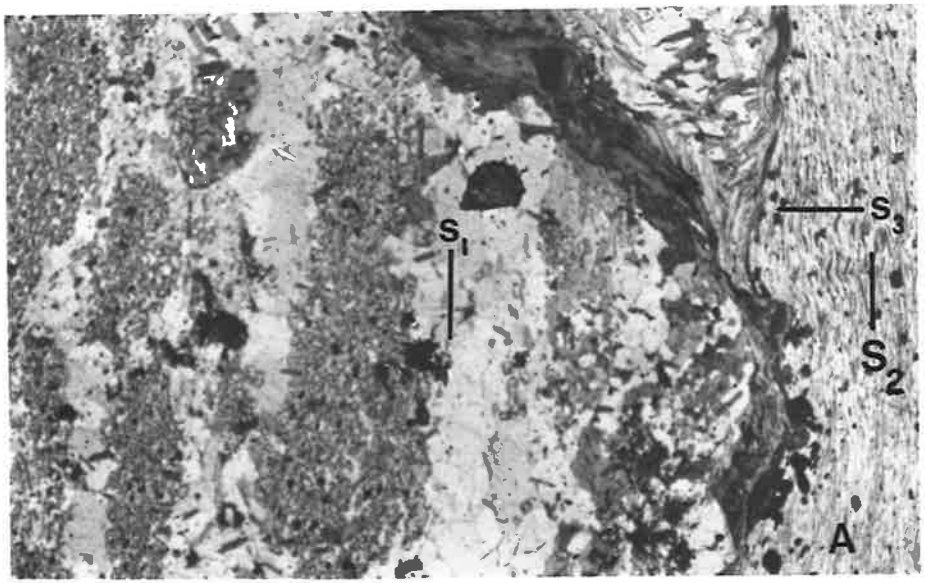
S1
S3
S2
A

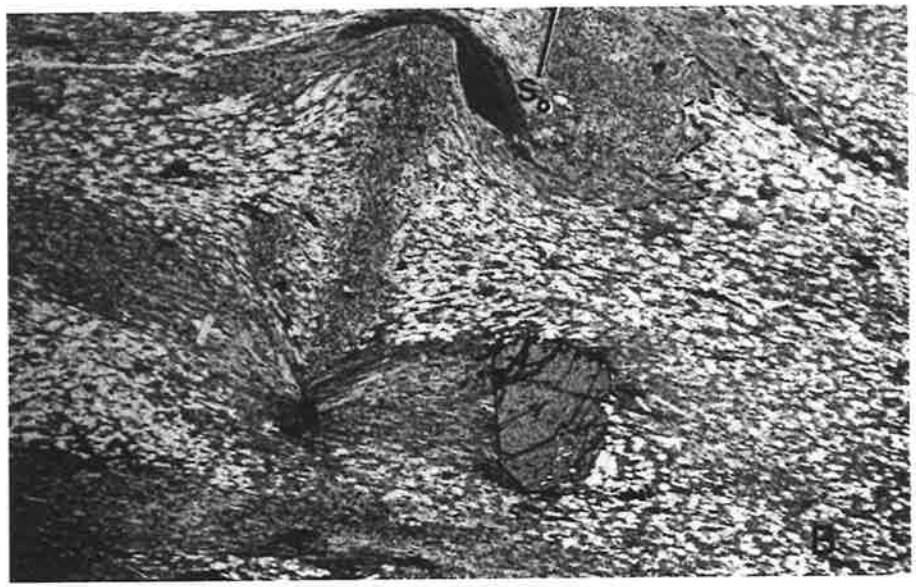
S0
B

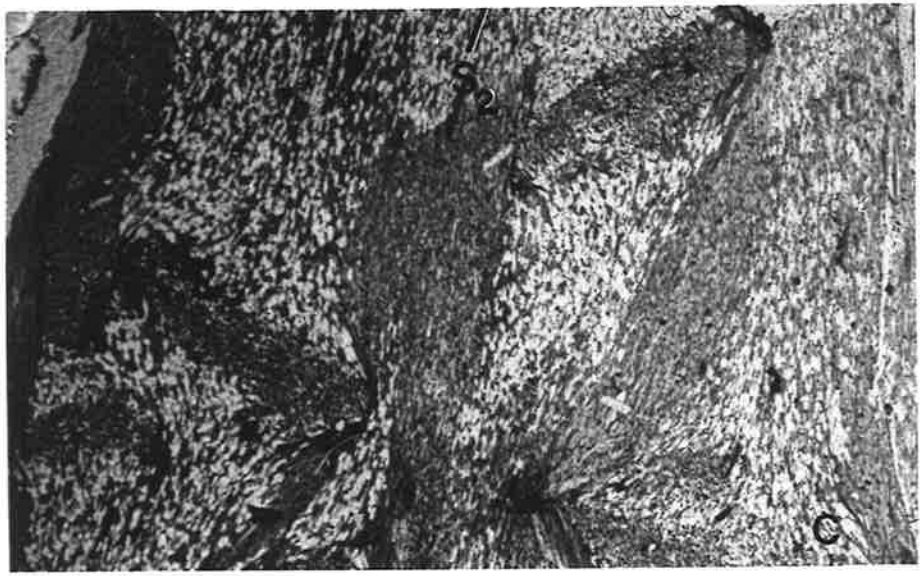
S2
C

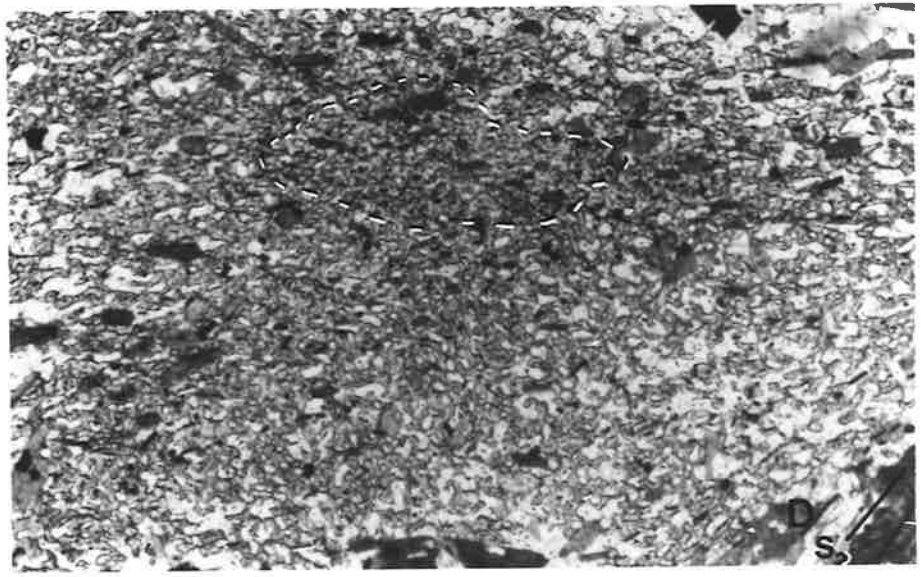
D
S0

Plate 27

(a) Syn-S_2 poikiloblastic andalusite. Quartz inclusions are slightly finer than the matrix and are elongate in the S_2 plane. There is some tendency for S_2 to deform around the porphyroblast which may indicate the crystal formed early syn-S_2 (supported by the finer size of the inclusions). Some F_3 crenulation of S_2 is visible. Section perpendicular to l_2. A405/H8b. Field of view 3.9 mm.

(b) Rotated syn-S_2 andalusite. Quartz inclusions, which are of similar size to the matrix, define a fabric which now appears locally discordant with S_2. Section perpendicular to l_2. A405/H8b. Scale bar = 1 mm. "Shadowmaster" optical projection drawing. Dashed lines indicate trend of schistosity (S_2). Probable coarse post- S_2 muscovites and biotites (shaded) outlined.

(c) Syn-S_2 andalusites. Rotation has occurred during crystallization. Quartz inclusions define an internal structure which is continuous with the sigmoidal pattern of the external fabric. Inclusions towards the margins of the andalusites are of the same grainsize as the matrix. Note the definite zones with much finer inclusions which formed pre-S_2. Section perpendicular to S_2. A405/H8a. Field of view 6.5 mm.

(d) Syn-S_2 overgrowths over two earlier, pre-S_2 andalusites with very fine equidimensional inclusions. Elongate inclusions in the overgrowth are continuous with S_2. Section perpendicular to l_2. A405/H8b. Field of view 3.9 mm.

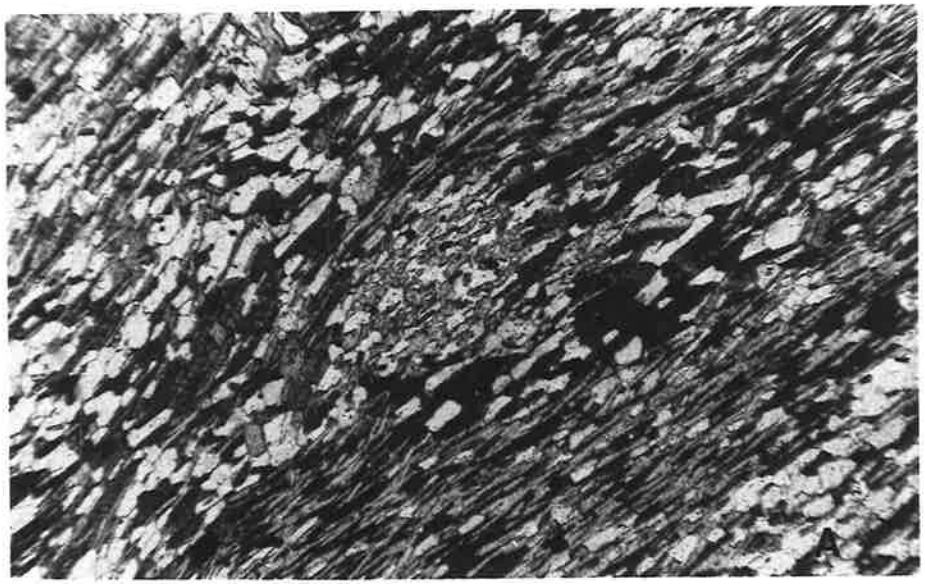
A

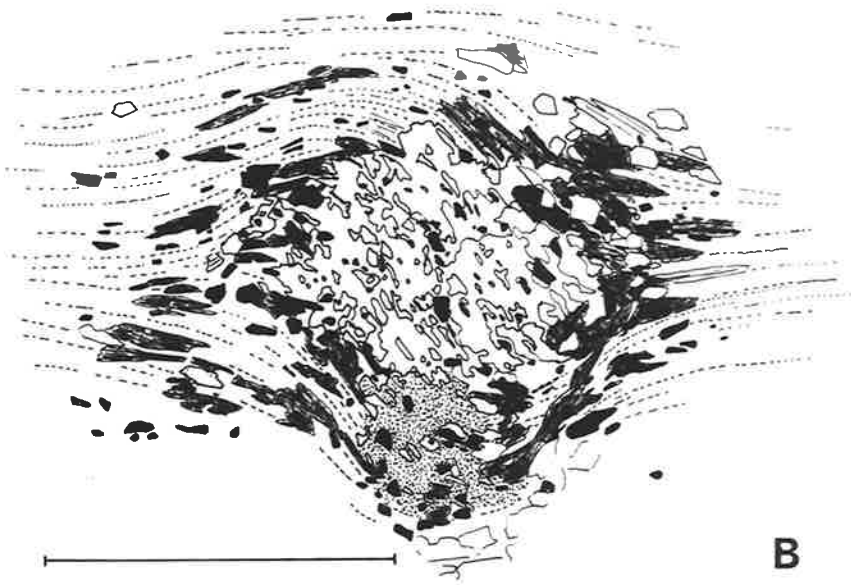
B

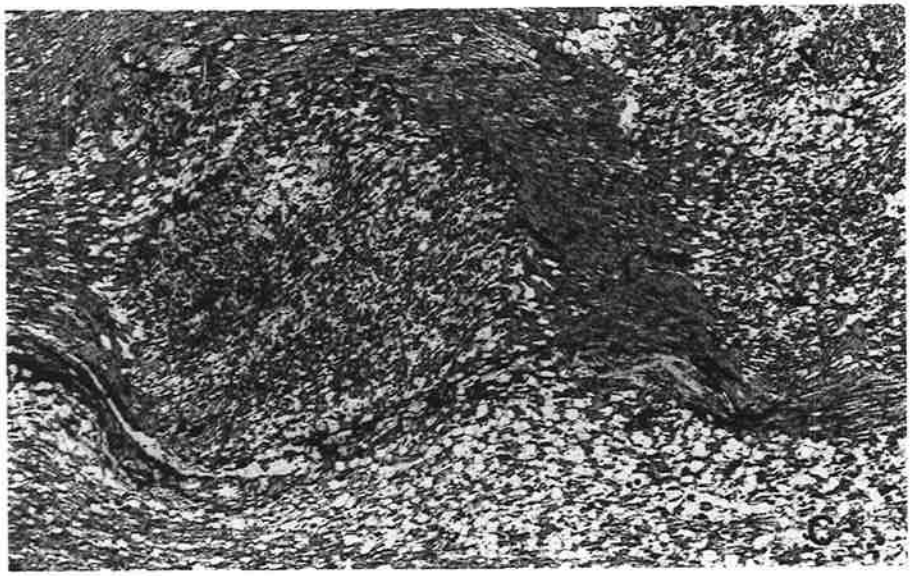
C

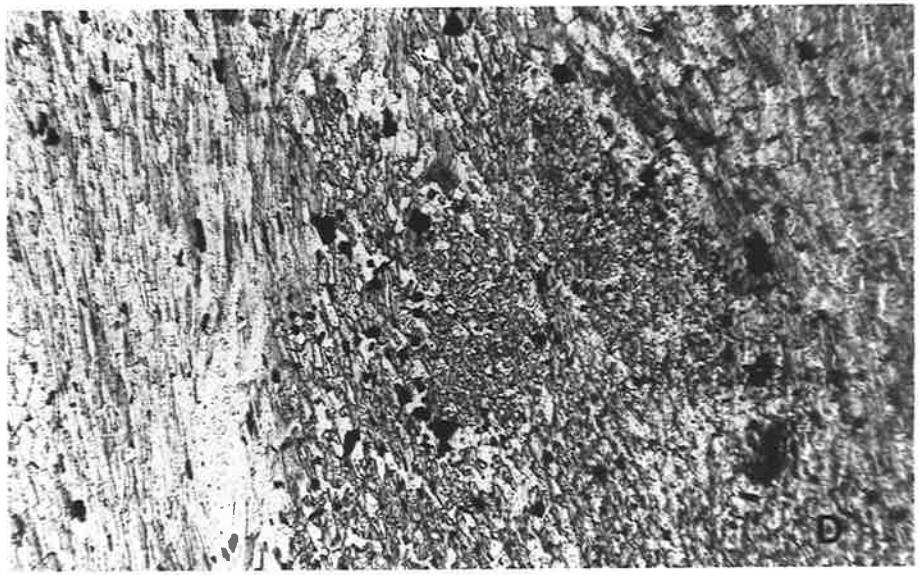
D

Plate 28

(a) A probable pre-S_2 staurolite aggregate. The slightly sigmoidal pattern of opaque inclusions (defining S_1) is continuous across the margins of adjacent crystals and is discordant with the external schistosity which is deformed about the aggregate, with the development of a quartz-filled pressure shadow area. Section perpendicular to l_3 and S_2. A405/BC34. Scale bar = 2.5 mm. "Shadowmaster" optical project drawing. Dashed lines indicate trend of schistosity (S_2). Probable post-S_2 biotites are outlined.

(b) Quartz inclusions in staurolite aggregates. Most inclusions are weakly aligned (see Plate 29(c)) to define a fold pattern which is discordant with S_2. This may be a pre-S_2 fold, however, recrystallization of the enclosing matrix and the development of F_3 crenulations has confused the textures. Section perpendicular to l_3. A405/BC37. Field of view 12.5 mm.

(c) Idioblastic staurolites associated with a ragged poikiloblastic andalusite. The sharp staurolite margins cut across the quartz inclusions of the andalusite. This would suggest these staurolites are later than the andalusite. Differing surface energies of andalusite and staurolite may be relevant, however. A405/MD5. Field of view 3.9 mm.

(d) Two intergrown staurolite crystals within a poikiloblastic andalusite. As their sharp margins cut across the andalusite inclusions, it seems probable that the aggregate formed post-andalusite rather than synchronously (although surface energies must also be considered). A405/BC37a(2). Field of view 3.1 mm.


A

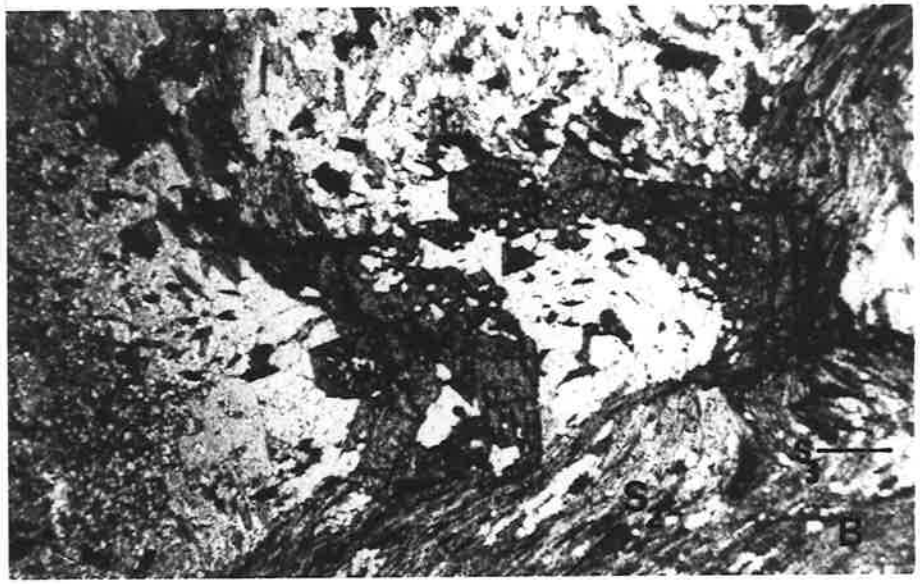
S1
S2
B

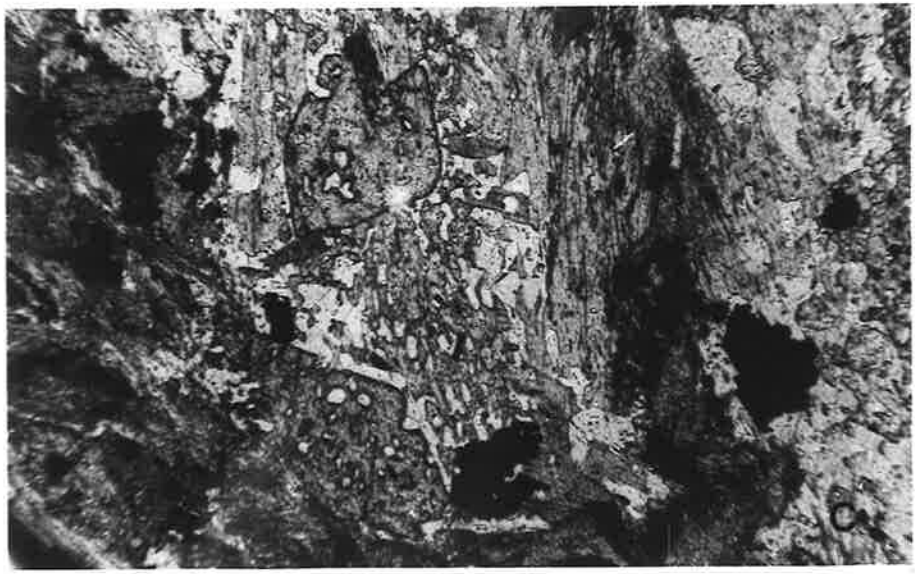
C

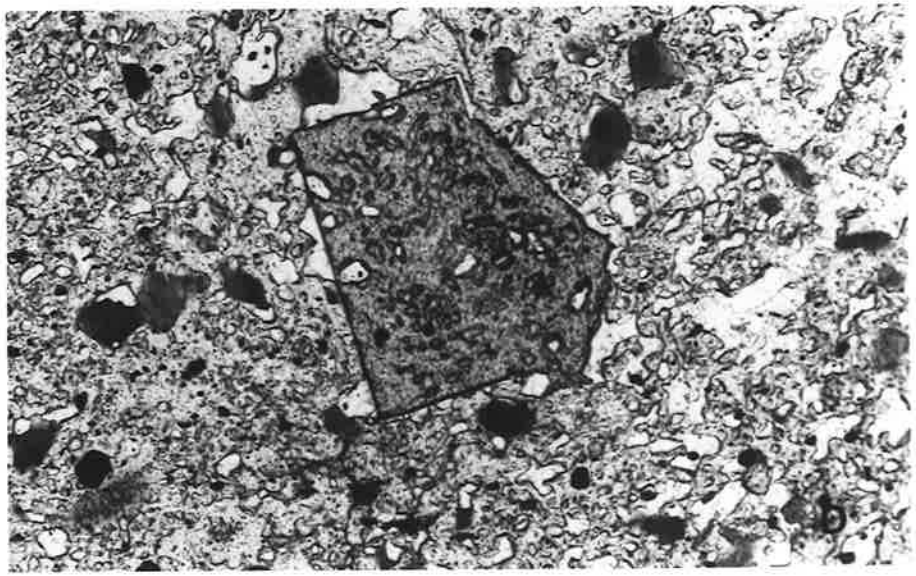
b

Plate 29

(a) A staurolite porphyroblast with opaque inclusions defining a pattern with similar orientation to the external fabric, abruptly truncates that fabric A405/E4E. Field of view 12.5 mm.

(b) Closer view of staurolite in (a). The crystal is possibly of pre-S_2 origin. Although inclusions have the same orientation as the S_2 matrix, the ragged appearance of the margins might suggest an earlier origin, with inclusions defining S_1 which is sub-parallel to S_2 as seen in nearby andalusites. Section perpendicular to l_3. A405/E4E. Field of view 3.9 mm.

(c) Closer view of staurolite aggregate in Plate 28(b). While fine quartz and opaque inclusions seem to define a pre-S_2 fold pattern, the intergrown staurolite and biotite at the fold hinge may have formed syn-S_2 or post-S_2. Section perpendicular to S_2 and l_3. A405/BC37. Field of view 5 mm.

(d) Quartz-filled pressure shadow in S_2 adjacent to a pre-S_2 andalusite. Section perpendicular to l_2. A405/BC34c. Field of view 14 mm.

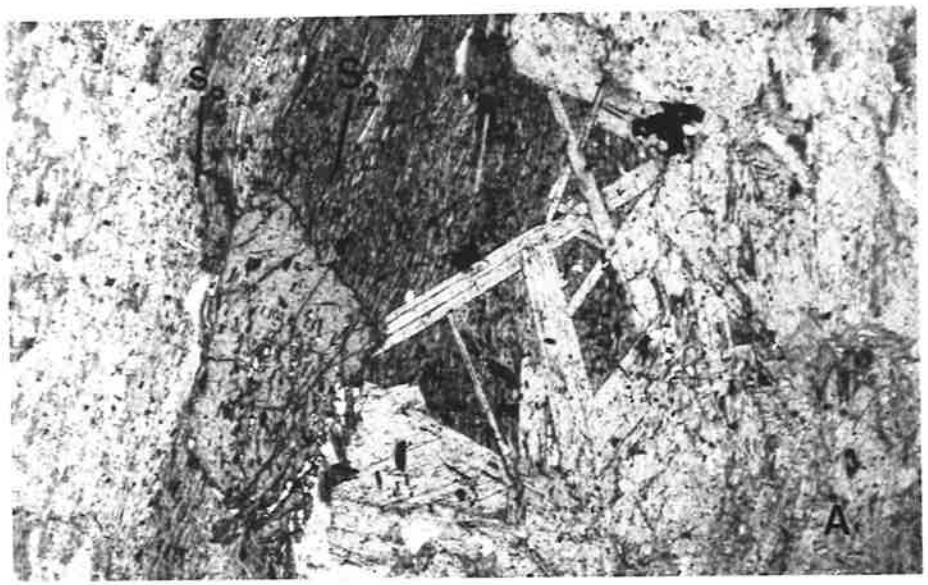
S1
S2
A


B

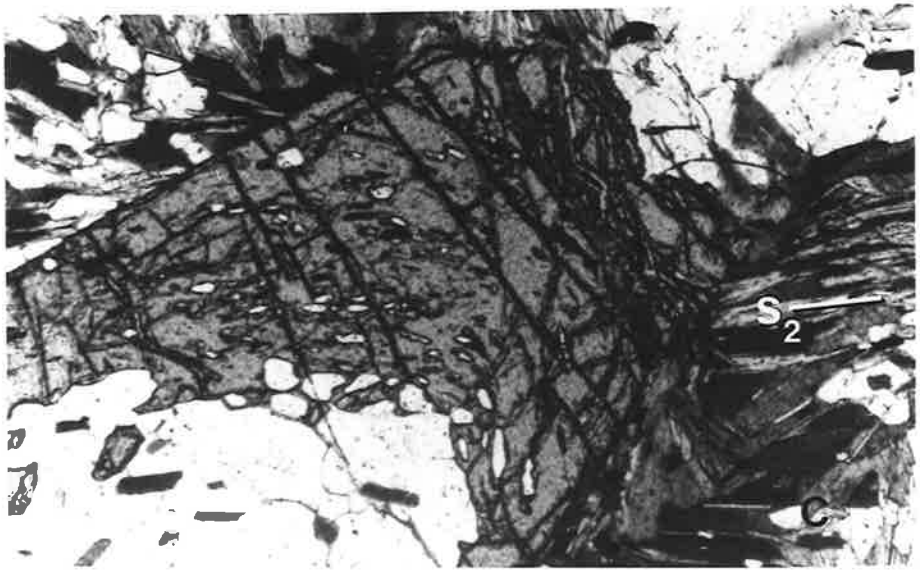
S2
C

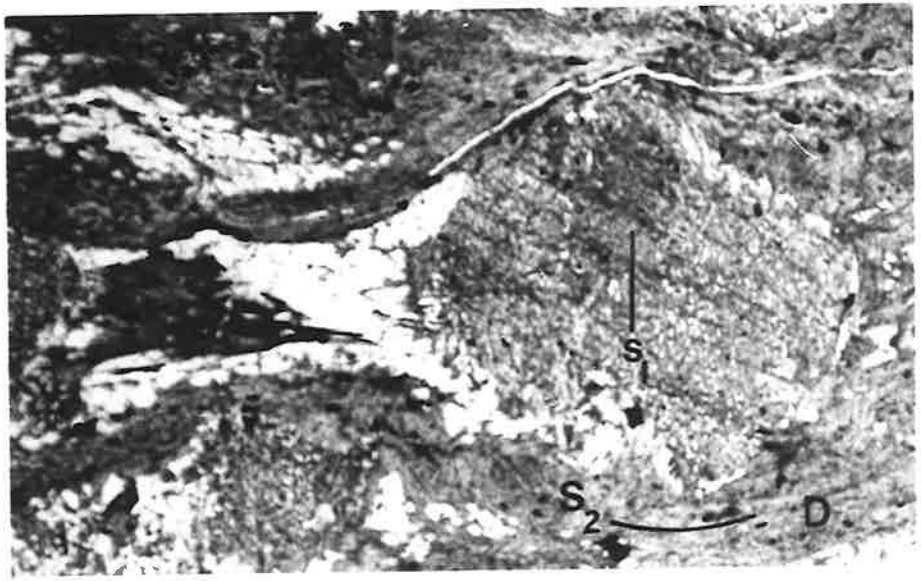
S1
S2
D

Plate 30

(a) F_3 crenulations of S_2 micas emanating from the margins of an augen structure in S_2. Some muscovite plates which largely fill the augen seem to have grown post-S_3. Section perpendicular to l_3. A405/BC42. Field of view 12.5 mm.

(b) F_3 crenulations in fibrolite mats. Earlier (syn-S_2?) fibrolite needles aligned in S_2. Later syn-S_3 fibrolite has formed in the axial planes of the crenulations. Section perpendicular to S_2 and approximately perpendicular to l_3. Relict andalusite grains (a) are present in trace amounts in the quartz-rich zones. A405/BC29. Field of view 12.5 mm.

(c) Fibrolite crystallized in S_3. Some earlier fibrolite is crenulated. While no andalusite remains in the rock, the abundance of coarse muscovite and biotite plates alludes to its breakdown to fibrolite. Section perpendicular to l_3. A405/BC42. Field of view 3.9 mm.

(d) Syn-S_3 biotites formed in pre-S_2 augen where the anisotropic control of S_2 is absent. Towards the margins of the augen where the anisotropic fabric of the S_2 schistosity is approached, the S_3 biotites are deflected from the average S_3 orientation into that of S_2. Section perpendicular to S_3. A405/BC27(3). Field of view 14 mm.

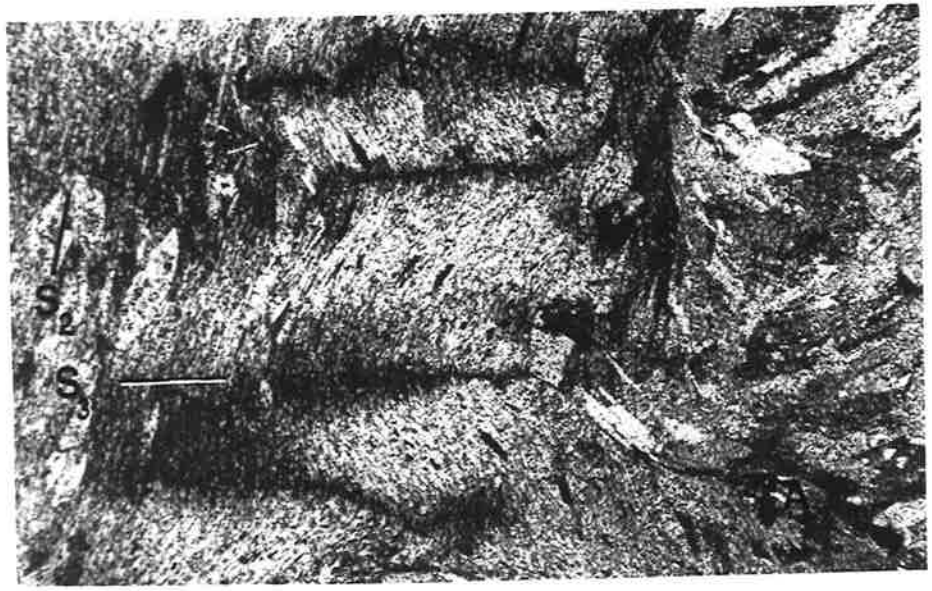
S2
S3


a
S3
S1
S2
B

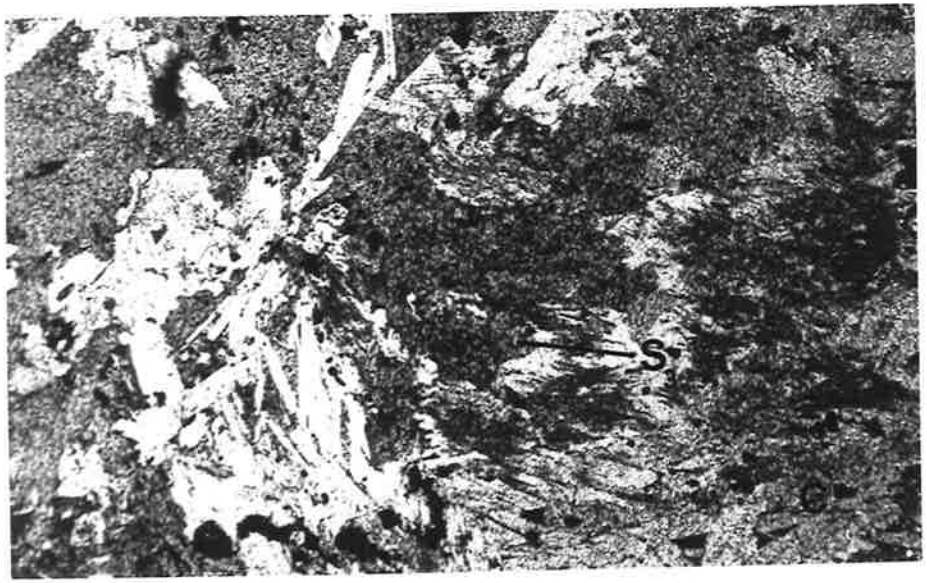
S1
C

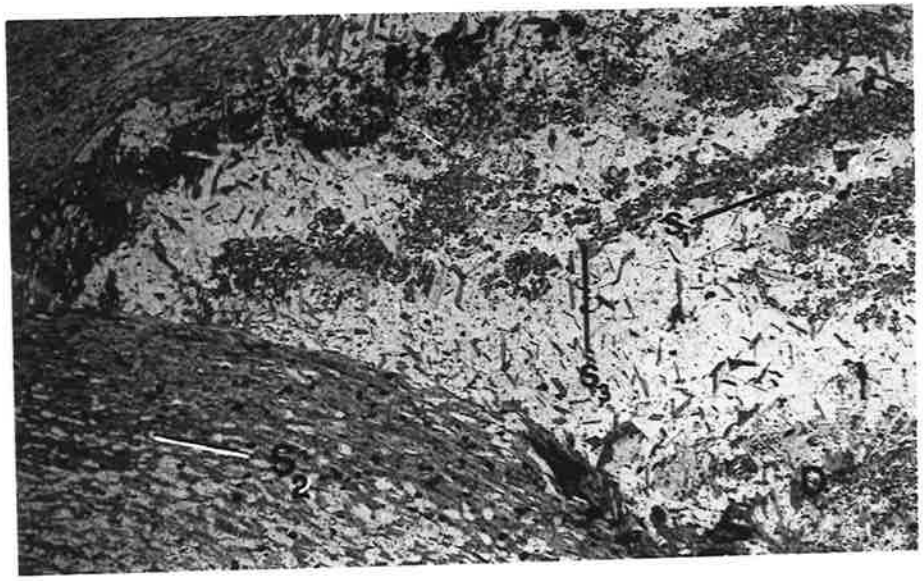
S1
S3
S2
D

Plate 31

(a) S_3 developed as a weak schistosity in quartz-rich augen with relict andalusite parallel to S_1. Syn-S_3 biotites are poorly aligned and are commonly deflected by quartz grains. The andalusites seem to be in optical continuity and are possibly relics after reaction with biotite to form sillimanite + quartz. Section perpendicular to S_3. A405/BC27(3). Field of view 14 mm.

(b) Crenulation of pre-S_3 fibrolite mats. Later syn-S_3 fibrolite needles have formed in the axial planes of the crenulations. Syn-S_2 biotite bands are slightly folded with S_3 as axial plane. Weakly aligned syn-S_3 biotites occur in the quartz-rich portions of the rock. Section perpendicular to S_3. A405/BC29. Field of view 14 mm.

(c) Orientation of biotites in metasiltstone has a large component of alignment in S_2 and a minor alignment in S_3. Section perpendicular to S_3. A405/E10. Field of view 14 mm.

(d) Post-S_2 idioblastic almandine garnet with ragged margin developed within a quartz-rich layer showing the effects of fine compositional control on garnet abundance and form. A405/E4E. Field of view 12.5 mm.


S2
S1
A

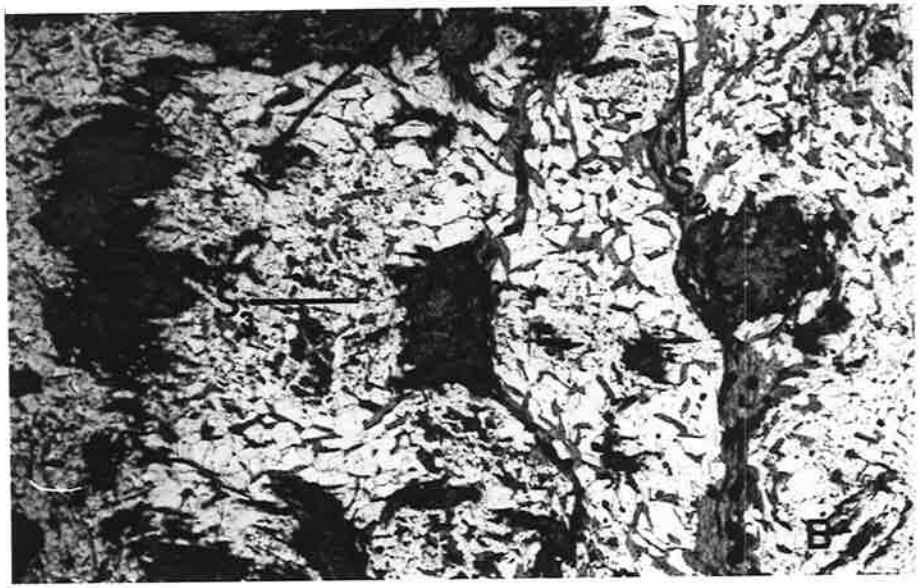
S2
B

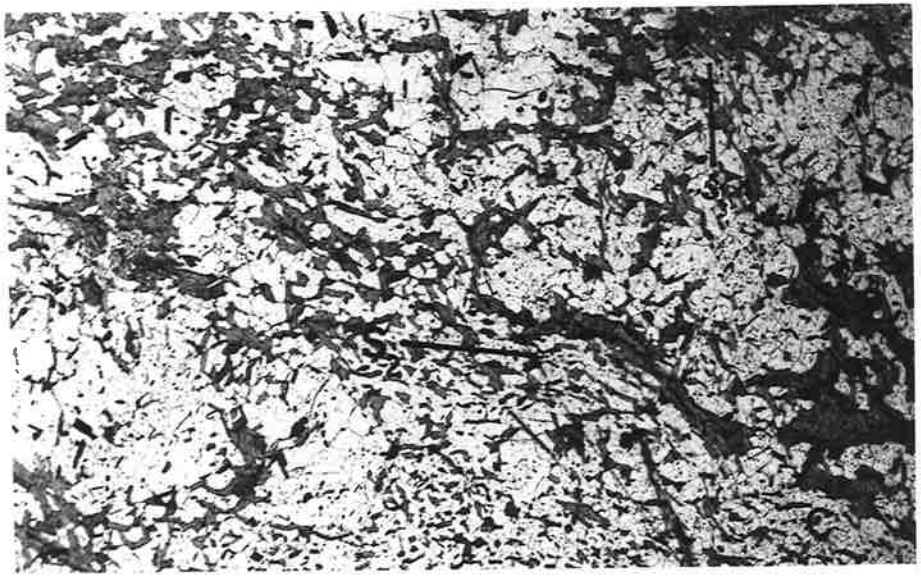
S1
C

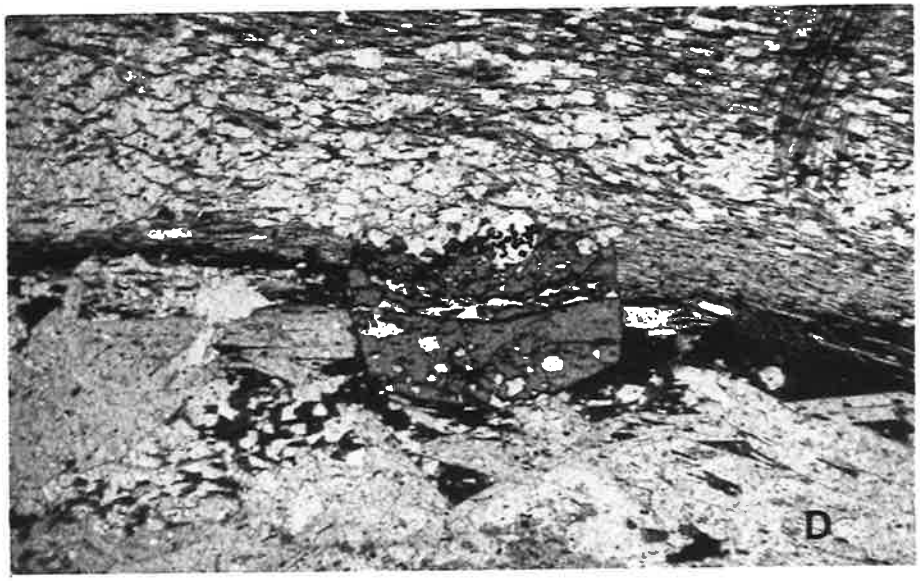
D

Plate 32

(a) Syn-S_2 garnet. A slight "snowball" structure is defined by opaque mineral and quartz inclusions. This pattern is continuous with S_2. Section perpendicular to S_2 and l_2. A405/E2A. Field of view 6.5 mm.

(b) A possible post-S_2 garnet. Opaque mineral inclusion pattern is continuous with the external S_2 fabric. Only very slight deflection of S_2 at the porphyroblast margins has occurred. Section perpendicular to S_2, l_2. A405/E2A(P). Field of view 6.5 mm.

(c) Sillimanite crystals with typical diamond-shaped cross sections considered to be directly replacing a poikiloblastic andalusite porphyroblast. Polars crossed. A405/E2A. Field of view 3.9 mm.

(d) Coarse sillimanite needle lying across earlier andalusite and a biotite-fibrolite mat. This crystal probably formed by direct polymorphic inversion of the skeletal andalusite. The coarse disoriented biotite plates which cut across and partly envelope the unstable andalusite are probably related to the formation of the nearby fibrolite (reaction system 2). A405/MD5. Field of view 3.1 mm.

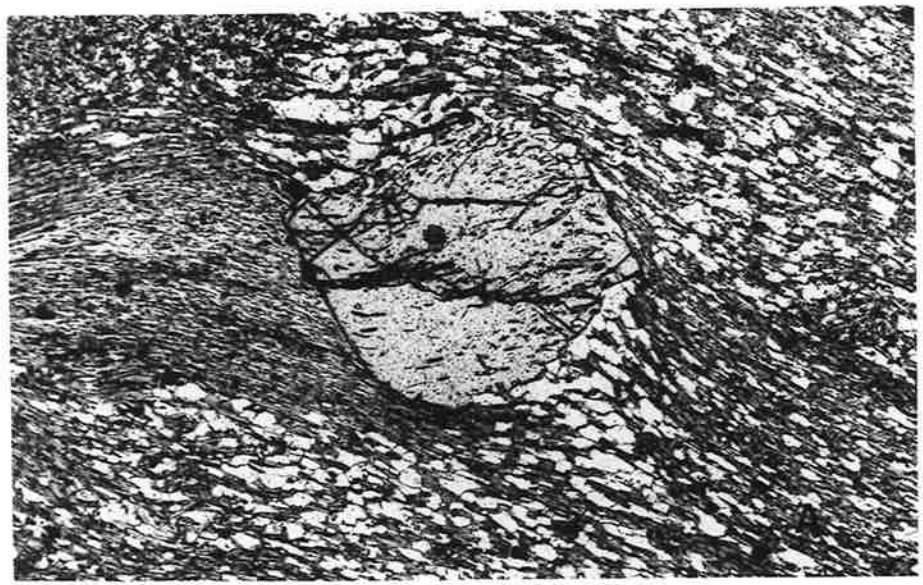

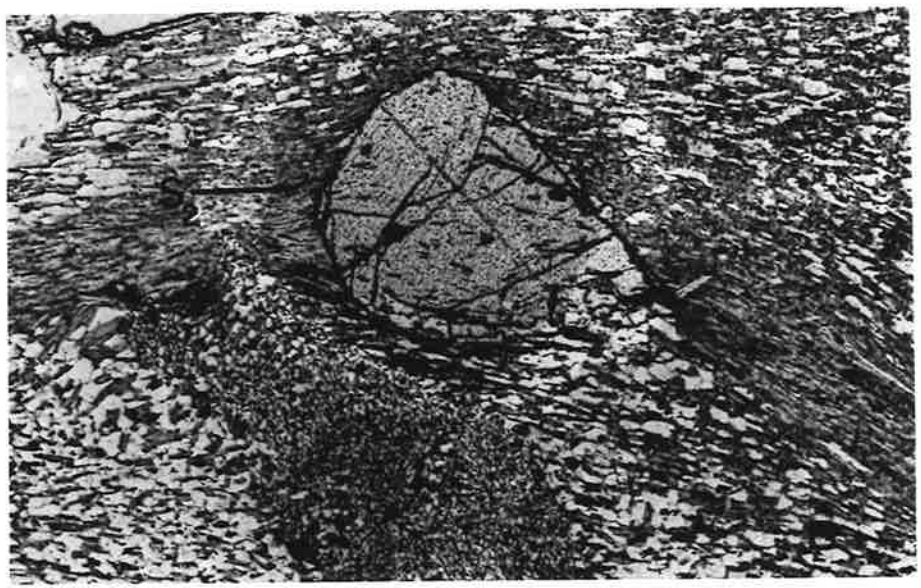

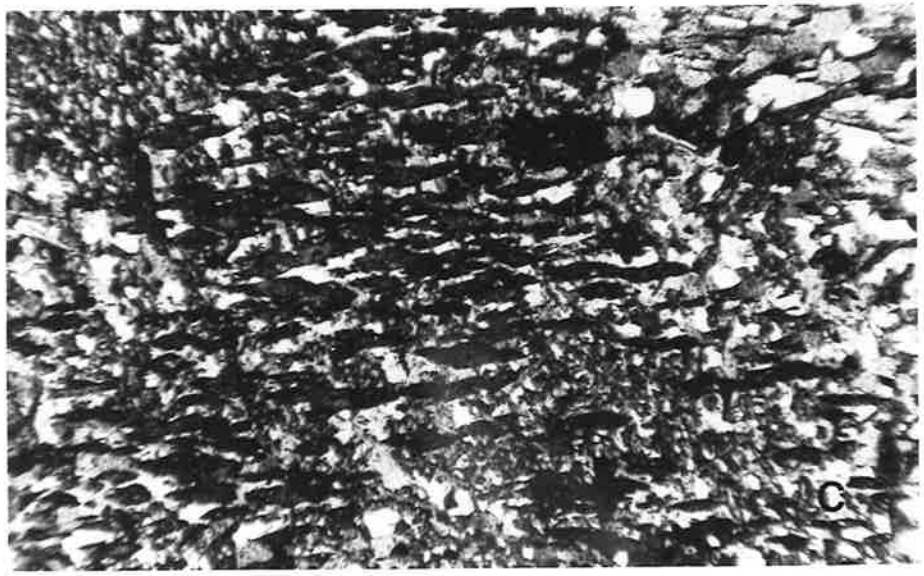
C


D

Plate 33

(a) Coarse plates of biotite forming a partial envelope around a poikiloblastic andalusite. Some biotites cut across and fill embayments in the andalusite. Nearby, fibrolite emanates from biotite into quartz and a fibrolite mat has formed from the breakdown of biotites in the matrix. A405/BC29. Field of view 3.9 mm.

(b) Skeletal andalusite enclosed by coarse, disoriented biotites. Mutual boundaries are diffuse (bottom left). A405/BC29. Field of view 3.9 mm.

(c) Relict andalusite within a fibrolite mat. The fibrolite has presumably formed from disoriented biotite crystals which replaced the andalusite (reaction 2(a)) and probably formed during a static phase as the needles form completely disoriented sprays, possibly mimicing the orientation of the earlier biotites. Coarser, prismatic sillimanite occurs nearby, probably a direct replacement of some relict andalusite. A405/BC29. Field of view 3.9 mm.

(d) Mat of fibrolite surrounding a poikiloblastic andalusite which is thought to be in the process of replacement by coarse disoriented biotite plates. Syn-S_3 biotites formed in the axial planes of crenulations of earlier fibrolite aligned in S_2. A405/MD5. Field of view 3.1 mm.

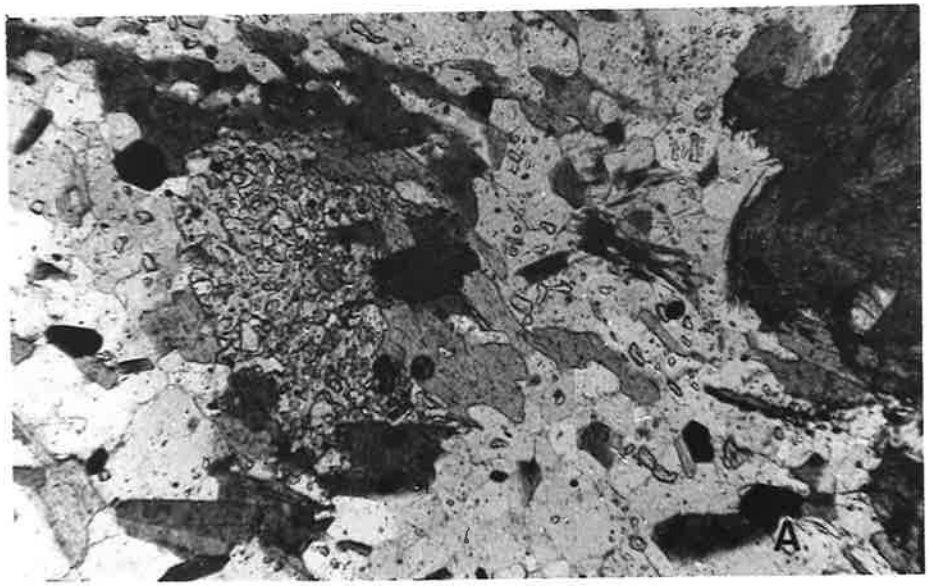
A

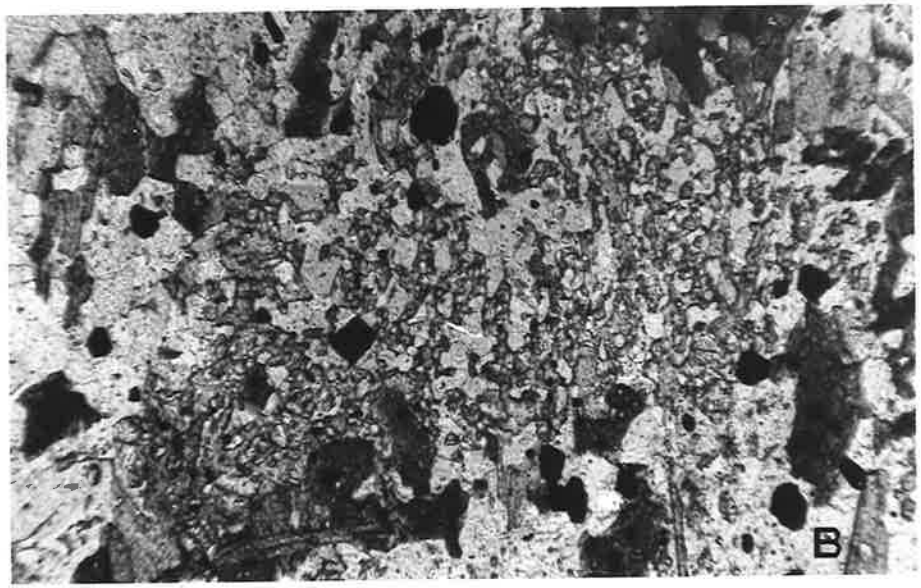
B

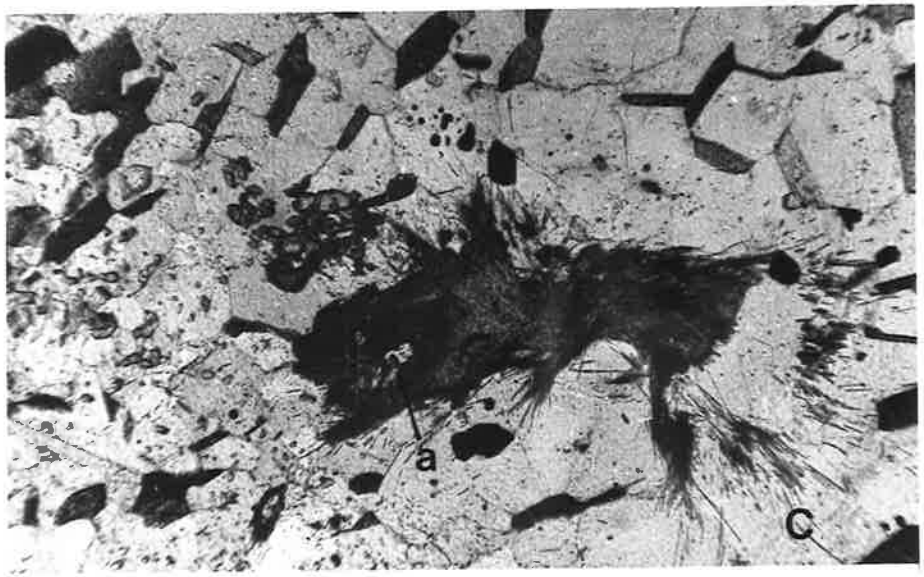
a
C


S
D

Plate 34

(a) Fibrolite mat adjacent to andalusites showing replacement by biotites. Much fibrolite parallels S_2 but some crystals show considerable deviation and probably formed during the static post-S_2 period, largely mimicing the orientation of biotites with diverse orientations. Section perpendicular to S_2 and l_3. A405/MD5. Field of view 3.9 mm.

(b) Fibrolite mats within and enclosing a recrystallized augen structure. No andalusite is present and there is no evidence of its replacement by biotite or muscovite. Either the fibrolite source was andalusite elsewhere in the rock, in which case the migration of Al would have to be greater than suggested by Carmichael (1969), or the fibrolite formed by the process of nucleation as suggested by Chinner (1961). Fibrolite orientation may be regarded as mimicing S_2 and S_3 biotites. Section perpendicular to S_2 and S_3, l_3. A405/E4E. Field of view 3.9 mm.

(c) Coarse idioblastic muscovites formed across and probably replacing earlier biotite crystals which are aligned in S_2. In the near vicinity of this texture andalusite is replaced by muscovite (Plate 34(d)). A405/E4E. Field of view 3.9 mm.

(d) Coarse muscovites replacing andalusite and quartz-biotite matrix. Relict matrix contains S_2-oriented biotites which give the impression of fanning out about the presumably pre-S_2 andalusites. Opaque inclusions in the andalusites, which are much finer than the enclosing matrix, are retained in the muscovites. The isolated small patches of andalusite are mostly in optical continuity with nearby larger andalusite relics. A405/E4E. Field of view 12.5 mm.


A

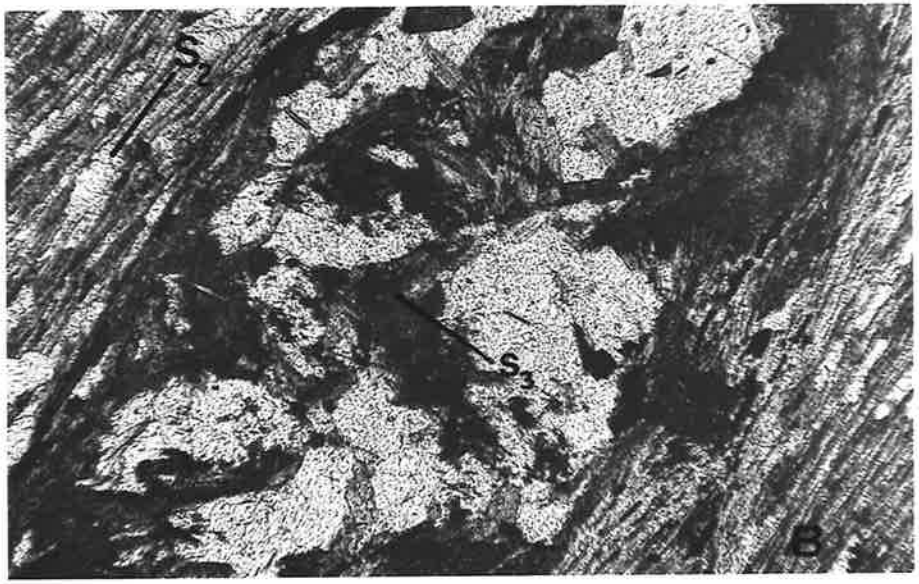
S_2
S_1
B

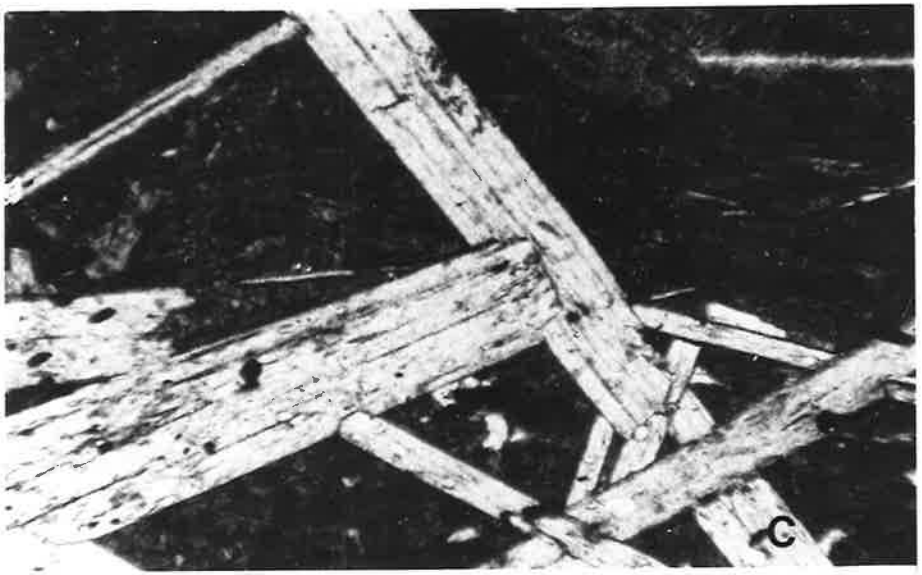
C

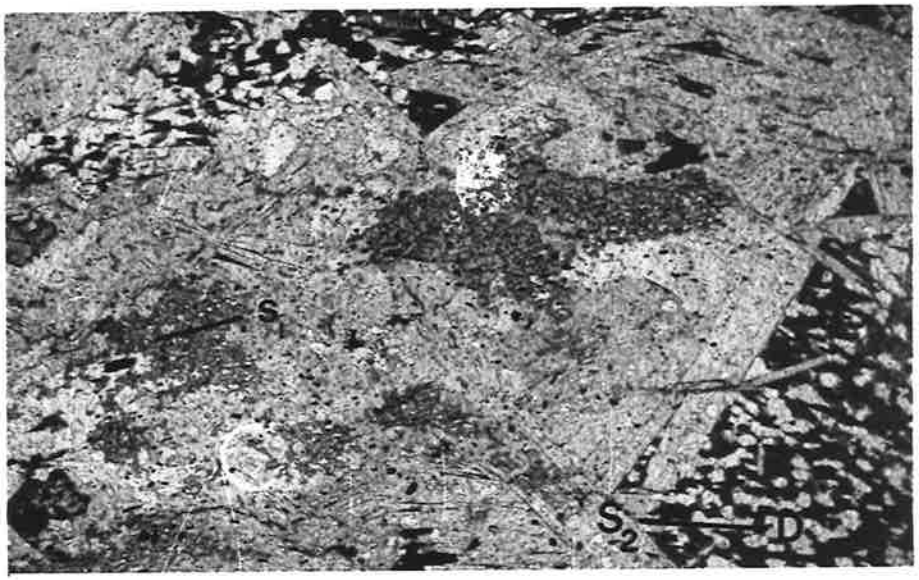
S
S_2
D

Plate 35

(a) Closer view of F_2 fold hinge zone as shown in Plate 32(a). S_2 appears to cut off an earlier schistosity defined by finer biotites. These biotites are assumed to be pre-S_2 because (i) the section is close to the S_3 plane and only 001 faces of S_3 biotites should be present (which they are not) and (ii) staurolites elsewhere in the rock show a relict fabric in their pattern of opaque inclusions which has a similar orientation. Coarse muscovites related to the breakdown of andalusite replace biotite and some quartz. Section perpendicular to l_2. A405/E4. Field of view 5 mm.

(b) Extensive muscovitization of pre-S_2 augen containing elongate poikiloblastic andalusites which possibly define an earlier schistosity (S_1) which is inclined at a low angle to S_2. Inclusions in the relict andalusite are elongate in this direction and are markedly finer than the enclosing matrix. A405/E4E(2). Field of view 12.5 mm.

(c) Relict skeletal andalusite in an aggregate of coarse muscovites. The extensive replacement of the andalusite and its quartz inclusions by muscovite (reaction 4a) has left isolated patches of andalusite in optical continuity. Opaque minerals have been unaffected and remain as inclusions in the muscovite. These are commonly elongate and are aligned in the same sense as quartz inclusions in the andalusite which seem to define a relict pre-S_2 schistosity. A staurolite crystal (St) is also enclosed by muscovite and it is uncertain whether any replacement of this mineral has occurred; its margins are straight and sharper than those of the unstable andalusite. A405/E4E. Field of view 3.9 mm.

(d) F_3 crenulations of S_2 micas. Crenulation axial planes are deflected by muscovite aggregates and staurolite porphyroblasts. The

Plate 35 (cont'd)

muscovite aggregates about which S_2 is also deformed provide evidence of the earlier presence of andalusite. Section perpendicular to l_3. A405/BC38(b). Field of view 14 mm.

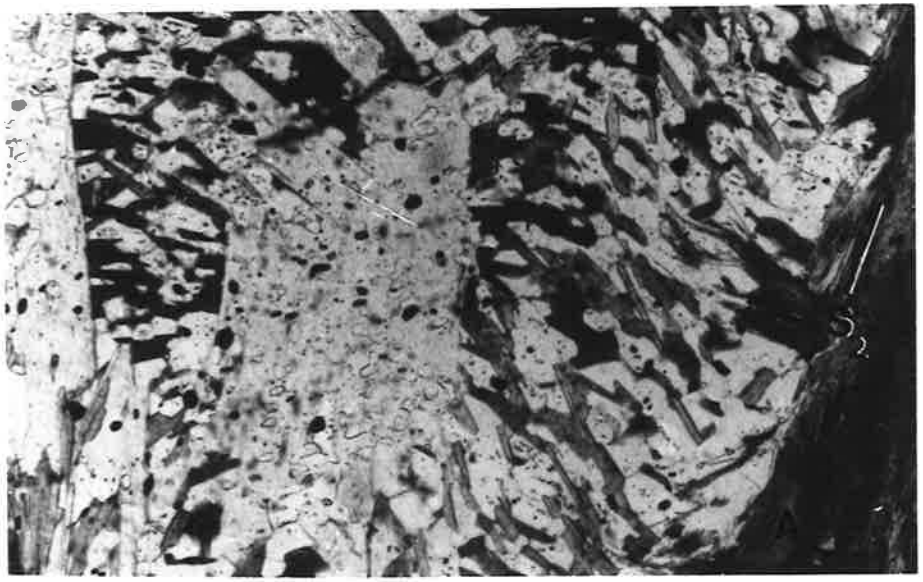
S2
A

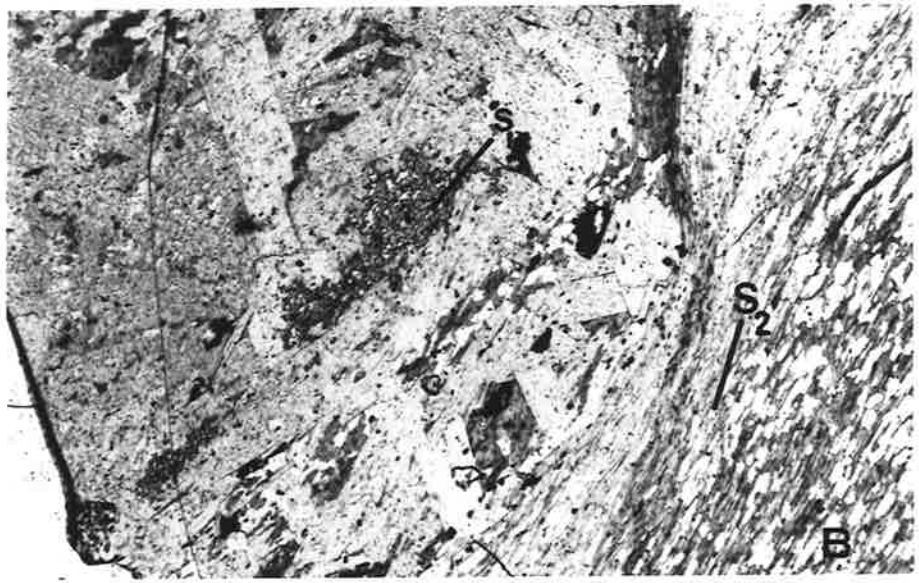
S1
S2
B

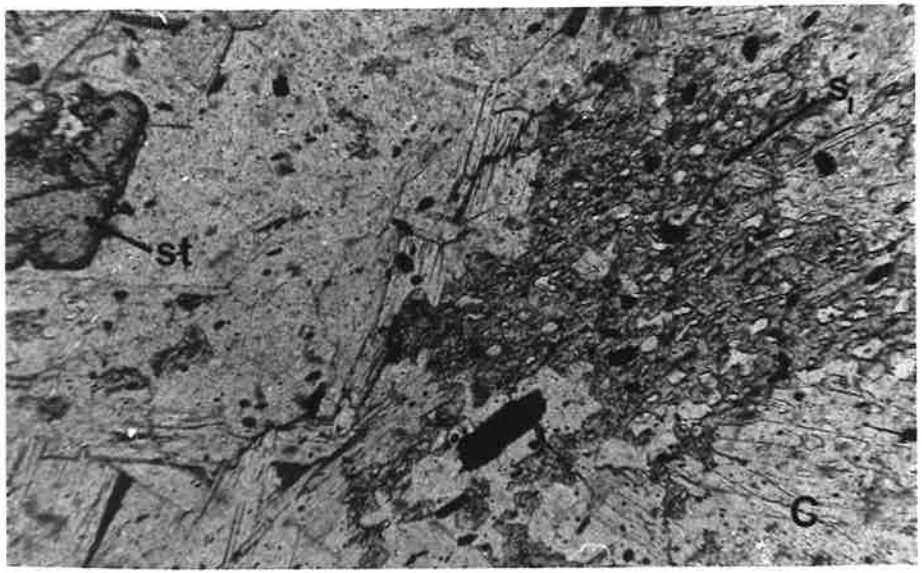
S1
st
C

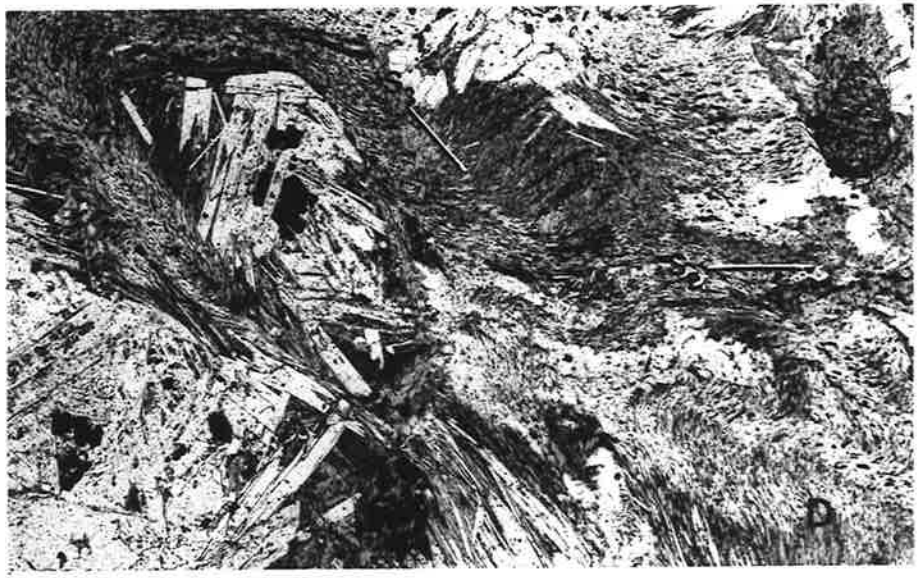
D

Plate 36

(a) Fibrolite and biotite inclusions in equidimensional disoriented muscovites (outlined). Needles of fibrolite are mostly disoriented also. Elongate muscovites which are largely aligned in S_3, however, contain well aligned inclusions of fibrolite and biotite. A coarse subidioblastic chlorite cuts across the earlier muscovite and fibrolite. A405/E6(1). Field of view 3.1 mm.

(b) Largely well aligned biotite and fibrolite inclusions in coarse muscovites (outlined). Inclusions tend to parallel the long dimension of the more elongate muscovites and can be seen to parallel the cleavage in some crystals. A405/E6(1). Field of view 3.1 mm.

(c) Aggregate of randomly oriented coarse muscovites cut by well aligned needles of fibrolite. Some biotite remains along cleavage planes of the muscovite. A405/BC42. Field of view 3.9 mm.

(d) Poikiloblastic andalusite cut by syn-S_3 biotites. In close proximity are fibrolite needles in quartz which have also formed in S_3. Section perpendicular to 1_3. A405/BC37a(3). Field of view 5 mm.

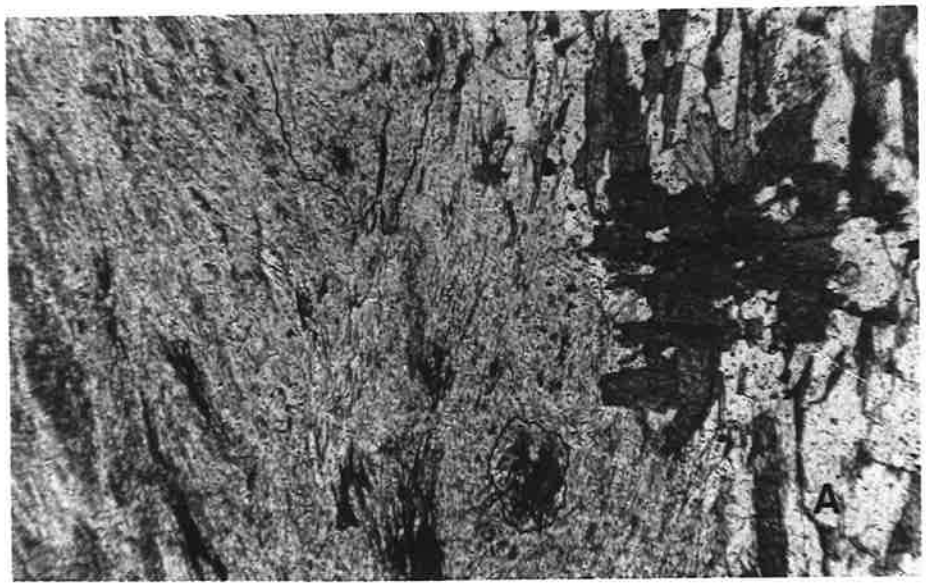
A

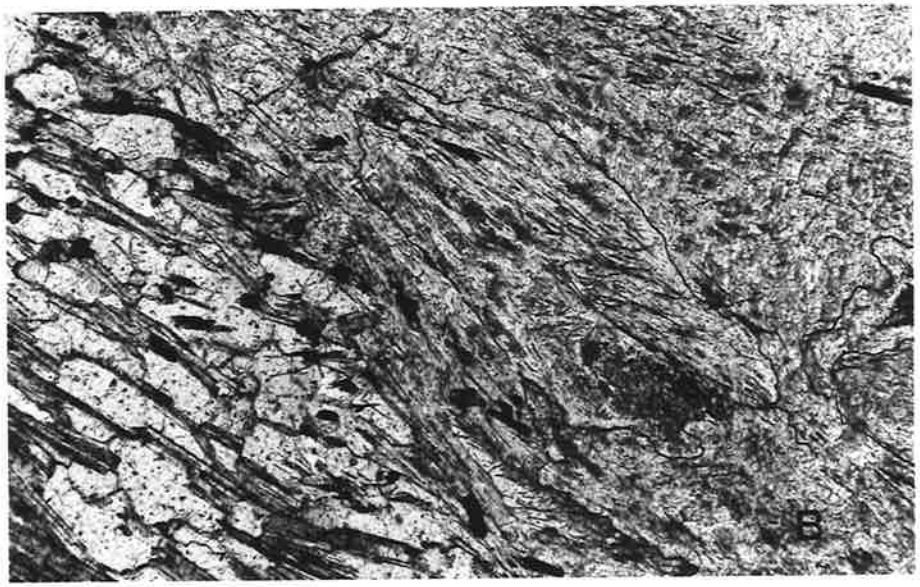
B


C

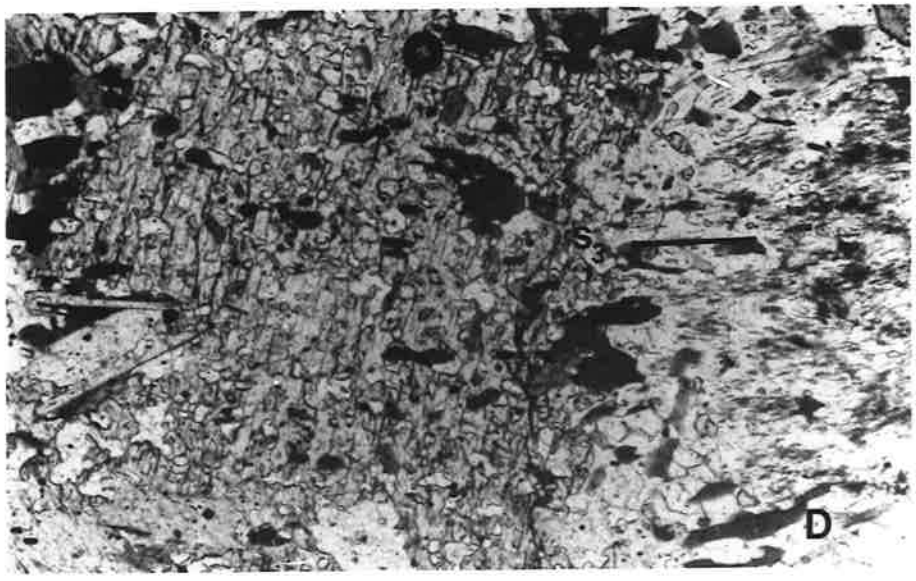
S3
D

Plate 37

(a) Coarse opaques associated with a fibrolite mat. The opaques are not intergrown with the fibrolite, however, and a poikiloblastic andalusite embayed by coarse biotites is present adjacent to the fibrolite mat. These are features consistent with the formation of the fibrolite via reaction system 2. A405/M21'. Field of view 5 mm.

(b) S_2 defined by narrow zones of strongly oriented biotites passing around earlier poikiloblastic andalusite porphyroblasts containing very fine weakly aligned quartz inclusions. A405/M21'. Field of view 14 mm.

(c) S_2 deformed about an earlier poikiloblastic andalusite in which quartz inclusions define an earlier planar structure S_1. Minor F_3 crenulations in S_2 micas have developed. The probable replacement of andalusite by coarse biotites is accompanied by the development of fibrolite mats adjacent to these areas. Section perpendicular to l_3. A405/M21'(P). Field of view 6.5 mm.

(d) Staurolite aggregate. The large crystal has a core choked with fine inclusions. A well defined rim is inclusion-free suggesting a later stage of slower growth. A405/BC37a(3). Field of view 5 mm.

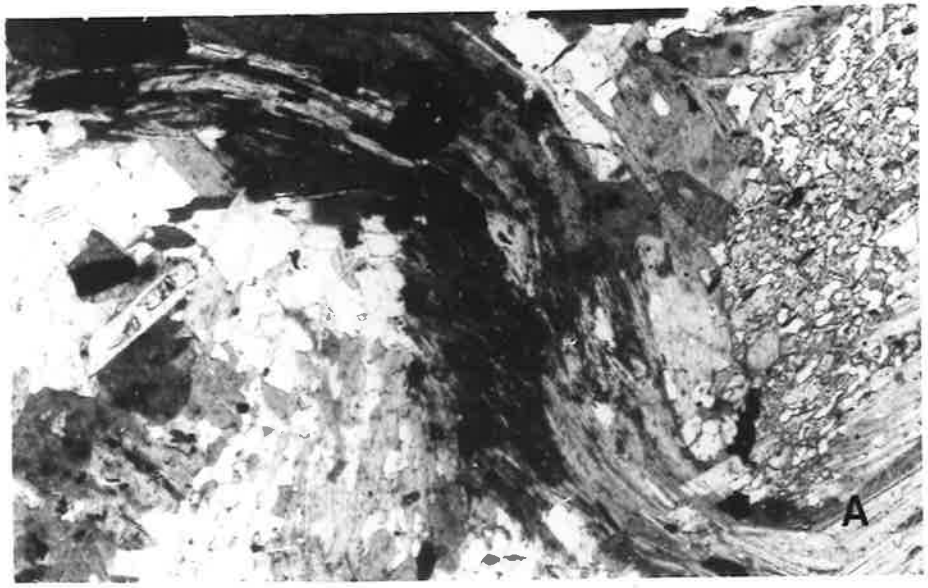
A


B

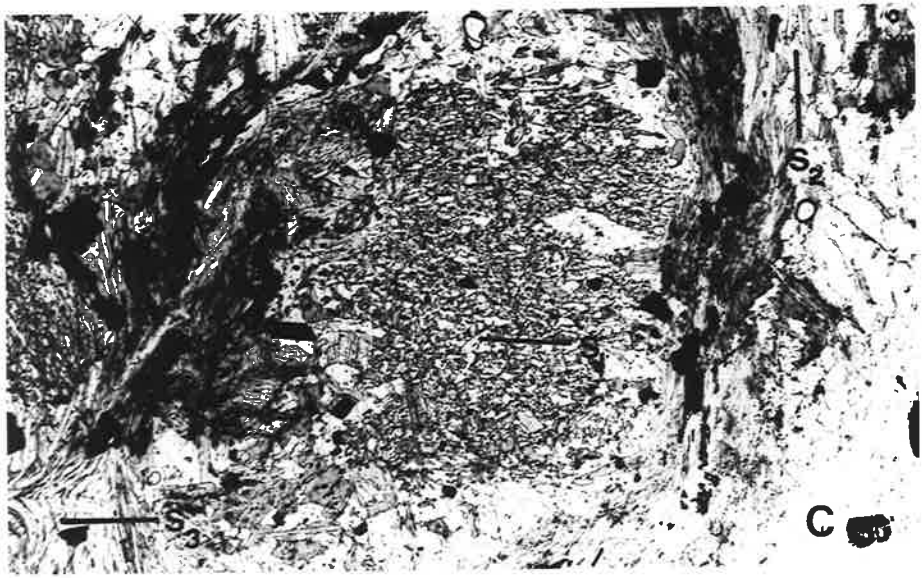
S_2
S_3
C

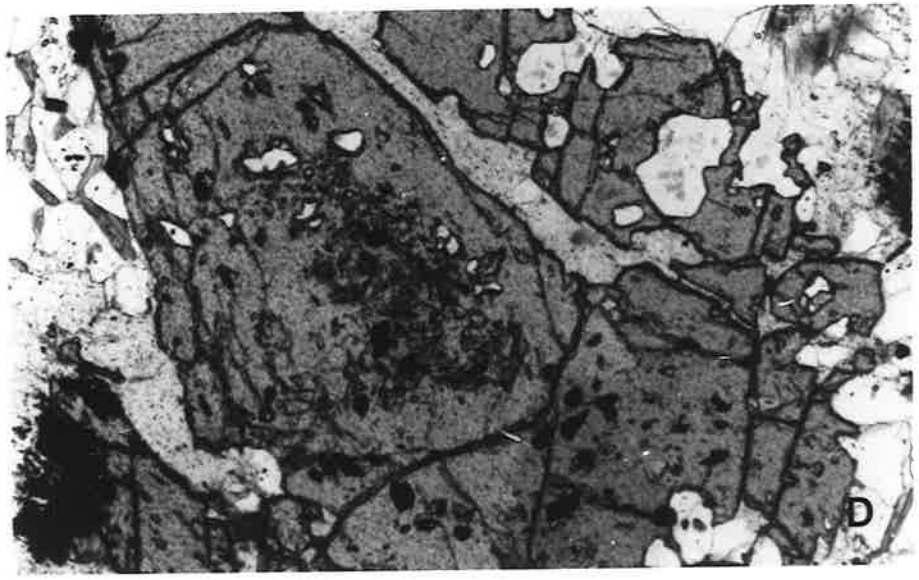
D

Plate 38

(a) Staurolite here appears stable in the presence of fibrolite as shown by the sharp boundaries of the staurolite crystals set in a fibrolite mat. A405/BC37a(3). Field of view 3.1 mm.

(b) Syn-S_3 biotites adjacent to poikiloblastic andalusites. These also cut across the andalusites and together with coarser disoriented biotites (b), appear to be replacing the andalusite. Fibrolite (f) and quartz formed in a separate domain. The smaller andalusite is partly replaced by coarse muscovite plates (m). A405/BC37a(3). Field of view 14 mm.

(c) Syn-S_3 fibrolite needles (f) in close proximity to andalusite porphyroblasts (a) which have broken down indirectly via reaction system 2. The fibrolite is largely aligned in S_3 which is also defined by weakly aligned biotites. The mimicing of biotite orientation has caused local variations in the orientations of the fibrolite needles. A405/BC37a(3). Field of view 14 mm.

(d) Post-S_2 staurolite. The variable size and shape of the quartz inclusions has been controlled by the pre-existing matrix. A405/BC37a(3). Field of view 5 mm.

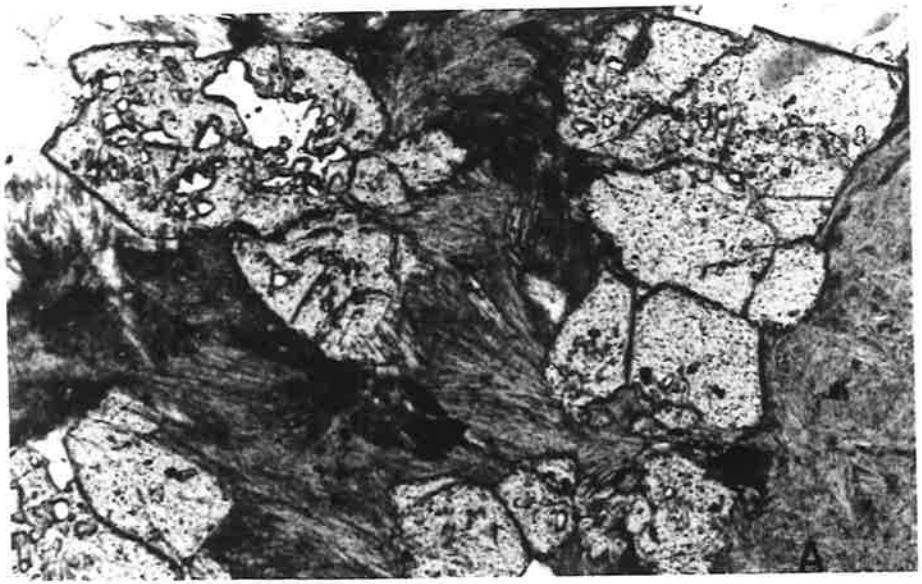
A

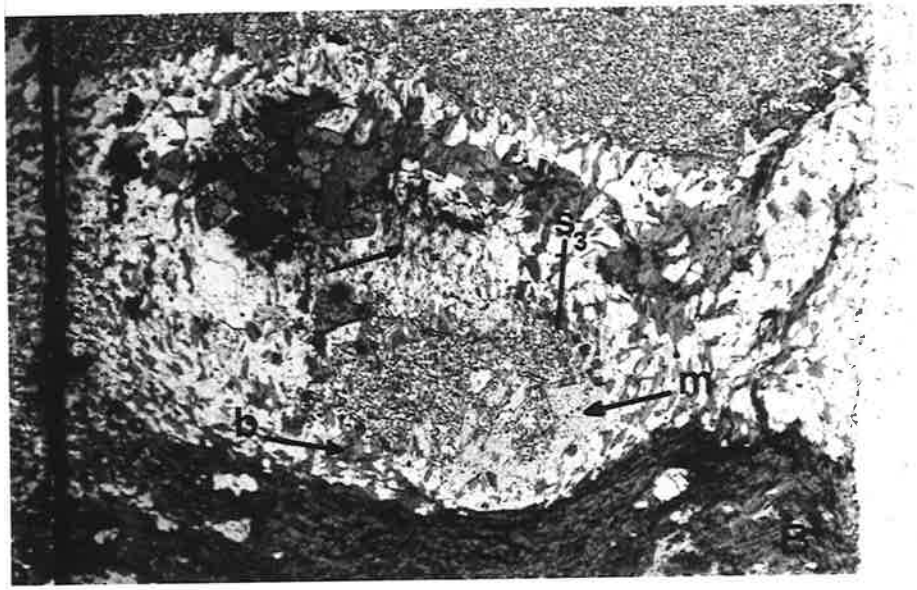
S_3
m
b
B

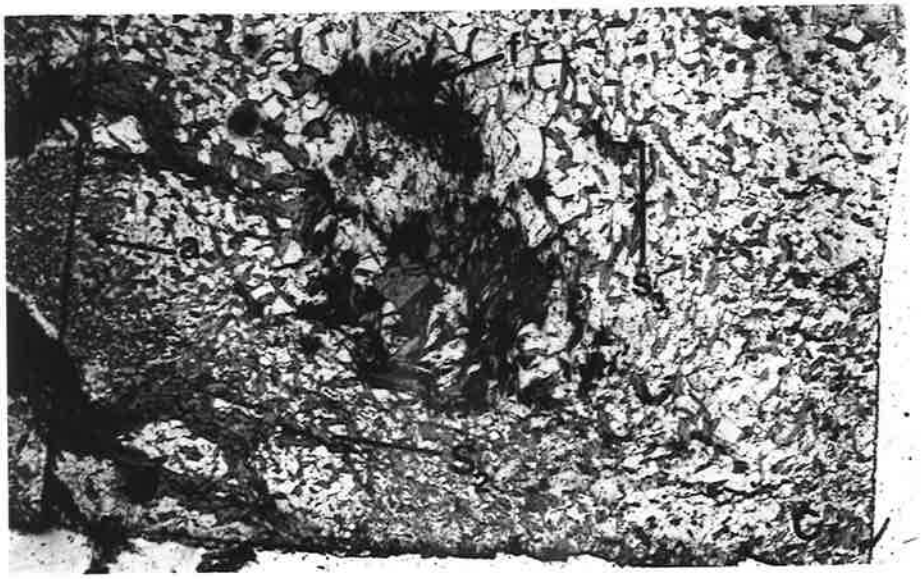
a
S
C

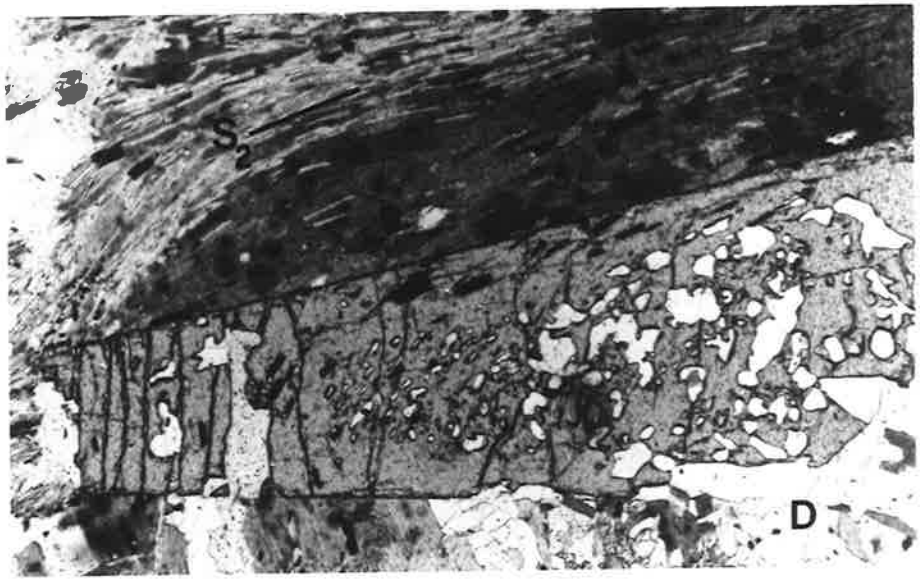
S_2
D

Plate 39

(a) Post-S_2 garnet. Inclusions are continuous with the external fabric. Those near the upper and lower margins of the crystal define a curved pattern which is also seen in the external schistosity which partly trends around the porphyroblast. A405/E2A(P). Scale bar = 2 mm. "Shadowmaster" optical projection drawing. Dashed lines indicate trend of schistosity (S_2). Probable post-S_2 coarse muscovites and biotites (shaded) are outlined. Biotite inclusions in garnet are shaded also.

(b) Truncation and minor deflection of S_2 schistosity around a garnet porphyroblast. The opaque inclusions are almost equidimensional and do not define any obvious pattern. Although the age relation of the porphyroblast with the schistosity is unresolved, the size of the inclusions suggests the garnet formed post-S_2, which is compatible with the high degree of truncation of S_2(but c.f. Ferguson and Harte, 1975). Section perpendicular to S_2 and 1_3. A405/E4E(1). Scale bar = 2.5 mm. "Shadowmaster" optical projection drawing. Dashed lines indicate trend of schistosity (S_2). Probable post-S_2 coarse muscovites and biotites (shaded) are outlined.

(c) Post-S_2 staurolite aggregate. The opaque inclusion pattern passes through the individual crystals and is continuous with the external S_2 fabric. Section perpendicular to S_2 and 1_3. A405/BC37a. Scale bar = 2 mm. "Shadowmaster" optical projection drawing. Dashed lines indicate trend of schistosity (S_2). Probable coarse post-S_2 muscovites and biotites (shaded) outlined. Also shown is a post-S_2 chlorite rosette (ch).

(d) Fibrolite needles passing into the coarse prismatic form of sillimanite which may reflect locally elevated temperatures following the formation of fibrolite, or alternatively, a decrease in the rate of reactions producing sillimanite. A405/M21' (b). Field of view 3.1 mm.

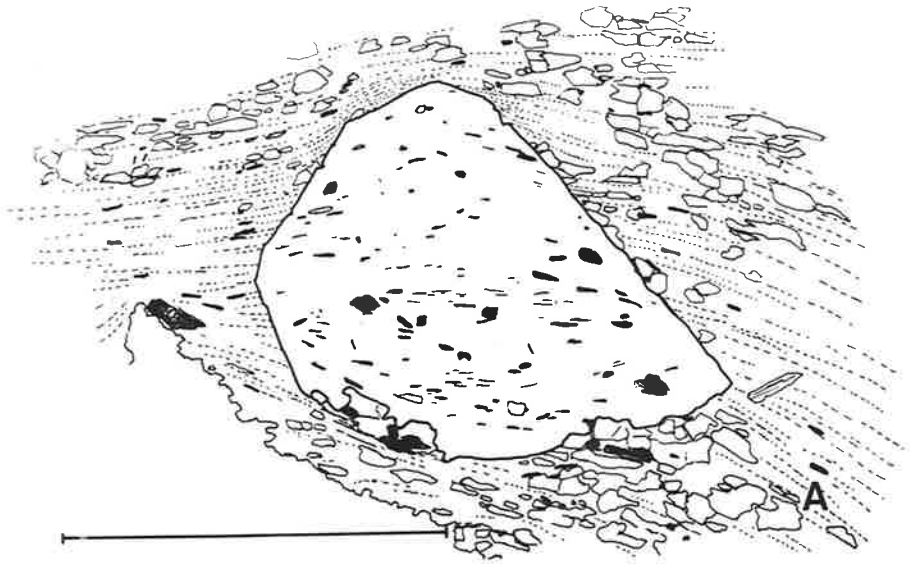
A

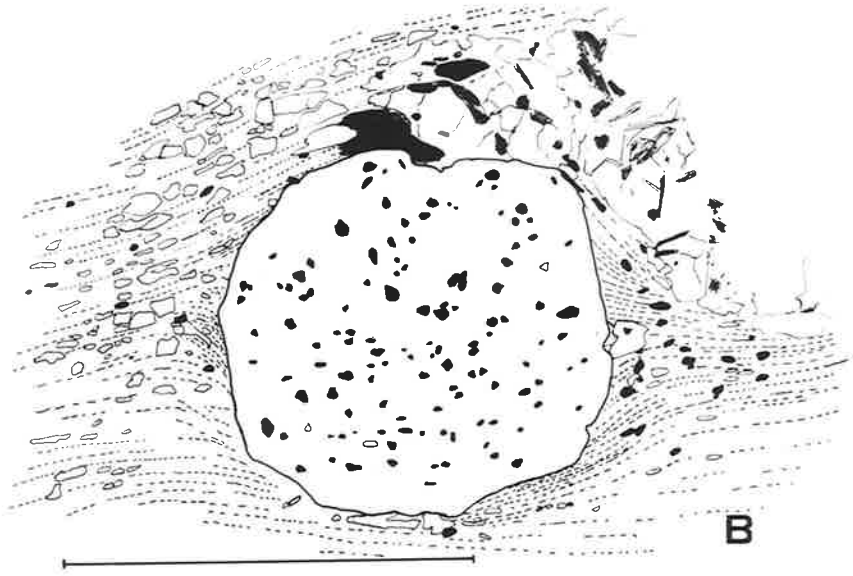
B


Ch
C

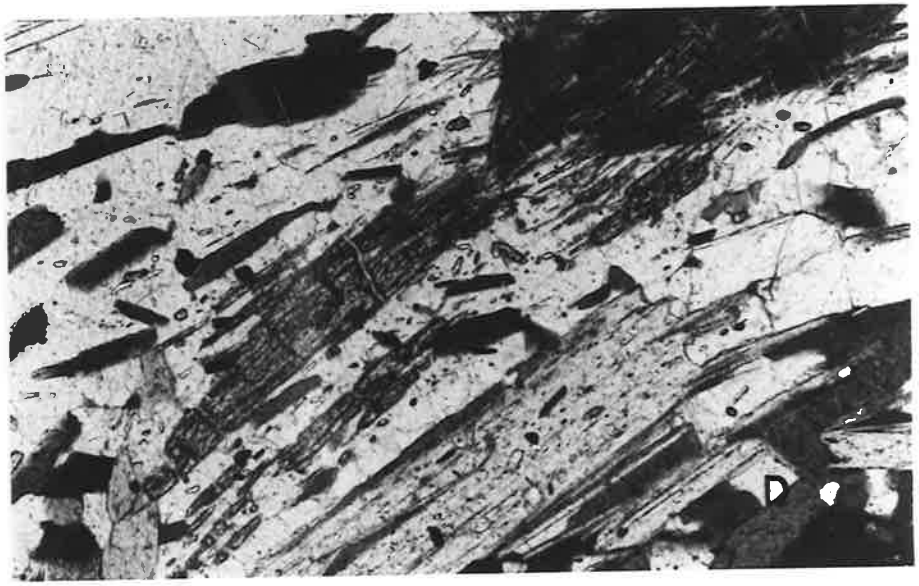
D

Plate 40

(a) F_3 crenulations of S_2 micas. The large muscovite aggregate, presumably a replacement of andalusite, appears to be pre-F_3. Section perpendicular to S_3 and l_3. A405/BC34(a). Field of view 14 mm.

(b) Pre-S_2 staurolite containing quartz and opaque mineral inclusions which define a sigmoidal inclusion pattern which is discordant with the S_2 schistosity. A small quartz-filled pressure shadow has developed. Section perpendicular to l_2, S_2. A405/BC38b. Field of view 14 mm.

(c) Quartz-rich augen structure in S_2. Post-S_2 recrystallization has destroyed any internal fabric. Some weak F_3 crenulations of S_2 micas can be seen. Section perpendicular to S_2 and S_3. A405/BC34(a). Field of view 14 mm.

(d) Andalusite inverting directly to prismatic sillimanite. Biotites, some formed in S_3, cut across the andalusite and presumably replace it. A fibrolite mat composed of needles aligned in S_2 is slightly crenulated and intersected by later fibrolite needles which have formed in S_3. Section perpendicular to l_3. A405/M21. Field of view 5 mm.

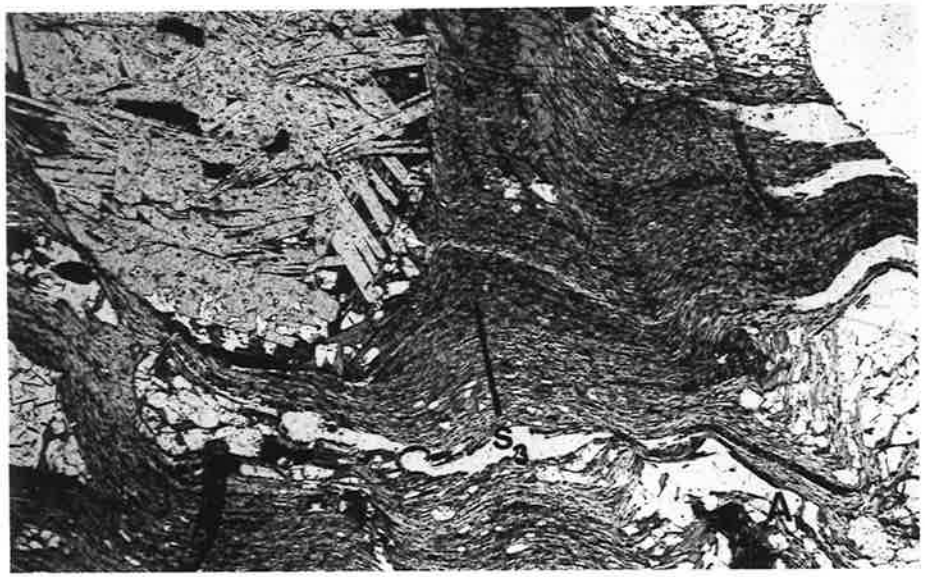
S_4
A

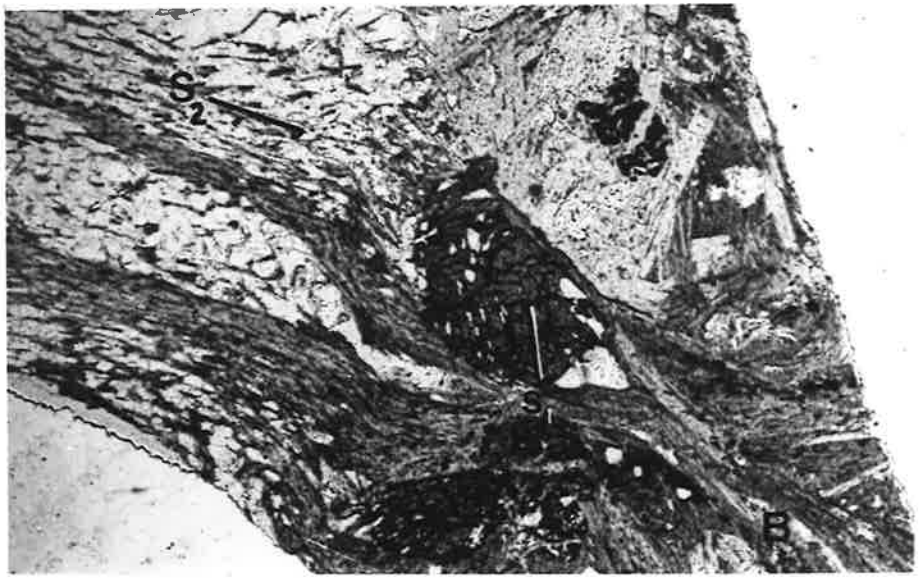
S_2
S_1
B

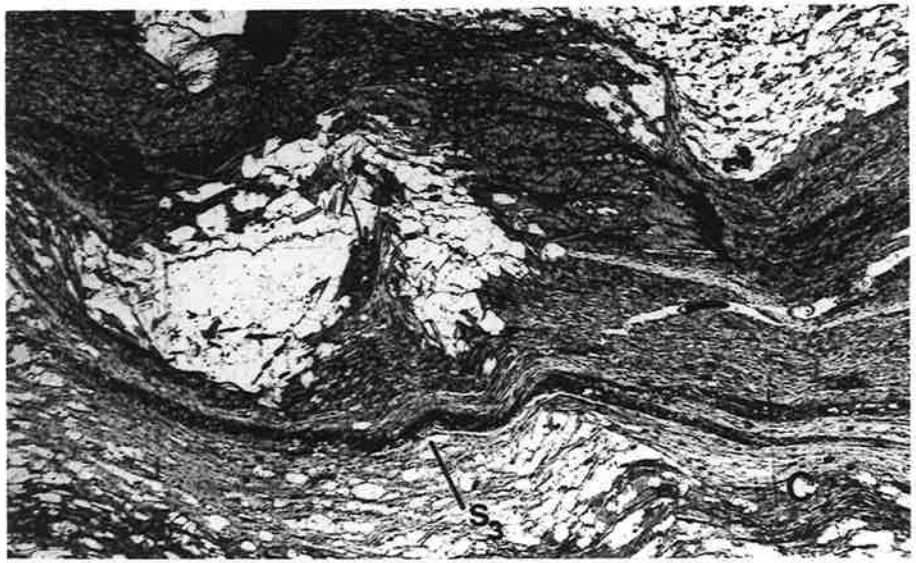
S_3
C

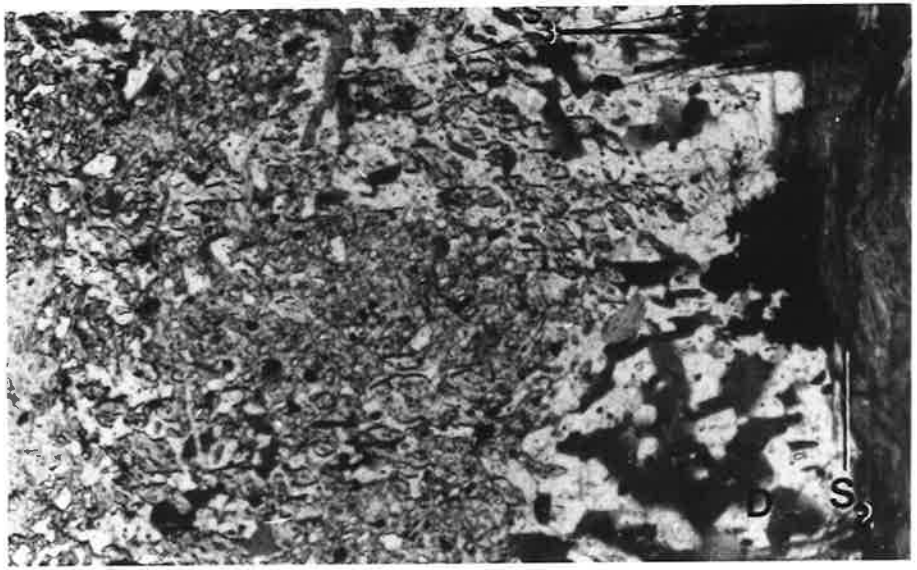
D
S_2

Plate 41

(a) Garnet associated with coarse post-S_2 muscovite crystal which is interpreted as replacing andalusite. This garnet is probably earlier than the muscovite because its margins are not sharp. A405/M10. Field of view 3.1 mm.

(b) Multistage andalusite porphyroblast. Distinct zones of fine equidimensional inclusions are present with an overgrowth containing coarser, elongate inclusions which has formed syn-S_2. Section perpendicular to S_2 and l_3. A405/H8b. Field of view 5 mm.

(c) Pre-S_2 andalusites with very fine equidimensional inclusions in a peraluminous schist layer within a metasiltstone. A405/M10. Field of view 14 mm.

(d) Fibrolite-biotite mats adjacent to staurolite porphyroblasts. Staurolite margins are sharp. Unstable andalusite (a) is common through the rock and though staurolites are associated with fibrolite needles, it is doubtful that they are being replaced. A405/MD5. Field of view 3.9 mm.

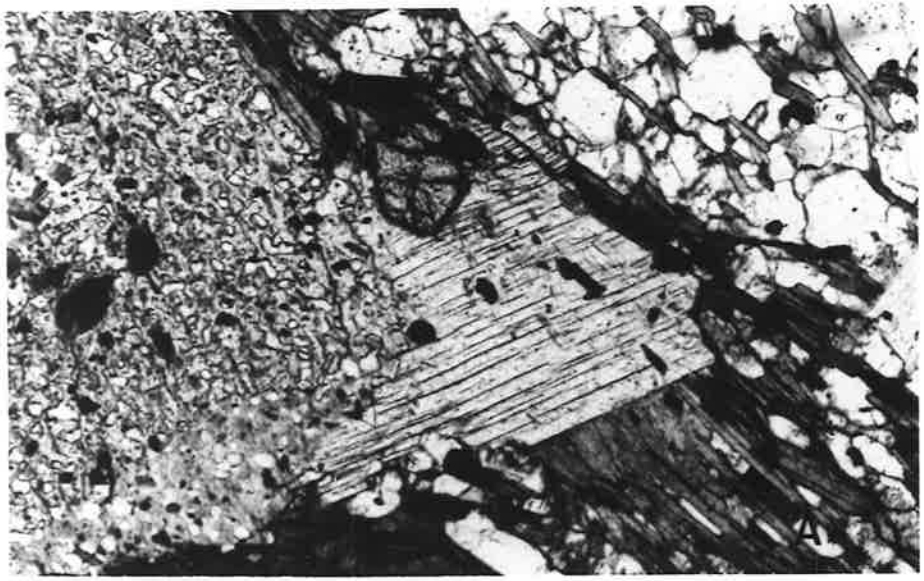
A

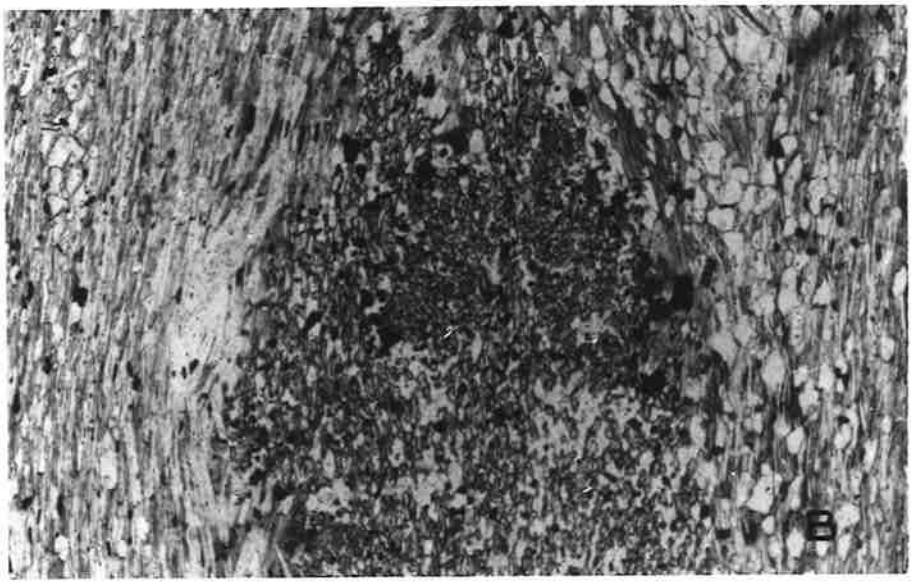
B

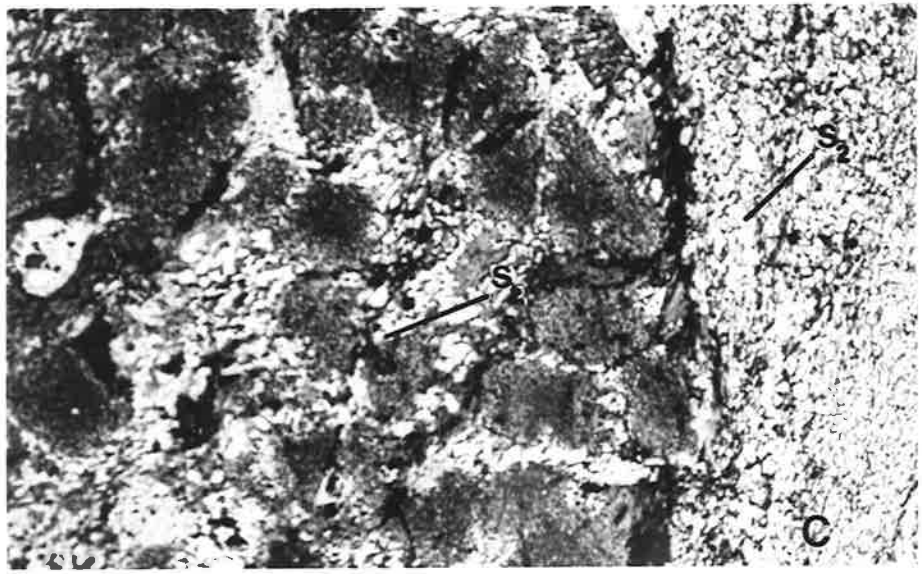
S2
S1
C


a
D

Plate 42

(a) Staurolite (St) in a coarse muscovite plate. Fibrolite mats occur adjacent to the muscovite and some pre-muscovite needles also cut across the crystal. It is proposed that the staurolite is merely a stable inclusion and that the muscovitization is associated with the breakdown of unstable andalusites. A405/E4E. Field of view 3.9 mm.

(b) Coarse muscovite plates related to the breakdown of andalusite envelope sub-idioblastic staurolite crystals. Some biotite crystals are also present. Mutual boundaries of these minerals are sharp. A405/E4E(2). Field of view 3.9 mm.

(c) Ragged poikiloblastic andalusite and staurolite porphyroblasts enclosed by fibrolite mats. There is some embayment of andalusite by biotite (b); it is uncertain whether the staurolite is stable relative to fibrolite. No muscovite is associated with the staurolite, however. A405/MD5. Field of view 3.9 mm.

(d) Post-S_2 chlorite rosettes. A405/E6(2). Field of view 3.9 mm.

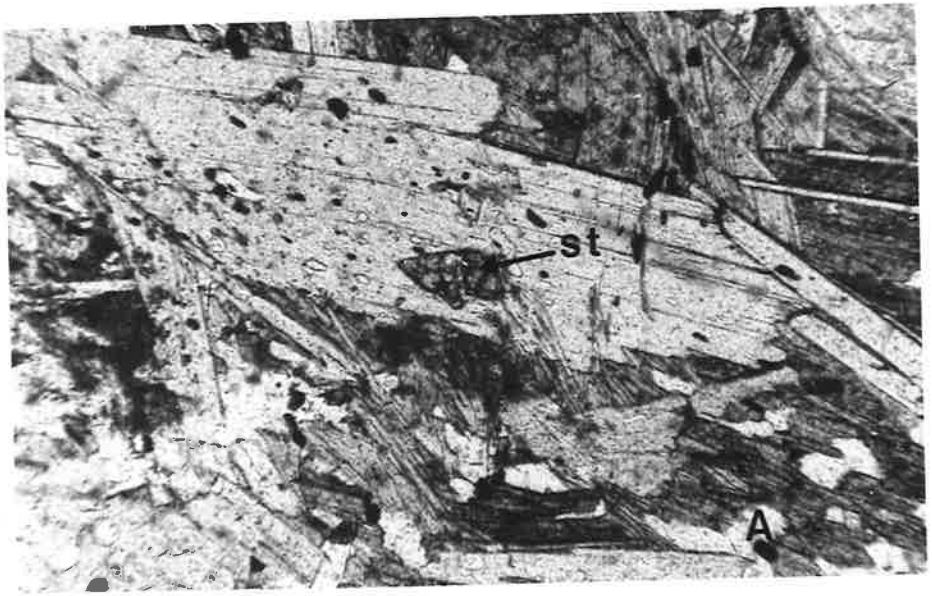
st
A


B


b
C

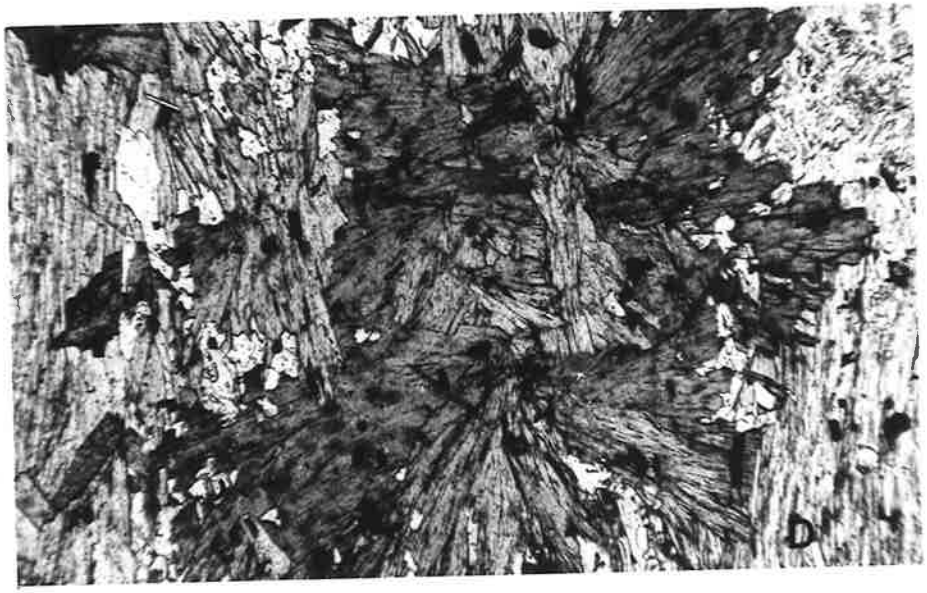
D

Plate 43

(a) Idioblastic garnets(g) in a calc-silicate band within a meta-sandstone. Disoriented stubby subidioblastic hornblendes, untwinned plagioclase and quartz form the bulk of the almost granoblastic texture. A405/M11. Field of view 3.1 mm.

(b) Granoblastic texture in calc-silicate. Dark minerals-hornblende, epidote. Lighter-quartz, plagioclase. A405/BC45. Field of view 12.5 mm.

(c) Typical granoblastic texture in calc-silicate composed of ovoid diopside, hornblende and scapolite crystals. Bedding (S_0) is recognized by the variation in relative proportions of these minerals. A matrix is commonly absent in certain layers, as seen here. A405/MCS2b. Field of view 14 mm.

(d) Granoblastic texture in impure marble. The common twinning of metamorphic calcite is evident. Diopside (di) tends to form roughly ovoid granular aggregates. Scapolite (Sc) forms irregularly shaped crystals. Plagioclase (pl) and hornblende (h) are minor in amount. A405/BC49(1). Field of view 12.5 mm.

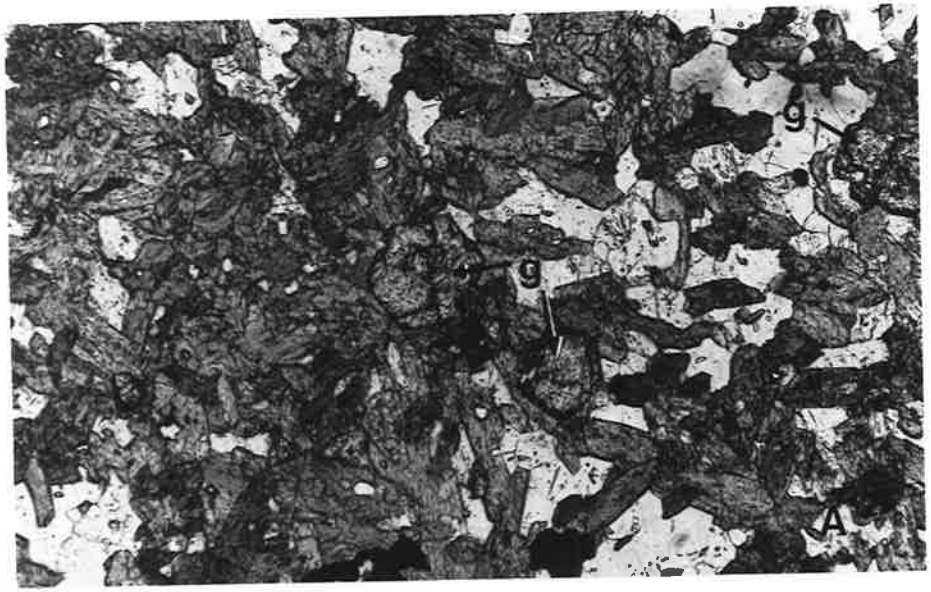
g
g
A

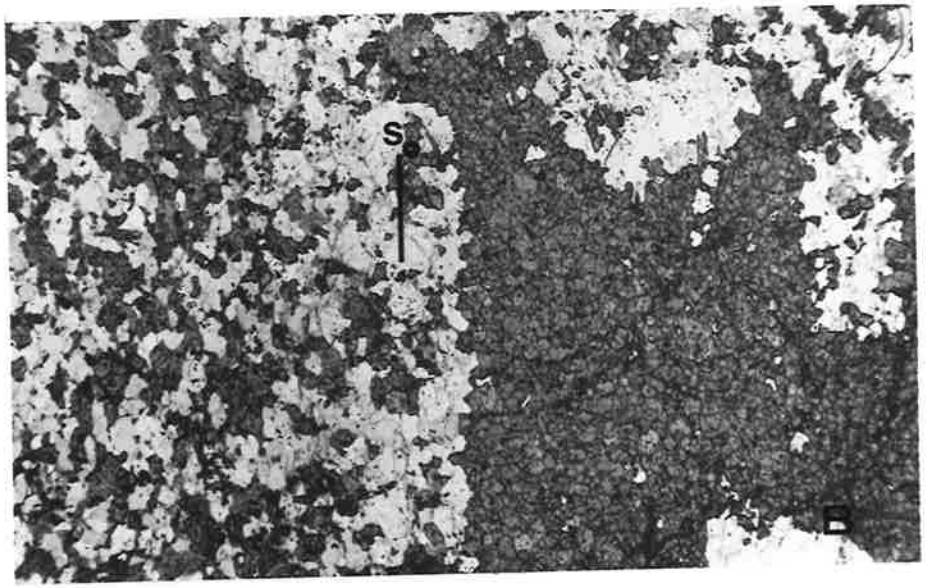
S
B

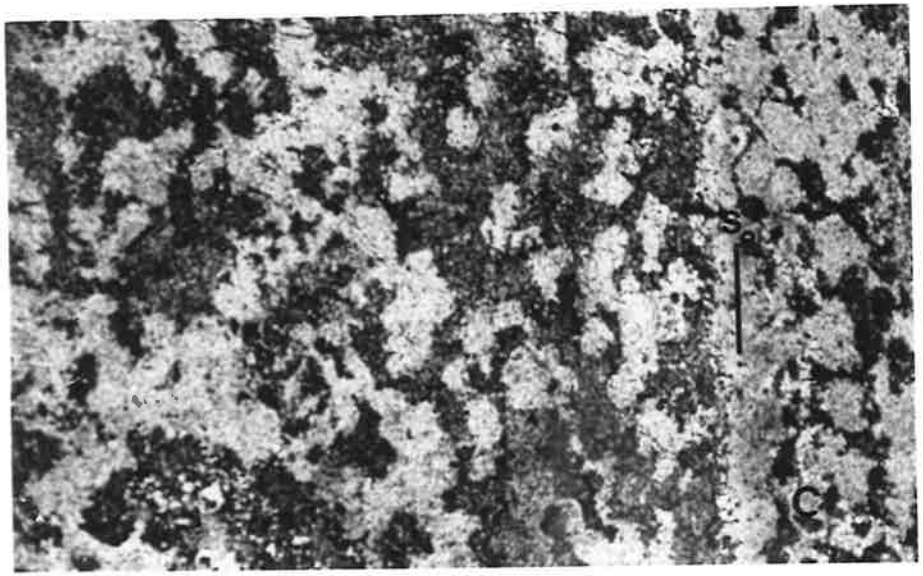
S
C

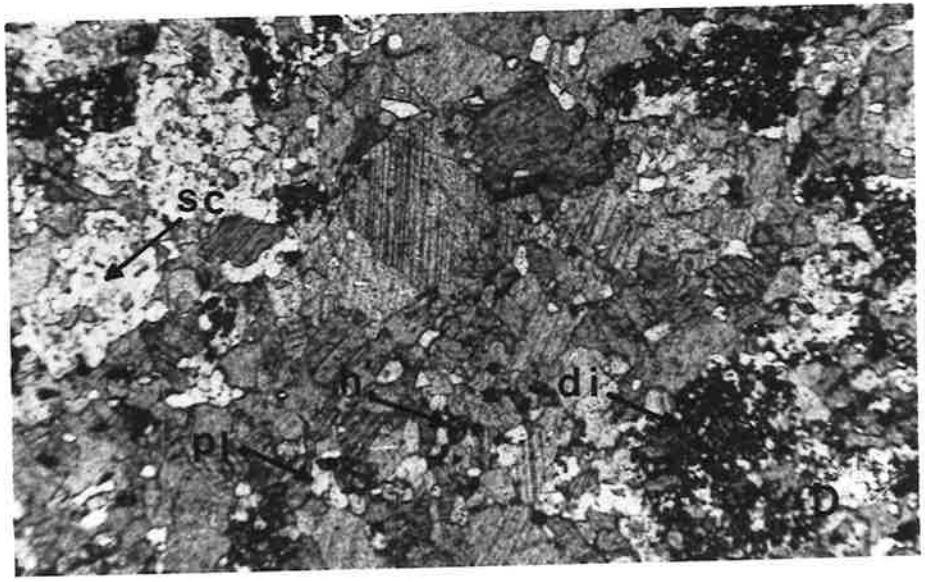
sc
h
di
pl
D

Plate 44

(a) Ovoid scapolite aggregates in a fine matrix of quartz, plagioclase and biotite. Biotites within the aggregates are aligned in S_2 but are markedly finer. Individual scapolite crystals contain few or no inclusions. It is suggested the scapolite crystallized syn-S_2. A405/M20. Field of view 14 mm.

(b) Ovoid aggregates of scapolite and individual scapolite crystals in a fine quartz, plagioclase, biotite matrix. Note the concentration of inclusions in the cores of most crystals and aggregates. A405/MCS2a. Field of view 14 mm.

(c) Ovoid scapolite aggregate. Note the radial development of the crystals. Inclusions tend to be concentrated towards the centre suggesting more rapid early growth. A405/MCS2a. Field of view 5 mm.

(d) Sharp boundary between quartz segregation and enclosing finer groundmass of quartz, plagioclase and biotite of a very micaceous metasiltstone. A405/E4A. Field of view 12.5 mm.

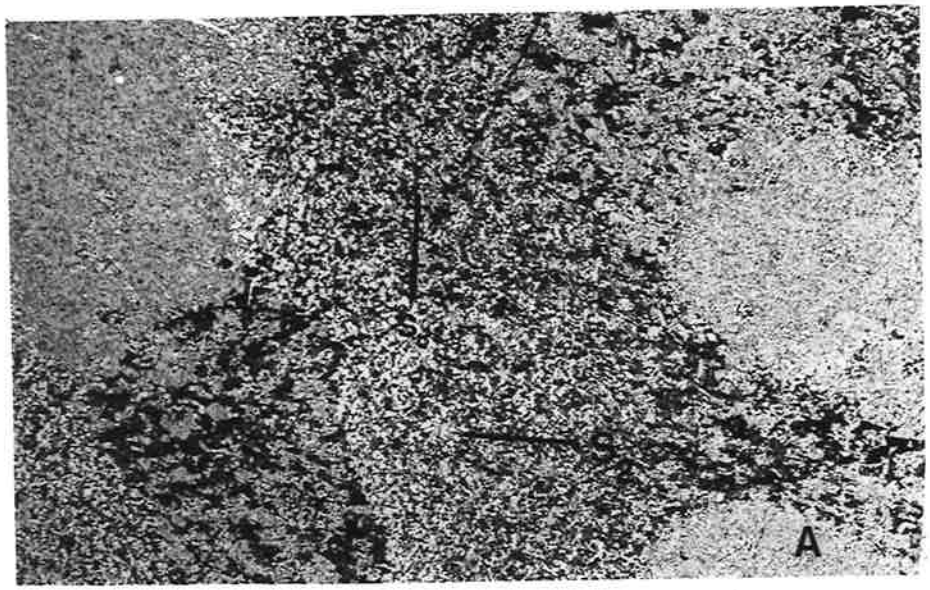
A

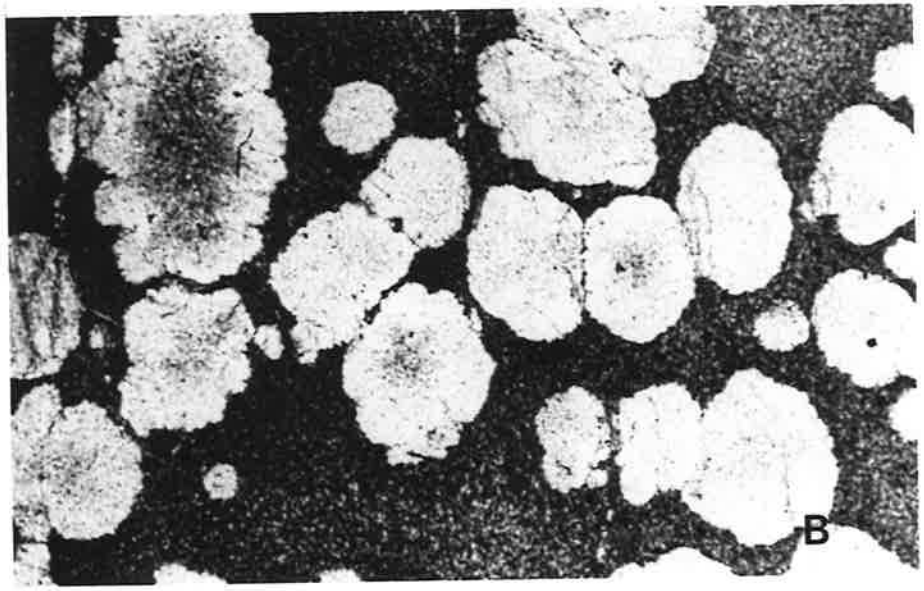
B

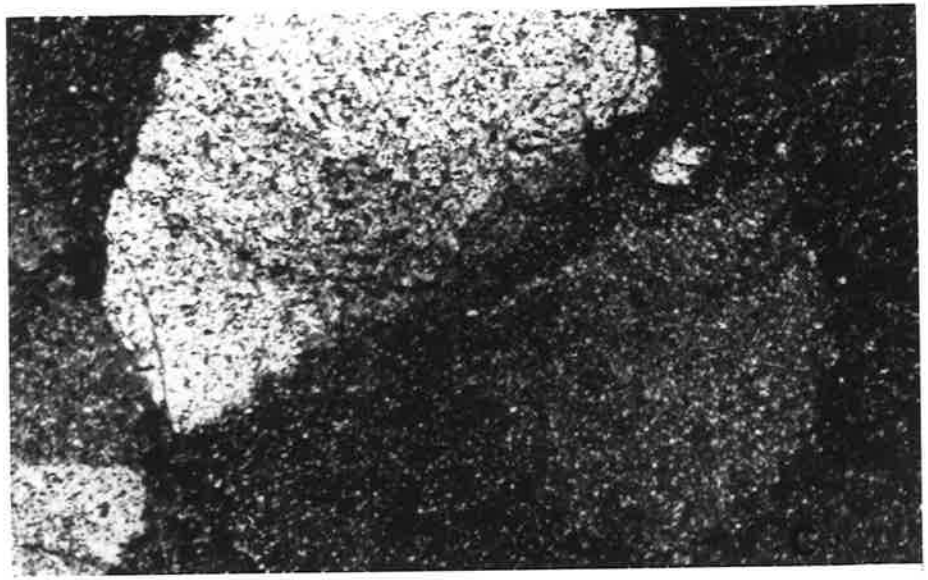

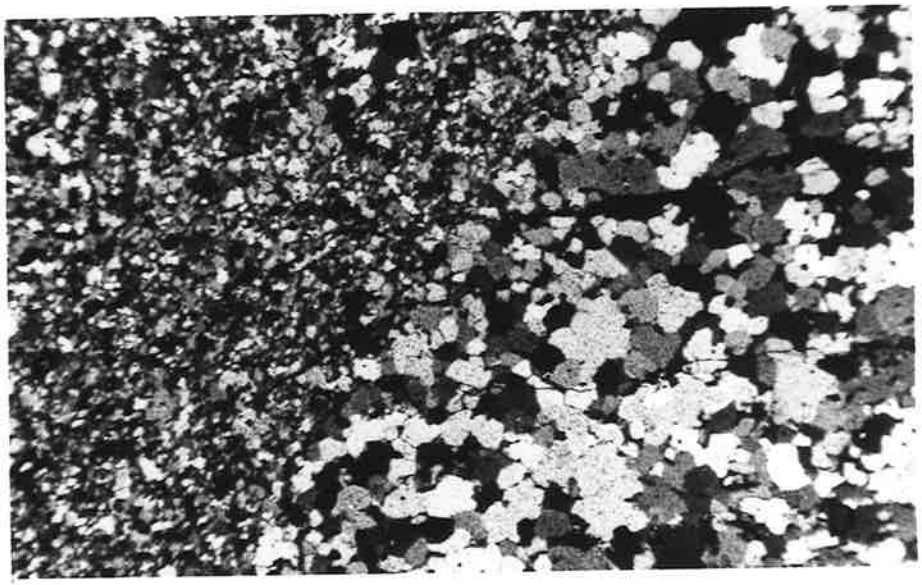

Plate 45

(a) Biotite-enriched core in quartz-biotite segregation. Much of the biotite has been replaced by chlorite with the release of magnetite. A405/BC27'. Field of view 12.5 mm.

(b) Combined Carlsbad and albite twinning in plagioclase crystals of a metadolerite showing relict igneous texture. Recrystallization and crystal re-orientation has been minimal. A405/E9S. Field of view 12.5 mm. Polars crossed.

(c) Elongate hornblende crystals defining S_2 in a metadolerite. The large plagioclase crystals are relict igneous phenocrysts. Recrystallization may have modified their form, but many still retain a subrounded outline which is probably igneous. A405/MD1. Field of view 12.5 mm.

(d) A possible relict igneous plagioclase phenocryst in a metadolerite. S_2-oriented elongate hornblendes are partly deflected by this crystal. Preferential seritization of the more calcic core is visible. A405/E7(1). Field of view 3.9 mm.

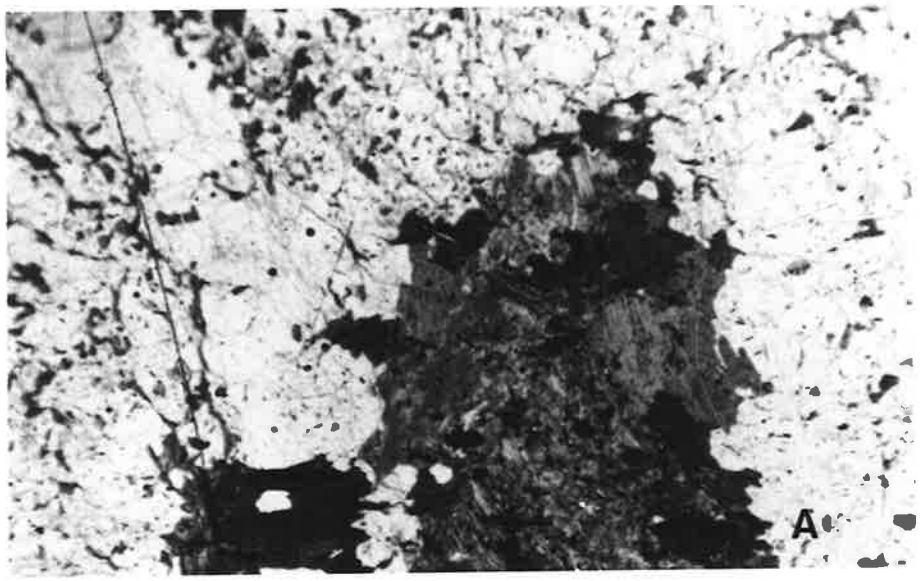
A


B

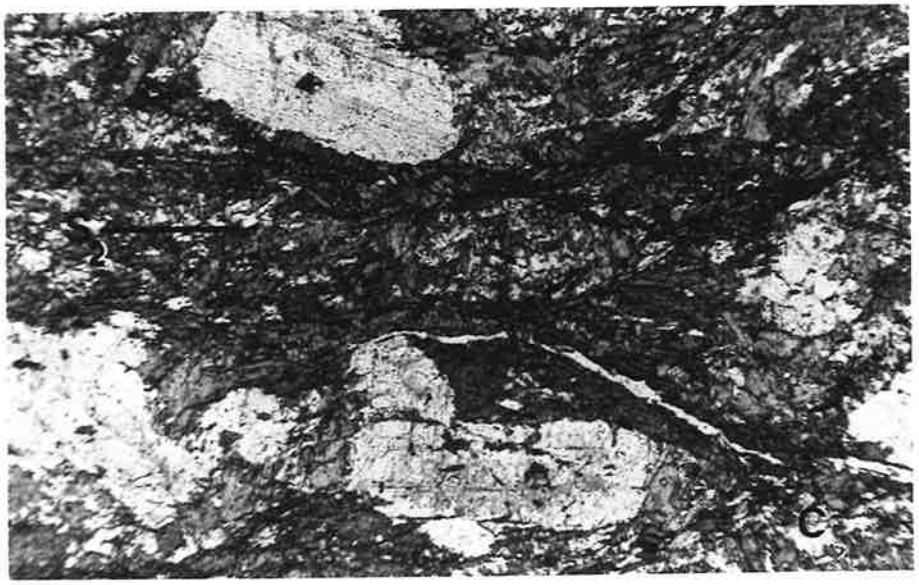
C

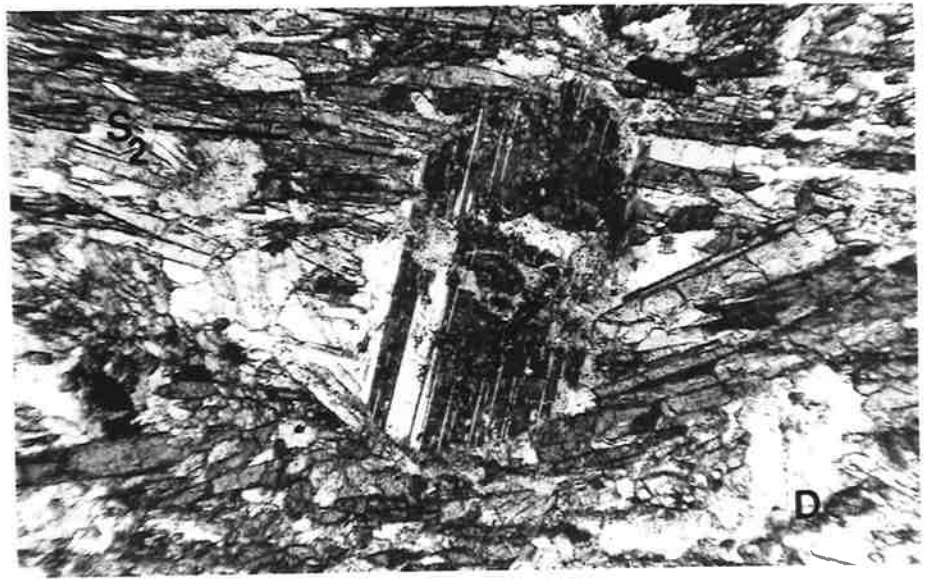
S_2
D

Plate 46

(a) Coarse, subidioblastic hornblendes defining S_2 cut across earlier rather stumpy hornblendes which are weakly aligned and may define an earlier schistosity. A405/MD1. Field of view 3.9 mm.

(b) Quartz + hornblende vein in andalusite schist adjacent to metadolerite dyke. A405/MD5. Field of view 3.9 mm.

(c) Aggregate of staurolite crystals which may have crystallized post S_2. No definite inclusion pattern is evident in the aggregate and the timing of porphyroblast growth is uncertain. Section perpendicular to S_2. A405/BC37a. Field of view 6.5 mm.

(d) Post-S_2 garnet. Note absence of any deflection of the schistosity at the crystal margins. A405/E4E(1). Field of view 6.5 mm.

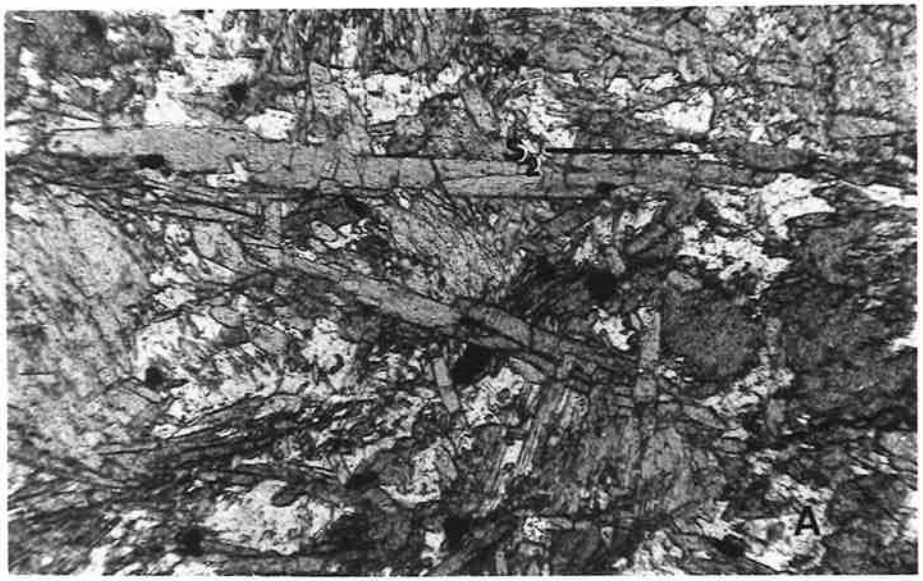
S_2
A


h
B

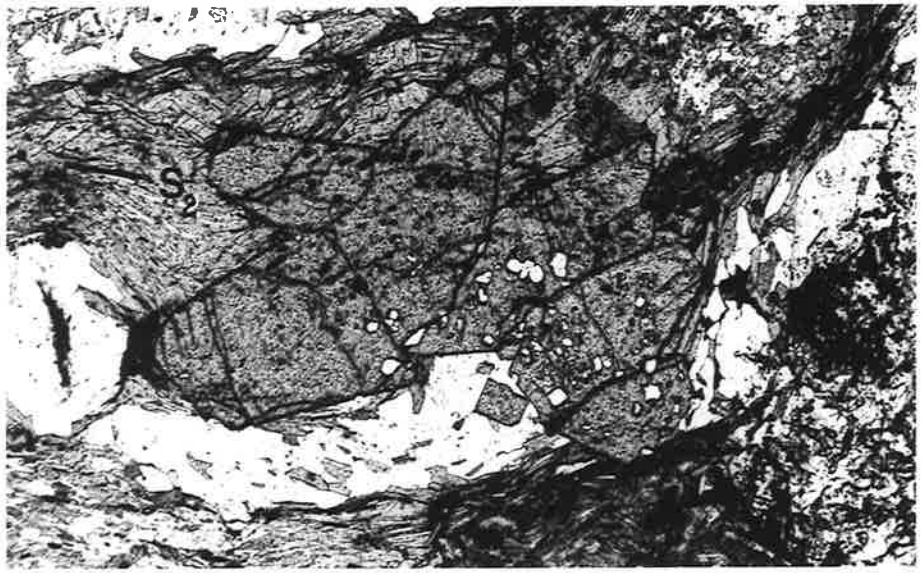
S_2

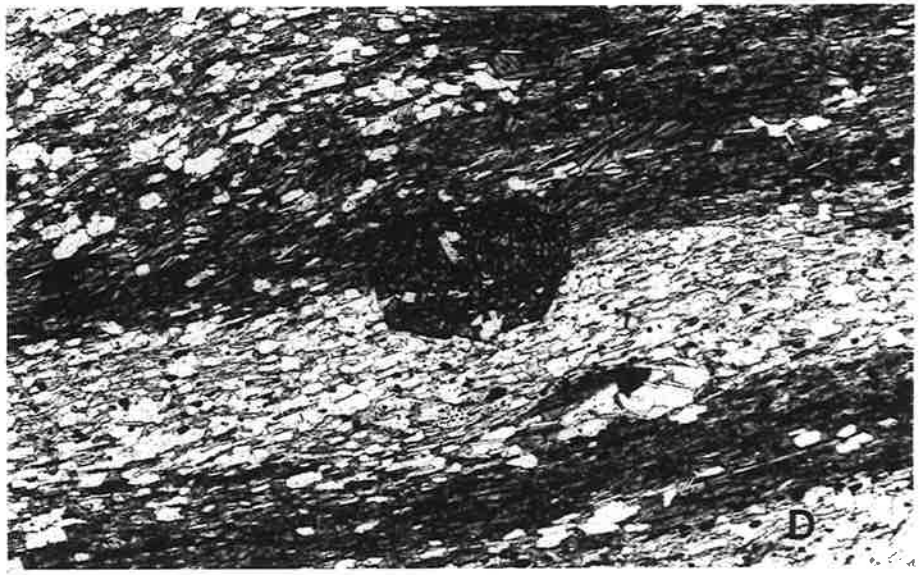
D